

## Supporting Information

### Sequence-sorted redox-switchable hetero[3]rotaxanes

Marius Gaedke, ‡<sup>[a]</sup> Henrik Hupatz, ‡<sup>[a]</sup> Felix Witte,<sup>[b]</sup> Susanne M. Rupf,<sup>[c]</sup> Clara Douglas,<sup>[a]</sup>  
Hendrik V. Schröder,<sup>[a,d]</sup> Lukas Fischer,<sup>[a]</sup> Moritz Malischewski,<sup>[c]</sup> Beate Paulus<sup>[b]</sup> and  
Christoph A. Schalley\*<sup>[a]</sup>

<sup>[a]</sup> Institut für Chemie und Biochemie, Freie Universität Berlin,  
Arnimallee 20, 14195 Berlin, Germany.

<sup>[b]</sup> Institut für Chemie und Biochemie, Freie Universität Berlin,  
Arnimallee 22, 14195 Berlin, Germany.

<sup>[c]</sup> Institut für Chemie und Biochemie, Freie Universität Berlin,  
Fabeckstr. 34/36 14195 Berlin, Germany.

<sup>[d]</sup>present address: Department of Chemical and Biological Engineering, Princeton University,  
Princeton, NJ08544, USA

\*Corresponding author e-mail: [c.schalley@fu-berlin.de](mailto:c.schalley@fu-berlin.de)

‡These authors contributed equally to this work.

## Table of Contents

1.	Experimental details.....	S02
1.1.	General methods.....	S02
1.2.	Synthesis of axle <b>AX</b> .....	S04
1.3.	Synthesis of macrocycle <b>NDIC7</b> .....	S13
1.4.	Synthesis of (pseudo)[3]rotaxanes.....	S19
2.	Isothermal titration calorimetry.....	S40
3.	Heteropseudo[3]rotaxane <sup>1</sup> H NMR experiments.....	S42
4.	Tandem mass spectrometry.....	S48
5.	Electrochemical measurements.....	S73
6.	UV/Vis experiments.....	S76
7.	Computational details .....	S77
8.	Crystallographic data.....	S78
9.	References.....	S81

# 1. Experimental details

## 1.1. General methods

All reagents and solvents were obtained from commercial sources and used without further purification. Dry solvents were purchased from Acros Organics (Geel, Belgium) and either directly used or treated with the M. Braun solvent purification system SPS 800. Wheel **TTFC8**,<sup>1</sup> 2,6-dimethoxybenzoxonitrile oxide stopper **St1**,<sup>2</sup> monovalent axle **A1**,<sup>3</sup> monovalent axle **A2**,<sup>3</sup> 1-bromo-6-(prop-2-yn-1-yloxy)hexane **S5**,<sup>4</sup> *tert*-butyl (3,5-dihydroxyphenyl)carbamate **S10**,<sup>3</sup> NDI building block **S13**,<sup>5</sup> **BC7**<sup>6</sup> and **NDIC8**<sup>3</sup> were synthesised according to literature procedures, sodium tetrakis[3,5-bis(trifluoromethyl)phenyl]borate (NaBArF<sub>24</sub>), 3,5-di-*tert*-butylbenzaldehyde **S1**, (4-cyanophenyl)methanaminium chloride **S2**, di-*tert*-butyl-dicarbonate, were bought at Sigma Aldrich or TCI Chemicals. Thin-layer chromatography was performed on silica gel-coated plates with fluorescent indicator F254 (Merck). For column chromatography, silica gel (0.04-0.063 mm, Merck), or Biotage SNAP and SNAP Ultra Cartridges were used on a Biotage Isolera One.

<sup>1</sup>H and <sup>13</sup>C NMR experiments were performed on JEOL ECX 400, JEOL ECZ 600, Bruker AVANCE 500 or Bruker AVANCE 700 instruments. Residual solvent signals were used as the internal standards. All shifts are reported in ppm and NMR multiplicities are abbreviated as s (singlet), d (doublet), t (triplet), m (multiplet) and br (broad). Coupling constants *J* are reported in Hertz. Compounds containing the tetrakis[3,5-bis(trifluoromethyl)phenyl]borate (BArF<sub>24</sub><sup>-</sup>) anion show <sup>13</sup>C NMR spectra with <sup>19</sup>F, <sup>10</sup>B and <sup>11</sup>B couplings. These signals are denoted as one signal.

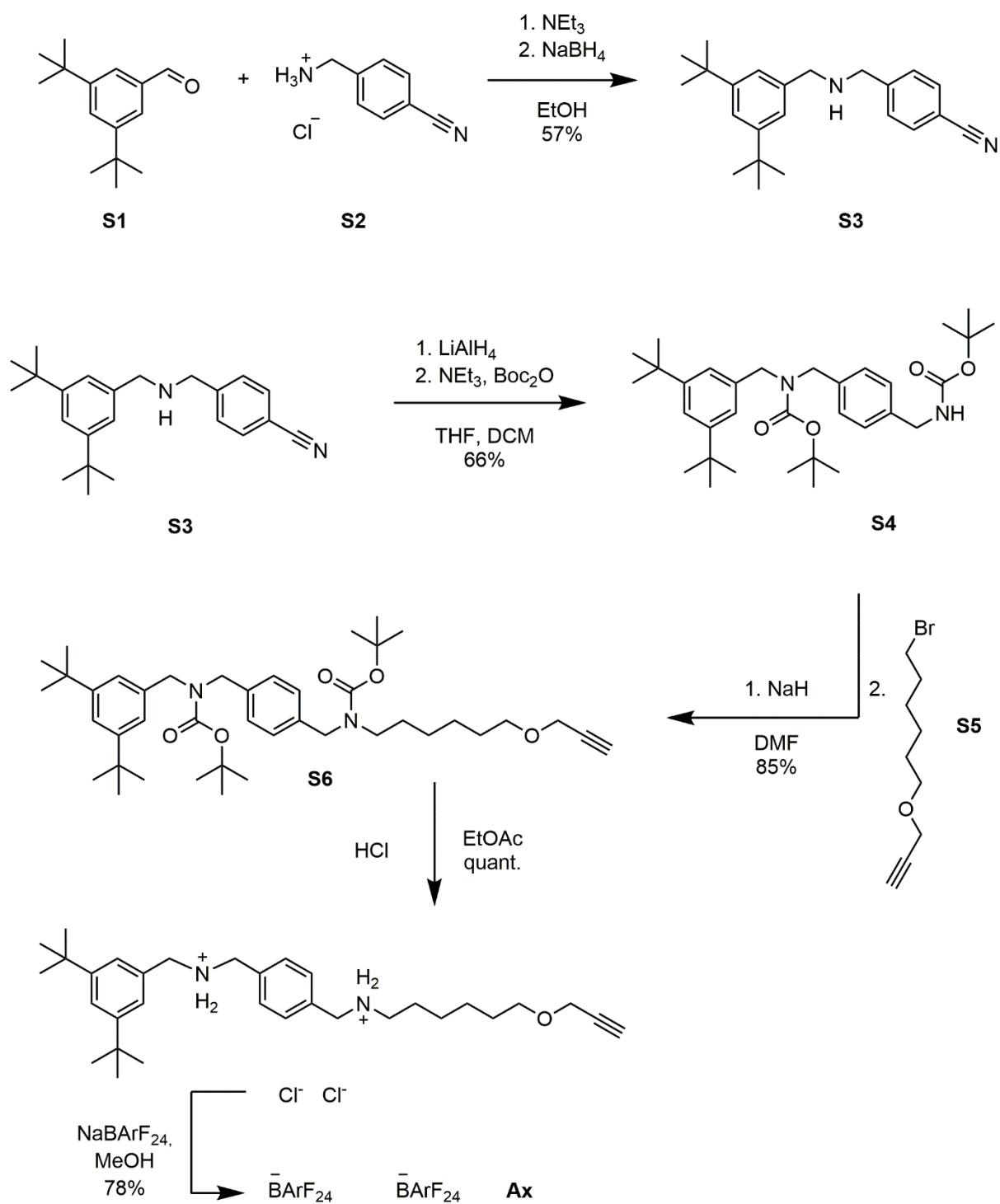
High-resolution ESI mass spectra were measured on an Agilent 6210 ESI-TOF device or a Synapt G2-S HDMS (Waters Co., Milford, MA, USA) mass spectrometer. HPLC grade solvents were used for sample preparation.

UV/Vis spectra were recorded with a Varian Cary 50 Bio spectrometer equipped with a xenon lamp. Solvents with HPLC grade and Suprasil glass cuvettes with a path-length of 1 cm were used.

CV measurements were carried out with an Autolab PGSTAT302N potentiostat in a 2 mL measuring cell in 1,2-dichloroethane with 0.1 M n-Bu<sub>4</sub>NBArF<sub>24</sub> as the conducting salt. The working electrode was made of glassy carbon, the reference Ag electrode was etched with conc. aq. HCl. A Pt wire worked as the counter electrode. The cyclic voltammogram traces were recorded with 25, 50, 100, 250, 500, 1000 mV/s scan rates, to ensure that the observed processes are reversible and diffusion-limited. In order to obtain the correct half-wave potentials, FeCp<sub>2</sub><sup>\*0</sup>/FeCp<sub>2</sub><sup>\*+</sup> (decamethylferrocene) was used as the reference. These values were afterwards referenced to FeCp<sub>2</sub>/FeCp<sub>2</sub><sup>+</sup> (ferrocene) as described in the literature.<sup>7</sup> The

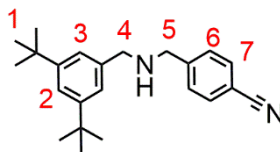
raw data were treated with Nova 1.5 by Metrohm and the plots were made with Origin 2020 by OriginLab.

## 1.2. Synthesis of axle Ax



**Scheme S1** General procedure for the synthesis of axle **Ax**.

### 4-(((3,5-di-tert-butylbenzyl)amino)methyl)benzonitrile S3



**S3**

3,5-Di-*tert*-butylbenzaldehyde (2.00 g, 9.16 mmol, 1.00 equiv.) and (4-cyanophenyl)-methanaminium chloride (1.53 g, 9.16 mmol, 1.00 equiv.) were dissolved in dry EtOH (400 ml) under argon atmosphere. Triethylamine (1.15 mL, 8.27 mmol, 0.90 equiv.) was added and the solution was refluxed for 5 h. After it was cooled to 0 °C, NaBH<sub>4</sub> (1.73 g, 45.8 mmol, 5.00 equiv.) was added and the solution was stirred under argon atmosphere overnight in the thawing ice bath. The reaction was then quenched by adding a concentrated aq. solution of NaHCO<sub>3</sub> until no more gas evolved. The solvent was removed under reduced pressure and the oily residue was dissolved in CH<sub>2</sub>Cl<sub>2</sub> (100 ml). The organic layer was washed with brine and dried over MgSO<sub>4</sub>. The solvent was removed under reduced pressure and the residue was purified by column chromatography (SiO<sub>2</sub>, CH<sub>2</sub>Cl<sub>2</sub>/MeOH 100:1 → 50:1, R<sub>f</sub> ~ 0.4 in CH<sub>2</sub>Cl<sub>2</sub>/MeOH = 50:1) yielding the amine as a white solid (1.76 g, 5.26 mmol, 57%).

**<sup>1</sup>H NMR** (500 MHz, CD<sub>2</sub>Cl<sub>2</sub>): δ = 1.33 (s, 18H, 1), 3.76 (s, 2H, 5), 3.87 (s, 2H, 4), 7.16 (d, *J* = 1.8 Hz, 2H, 3), 7.32 (t, *J* = 1.9 Hz, 1H, 2), 7.48 – 7.52 (m, 2H, 6), 7.60 – 7.64 (m, 2H, 7) ppm.

**<sup>13</sup>C NMR** (125 MHz, CD<sub>2</sub>Cl<sub>2</sub>): δ = 31.8, 35.3, 111.1, 119.6, 121.6, 122.9, 129.2, 132.7, 139.9, 147.2, 151.4.ppm. **HRMS (MeOH)**: *m/z* calcd. for [C<sub>23</sub>H<sub>31</sub>N<sub>2</sub>]<sup>+</sup>: 335.2482 [M+H]<sup>+</sup>, found: 335.2495

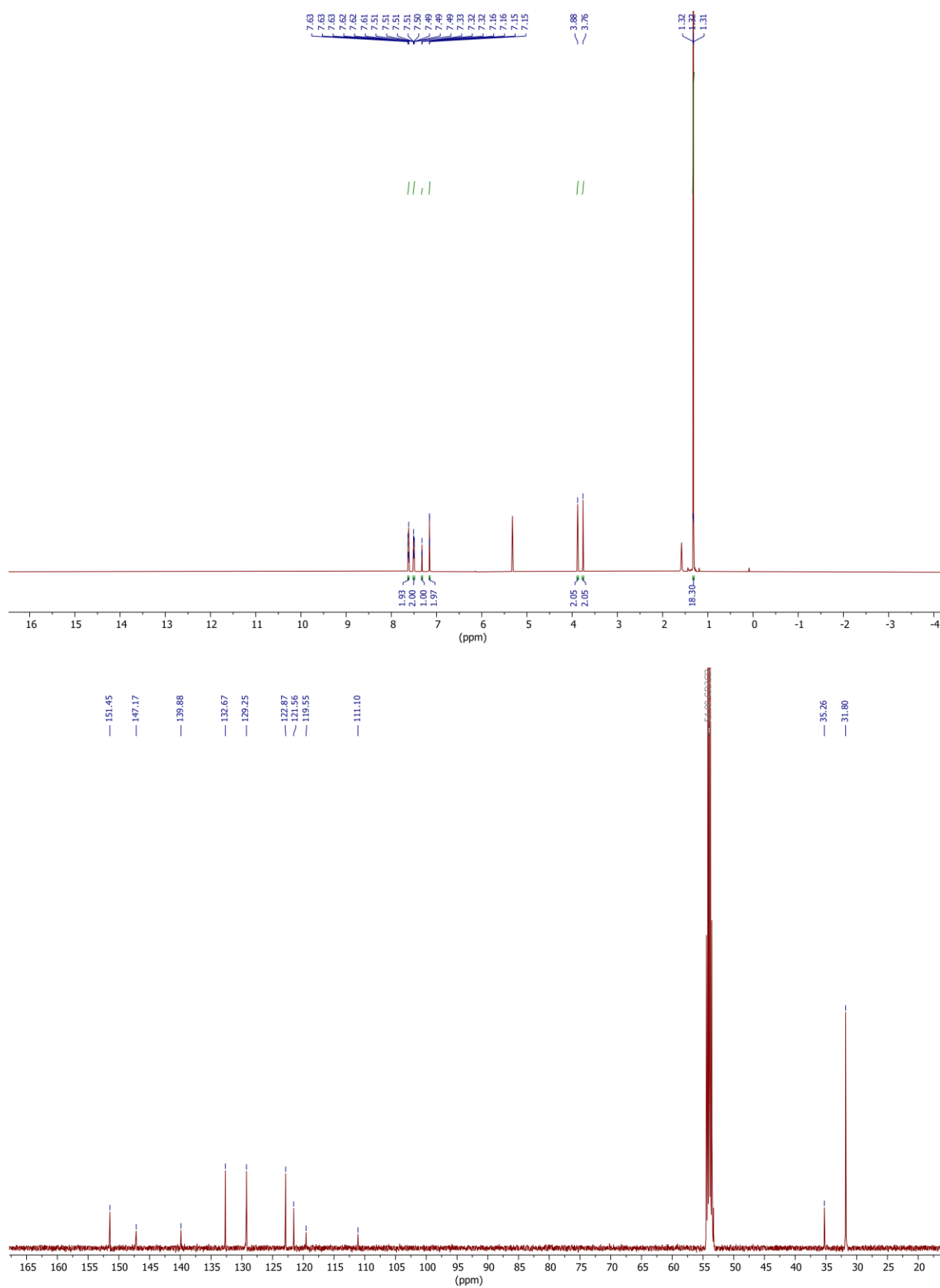
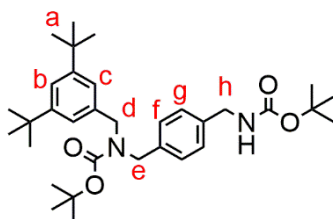


**Fig. S1**  $^1\text{H}$  (top) and  $^{13}\text{C}$  (bottom) NMR spectra (500/126 MHz,  $\text{CD}_2\text{Cl}_2$ , 298 K) of amine **S3**.

**tert-butyl (4-(((tert-butoxycarbonyl)amino)methyl)benzyl)(3,5-di-tert-butylbenzyl)carbamate S4**



**S4**

Amine **S3** (1.76 g, 5.26 mmol, 1.00 equiv.) was dissolved in dry THF (400 ml) under argon atmosphere and cooled to 0 °C. LiAlH<sub>4</sub> (1.00 g, 26.3 mmol, 5.00 equiv.) was added and the solution was stirred under argon atmosphere for 24 h in the thawing ice bath. The reaction was quenched by adding a concentrated aq. solution of Na<sub>2</sub>SO<sub>4</sub> until no more gas evolved. The precipitate was filtered off and the solvent was removed under reduced pressure. The residue was dissolved in CH<sub>2</sub>Cl<sub>2</sub> (100 mL), washed with water and brine and dried over MgSO<sub>4</sub>. The solvent was removed under reduced pressure. The raw product (1.75 g, 5.2 mmol, 1.00 equiv.) was dissolved in CH<sub>2</sub>Cl<sub>2</sub> (50 mL) and cooled to 0 °C. Triethylamine (1.26 g, 12.4 mmol, 2.40 equiv.) and di-*tert*-butyl-dicarbonate (2.49 g, 11.4 mmol, 2.20 equiv.) was added. The reaction mixture was stirred overnight in the thawing ice bath. Afterwards, it was quenched by adding a concentrated aq. solution of NaHCO<sub>3</sub>. The organic layer was washed with water and brine and dried over MgSO<sub>4</sub>. The solvent was removed under reduced pressure and the residue was purified by column chromatography (SiO<sub>2</sub>, CH<sub>2</sub>Cl<sub>2</sub>/MeOH 100:1 → 20:1, R<sub>f</sub> ~ 0.4 in CH<sub>2</sub>Cl<sub>2</sub>/MeOH = 100:1) yielding the protected diamine as a colorless sticky oil (1.88 g, 3.48 mmol, 66%).

**<sup>1</sup>H NMR** (700 MHz, CDCl<sub>3</sub>): δ = 1.31 (s, 18H, 1), 1.47 (s, 9H, *tert*-butyl), 1.50 (s, 9H, *tert*-butyl), 4.30 (m, 4H, 4,5), 4.40 (s, 2H, 8), 4.40 (s<sub>br</sub>, 1H, NH), 6.99 – 7.09 (m, 2H, 3), 7.11 – 7.25 (m, 4H, 6, 7), 7.31 (t, *J* = 1.9 Hz, 1H, 2) ppm. **<sup>13</sup>C NMR** (176 MHz, CDCl<sub>3</sub>): δ = 28.6, 31.8, 34.9, 44.6, 48.9, 49.2, 49.7, 50.2, 80.0, 121.3, 122.0, 122.4, 127.8, 128.5, 137.4, 137.9, 151.0, 154.9, 156.2 ppm. **HRMS (MeOH)**: *m/z* calcd. for [C<sub>33</sub>H<sub>50</sub>N<sub>2</sub>O<sub>4</sub>]<sup>+</sup>: 577.3403 [M+K]<sup>+</sup>, found: 577.3436; *m/z* calcd. for [C<sub>33</sub>H<sub>50</sub>N<sub>2</sub>O<sub>4</sub>]<sup>+</sup>: 561.3663 [M+Na]<sup>+</sup>, found: 561.3696.

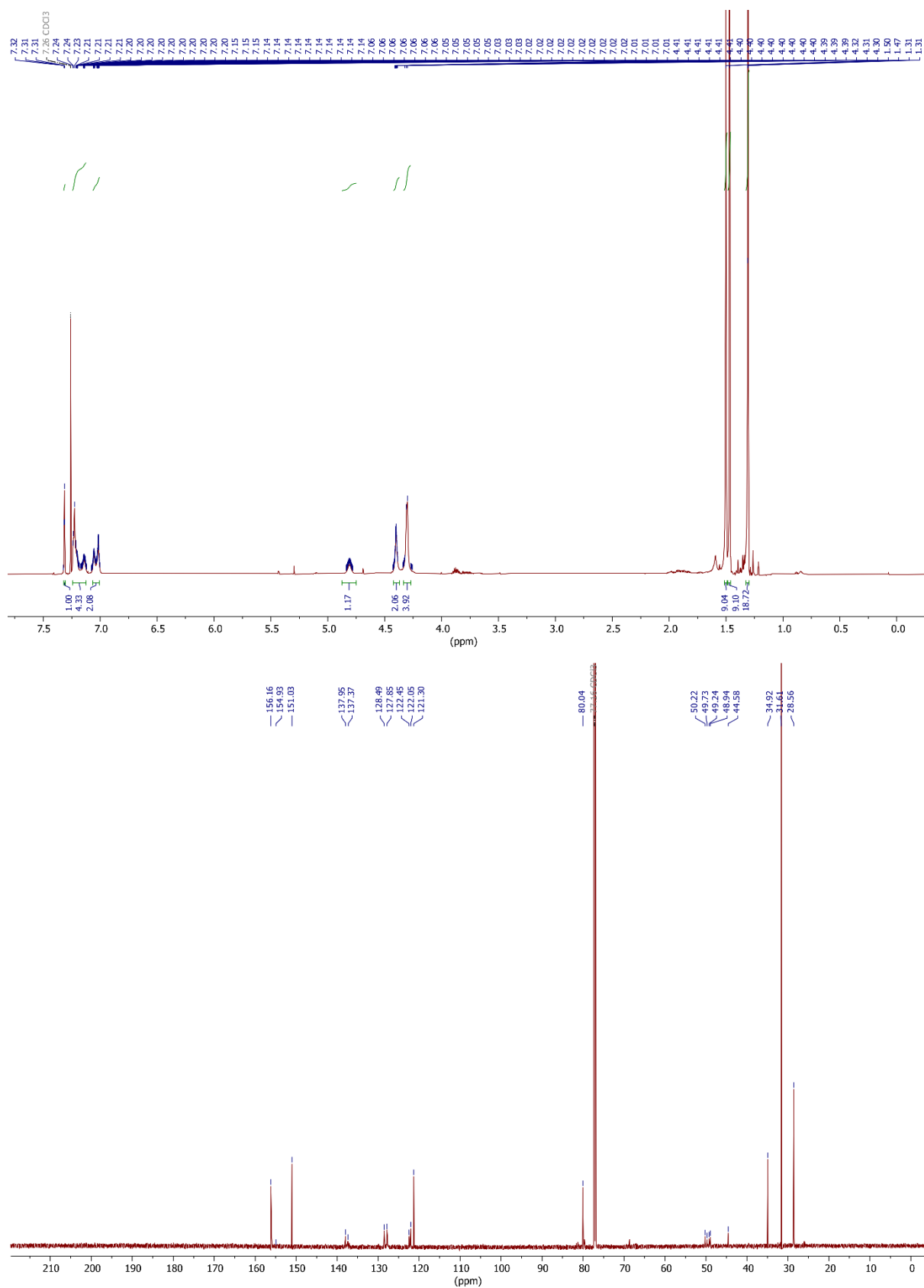
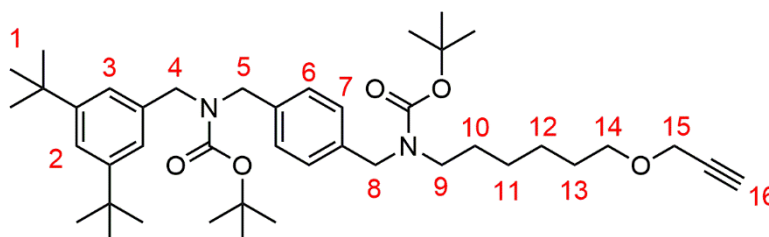


**Fig. S2** <sup>1</sup>H (top) and <sup>13</sup>C (bottom) NMR spectra (700/176 MHz, CDCl<sub>3</sub>, 298 K) of carbamate **S4**.

***tert*-butyl (4-(((*tert*-butoxycarbonyl)(6-(prop-2-yn-1-yloxy)hexyl)amino)methyl)benzyl)(3,5-di-*tert*-butylbenzyl)carbamate **S6****



**S6**

Carbamate **S4** (1.99 g, 3.8 mmol, 1.00 equiv.) was dissolved in dry DMF (50 ml) under argon atmosphere and cooled to 0 °C. NaH (0.2 g, 4.9 mmol, 1.30 equiv.) was added slowly and portion-wise, the mixture stirred for 10 min in the ice bath and became pink. **S5** (1.00 g, 4.5 mmol, 1.20 equiv.) was added and the mixture was stirred under argon atmosphere in the thawing ice bath overnight. The reaction was quenched by adding H<sub>2</sub>O (50 mL). The solvent was removed under reduced pressure and the residue was dissolved in CH<sub>2</sub>Cl<sub>2</sub> (100 mL), washed with water and dried over MgSO<sub>4</sub>. The solvent was removed under reduced pressure. The crude product was purified by column chromatography (SiO<sub>2</sub>, cyclohexane/Et<sub>2</sub>O 9:1 -> 8:2, R<sub>f</sub> ~ 0.5 in cyclohexane/Et<sub>2</sub>O 8:2) yielding **S6** as a colorless sticky oil (2.19 g, 3.23 mmol, 85%).

**<sup>1</sup>H NMR** (700 MHz, CDCl<sub>3</sub>): δ = 1.24 – 1.29 (m, 2H, 11), 1.31 (s, 18H, 1), 1.33 – 1.39 (m, 2H, 12), 1.42 – 1.53 (m, 20H, *tert*-butyl, 10), 1.55 – 1.62 (m, 2H, 13), 2.40 (t, *J* = 2.4 Hz, 1H, 16), 3.08 – 3.22 (m, 2H, 9), 3.49 (t, *J* = 6.6 Hz, 2H, 14), 4.12 (d, *J* = 2.4 Hz, 2H, 15), 4.25 – 4.33 (m, 2H, 4/5), 4.35 – 4.46 (m, 4H, 8,4/5), 7.00 – 7.08 (m, 2H, 3), 7.11 – 7.22 (m, 4H, 6,7), 7.32 (t, *J* = 1.9 Hz, 1H, 2) ppm. **<sup>13</sup>C NMR** (176 MHz, CDCl<sub>3</sub>): δ = 26.0, 26.8, 28.2, 28.6, 29.6, 30.5, 31.6, 34.9, 47.1, 48.9, 49.3, 50.0, 50.1, 58.2, 70.2, 74.2, 79.7, 80.0, 80.2, 121.3, 122.1, 122.5, 127.2, 127.8, 128.3, 137.1, 137.4, 137.8, 151.0, 156.2 ppm. **HRMS (MeOH)**: *m/z* calcd. for [C<sub>42</sub>H<sub>64</sub>N<sub>2</sub>O<sub>5</sub>]<sup>+</sup>: 715.4452 [M+K]<sup>+</sup>, found: 715.4473; *m/z* calcd. 699.4713 [M+Na]<sup>+</sup>, found: 699.4732.

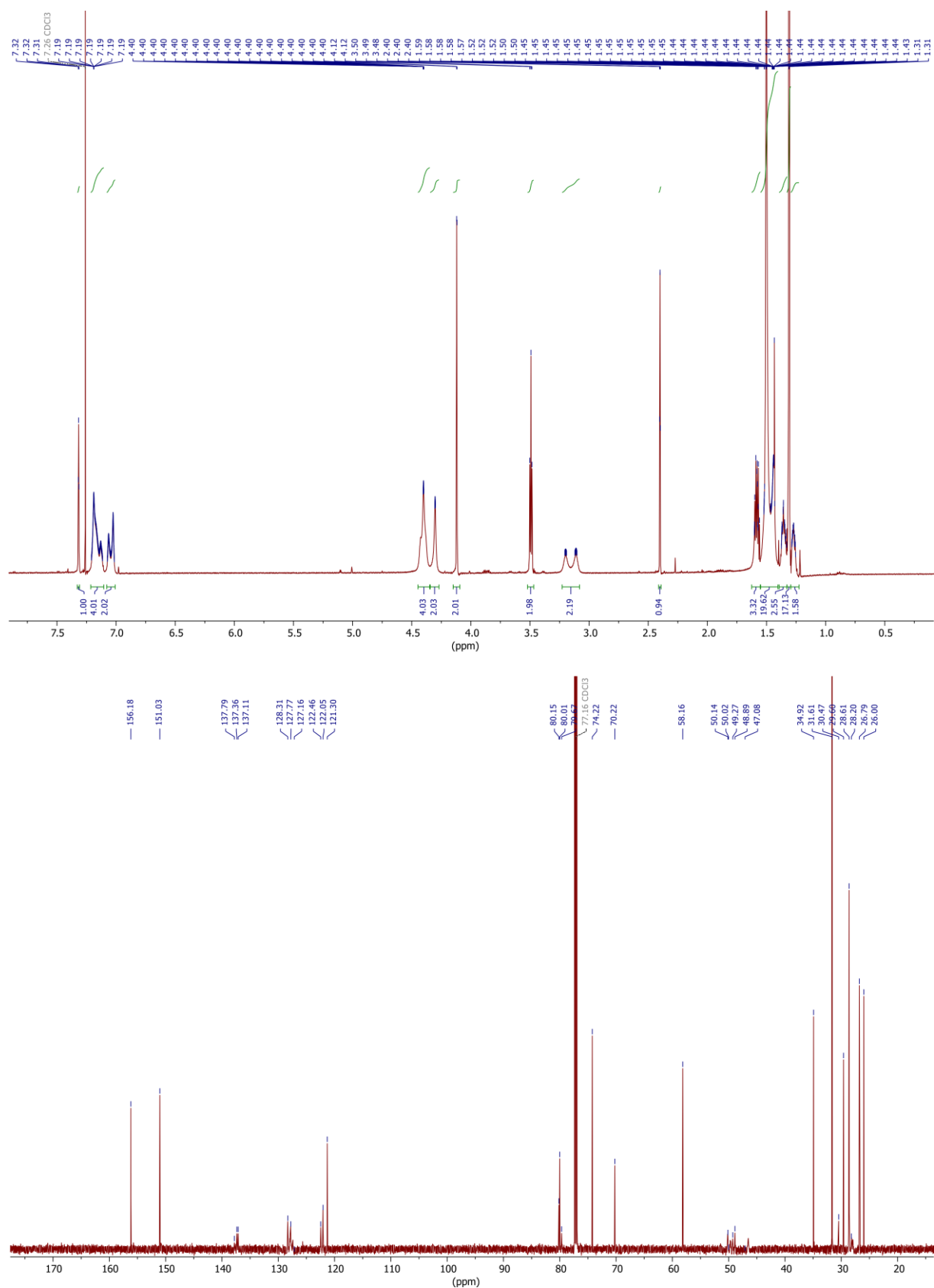
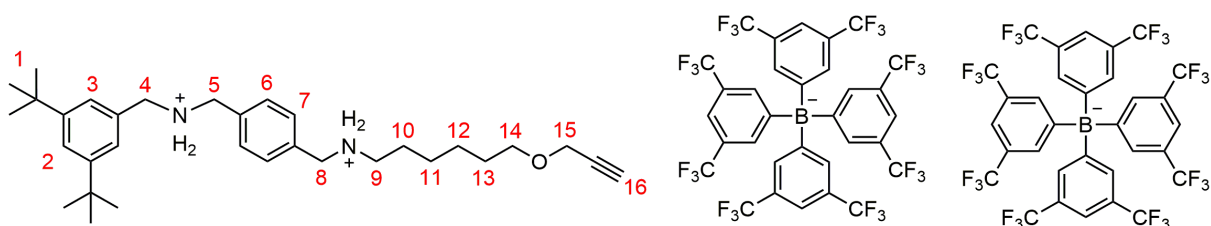


**Fig. S3** <sup>1</sup>H (top) and <sup>13</sup>C (bottom) NMR spectra (700/176 MHz, CDCl<sub>3</sub>, 298 K) of carbamate **S6**.

**N-(4-(((3,5-di-tert-butylbenzyl)ammonio)methyl)benzyl)-6-(prop-2-yn-1-yloxy)hexan-1-aminium tetrakis(3,5-bis(trifluoromethyl)phenyl)borate **Ax****



**Ax**

Carbamate **S6** (0.43 g, 0.61 mmol, 1.00 equiv.) was dissolved in EtOAc (20 ml) and cooled to 0 °C. conc. HCl (3 mL) was added. The mixture was stirred in the thawing ice bath overnight. The solvent was removed under reduced pressure and a portion (0.10 g, 0.18 mmol, 1.00 equiv.) was dissolved in MeOH (20 mL). NaBARF<sub>24</sub> (0.32 g, 0.36 mmol, 2.00 equiv.) was added and the mixture stirred for 3 h at r.t.. The solvent was removed under reduced pressure, the crude product was dissolved in CH<sub>2</sub>Cl<sub>2</sub> (50 mL), washed with water and dried over MgSO<sub>4</sub>. Removal of the solvent yielded **Ax** as a colorless sticky oil (0.31 g, 0.14 mmol, 78% combined). **<sup>1</sup>H NMR** (700 MHz, CD<sub>2</sub>Cl<sub>2</sub>): δ = 1.31 (s, 18H, 1), 1.35 – 1.40 (m, 2H, 12), 1.40 – 1.46 (m, 2H, 11), 1.51 (tt, *J* = 7.0, 5.5 Hz, 2H, 13), 1.74 (m, 2H, 10), 2.53 (t, *J* = 2.4 Hz, 1H, 16), 3.16 (t, *J* = 6.9 Hz, 2H, 9), 3.52 (t, *J* = 5.7 Hz, 2H, 14), 4.06 (d, *J* = 2.4 Hz, 2H, 15), 4.27 (s, 2H, 8), 4.35 (s, 2H, 4/5), 4.37 (s, 2H, 4/5), 7.18 (d, *J* = 1.8 Hz, 2H, 3), 7.49 (m, 4H, 6,7), 7.56 (sbr, 8H, BARF<sub>24</sub>), 7.64 (t, *J* = 1.8 Hz, 1H, 2), 7.72 (sbr, 16H, BARF<sub>24</sub>). **<sup>13</sup>C NMR** (151 MHz, CD<sub>2</sub>Cl<sub>2</sub>): δ = 24.6, 25.2, 25.6, 28.3, 31.4, 35.5, 48.8, 52.3, 52.4, 54.7, 58.2, 71.3, 75.7, 79.8, 118.1, 122.5, 124.0, 125.0, 126.1, 126.4, 127.7, 127.9, 129.4, 131.7, 131.8, 132.0, 132.0, 135.4, 154.2, 162.3 ppm. **HRMS (MeOH)**: *m/z* calcd. for [C<sub>32</sub>H<sub>50</sub>N<sub>2</sub>O]<sup>2+</sup>: 477.3845 [M-H]<sup>+</sup>, found: 477. 3849.

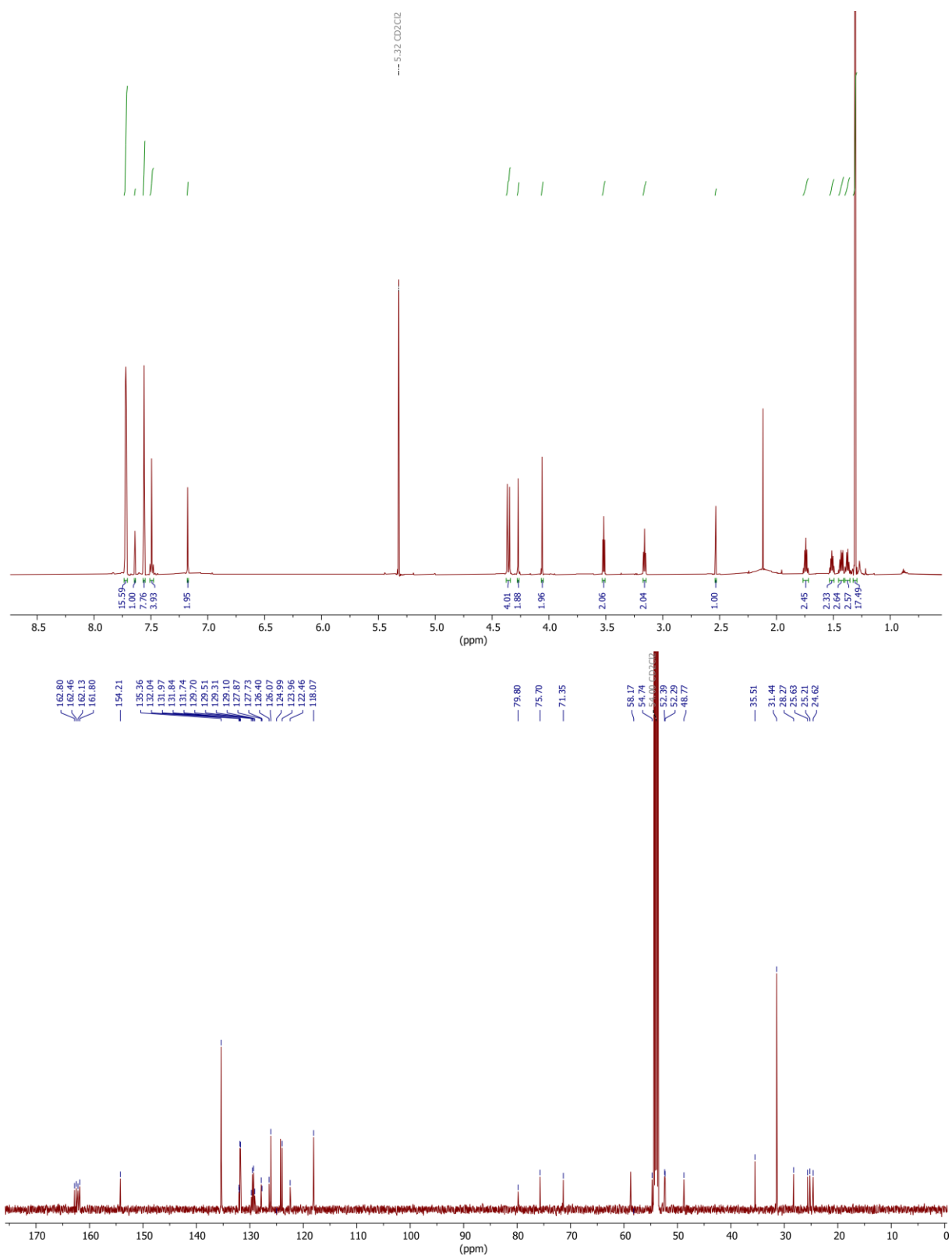
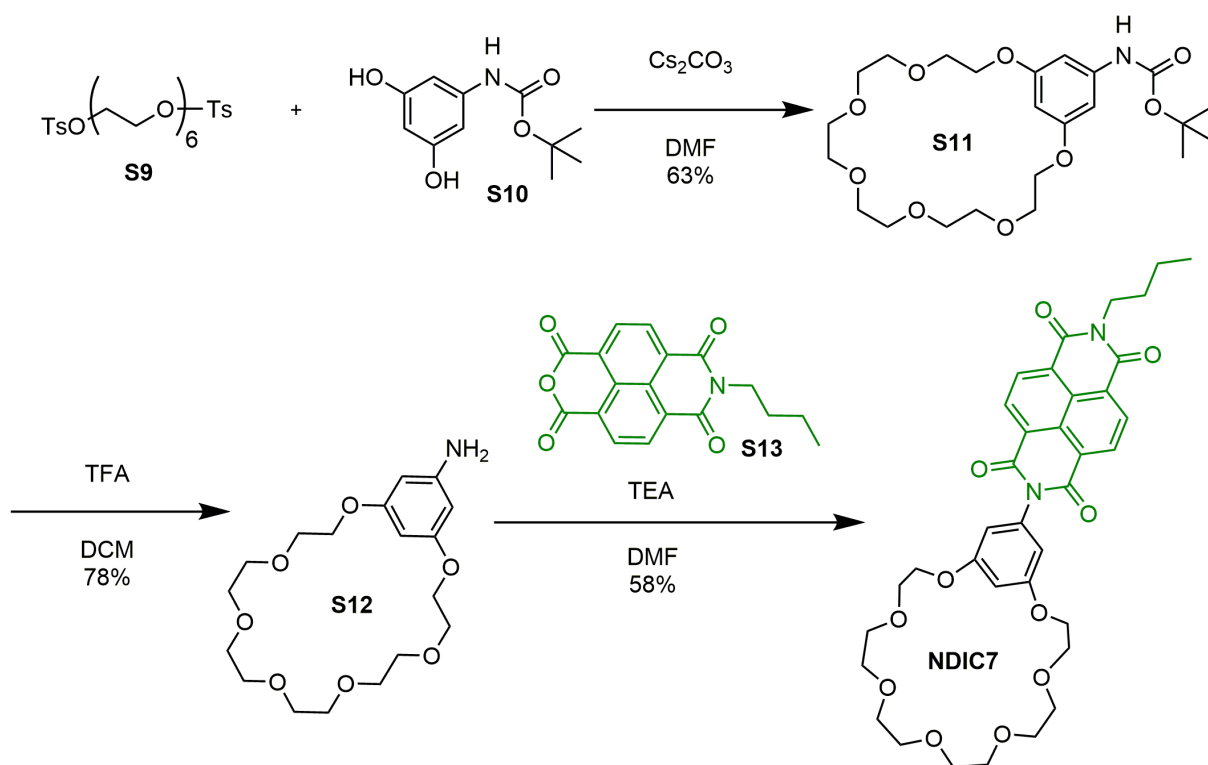


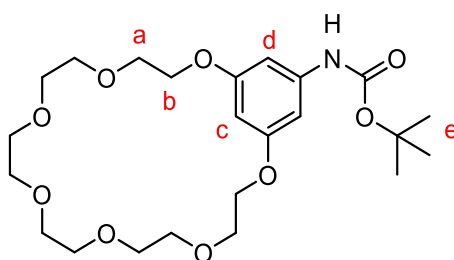
**Fig. S4** <sup>1</sup>H (top) and <sup>13</sup>C (bottom) NMR spectra (700/151 MHz, CD<sub>2</sub>Cl<sub>2</sub>, 298 K) of axle **Ax**.

### 1.3. Synthesis of macrocycle NDIC7



**Scheme S2** General procedure for macrocycle **NDIC7**.

#### **tert-butyl 2,5,8,11,14,17,20-heptaoxa-1(1,3)-benzenacycloicosaphane-15-ylcarbamate S11**



Ditosylate **S9** (525 mg, 0.89 mmol, 1.00 equiv.) was dissolved in dry DMF (100 mL) under argon atmosphere. In a separate vessel, K<sub>2</sub>CO<sub>3</sub> (492 mg, 3.56 mmol, 4.00 equiv.) and diol **S10** (201 mg, 0.89 mmol, 1.00 equiv.) were dissolved in dry DMF (200 mL) and stirred at 60 °C under argon atmosphere. The ditosylate solution was added portion-wise over 2 h, afterwards the solution was stirred for 5 days at 80 °C. The solution was cooled to r.t. and filtered. The solvent was removed under reduced pressure. The residue was dissolved in CH<sub>2</sub>Cl<sub>2</sub> (100 mL) and washed with water and brine and dried over MgSO<sub>4</sub>. The solvent was removed under reduced pressure and the residue was purified by column chromatography (SiO<sub>2</sub>, CH<sub>2</sub>Cl<sub>2</sub>/EtOAc 30% → 100% EtOAc, R<sub>f</sub> ~ 0.2 in CH<sub>2</sub>Cl<sub>2</sub>/EtOAc = 1:1) yielding **S11** as a yellowish oil (256 mg, 0.56 mmol, 63%).

**<sup>1</sup>H NMR** (500 MHz, CDCl<sub>3</sub>): δ = 1.49 (s, 9H, e), 3.61 – 3.65 (m, 12H, CH<sub>2</sub>-O), 3.68 (m, 4H, CH<sub>2</sub>-O), 3.76 – 3.81 (m, 4H, a), 4.12 – 4.16 (m, 4H, b), 6.35 (t, *J* = 2.2 Hz, 1H, c), 6.48 (s, 1H, NH), 6.59 (d, *J* = 2.2 Hz, 2H, d) ppm. **<sup>13</sup>C NMR** (176 MHz, CDCl<sub>3</sub>): δ = 28.4, 67.9, 69.7, 70.7, 70.7, 71.1, 71.3, 80.6, 97.9, 98.1, 140.2, 152.6, 160.4 ppm. **HRMS (MeOH)**: *m/z* calcd. for [C<sub>23</sub>H<sub>37</sub>NO<sub>9</sub>]<sup>+</sup>: 494.2366 [M+Na]<sup>+</sup>, found: 494.2389; 510.2105 [M+K]<sup>+</sup>, found: 510.2131.

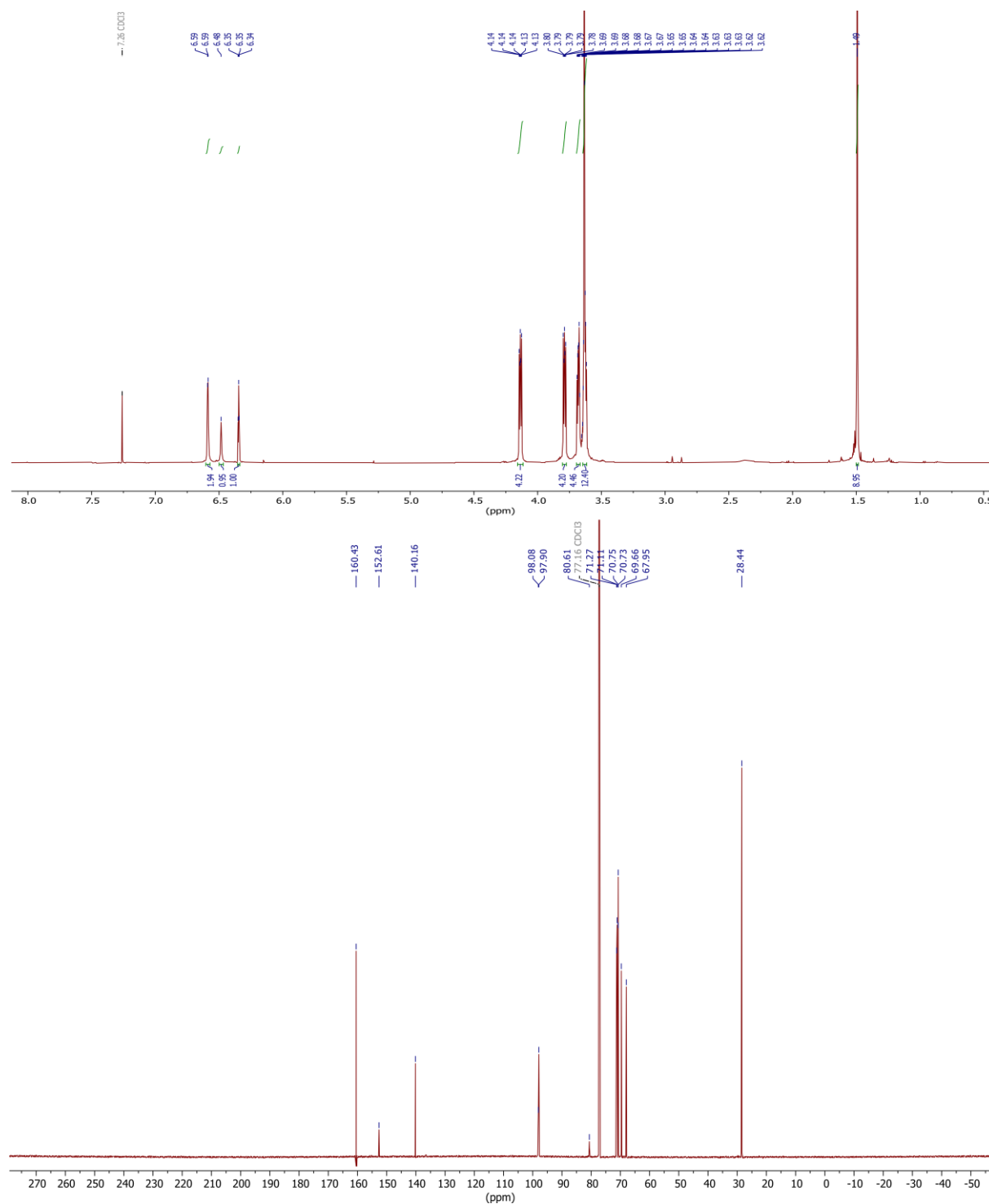


**Fig. S5** <sup>1</sup>H (top) and <sup>13</sup>C (bottom) NMR spectra (500/176 MHz, CDCl<sub>3</sub>, 298 K) of crown ether S11.



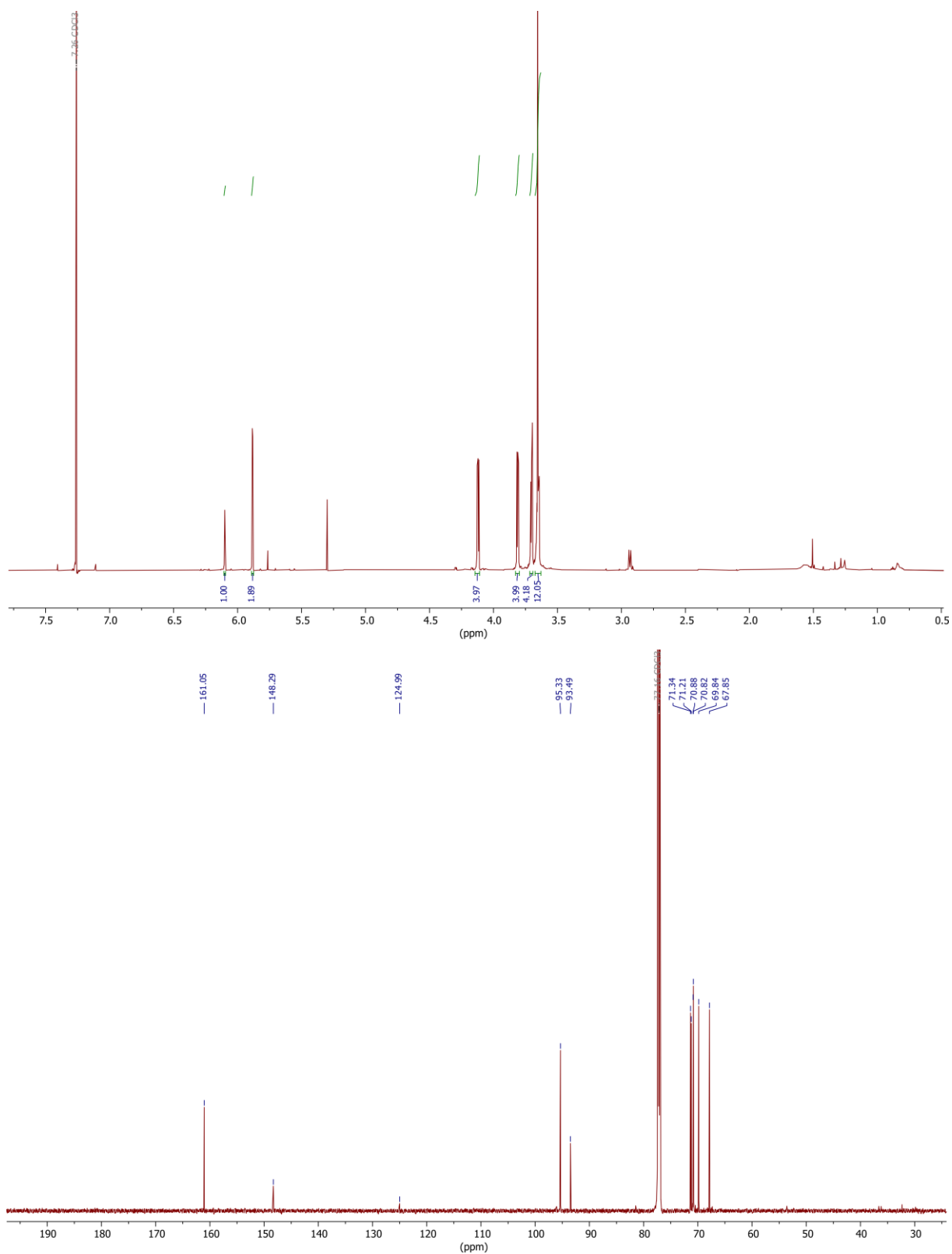
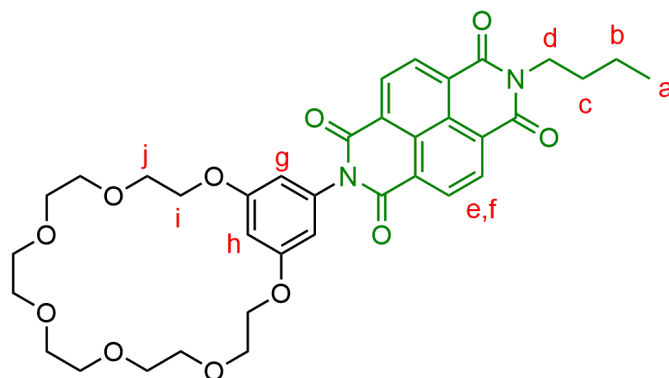


**Fig. S6**  $^1\text{H}$  (top) and  $^{13}\text{C}$  (bottom) NMR spectra (700/176 MHz,  $\text{CDCl}_3$ , 298 K) of crown ether **S12**.

**2-(2,5,8,11,14,17,20-heptaoxa-1(1,3)-benzenacycloicosaphane-15-yl)-7-butylbenzo[*lmn*][3,8]phenanthroline-1,3,6,8(2H,7H)-tetraone NDIC7**



NDI **S13** (146 mg, 0.48 mmol, 1.10 equiv.) was dissolved in dry DMF (18 mL) and stirred for 20 min at 70°C under argon. Triethylamine (0.18 mL, 1.31 mmol, 3.00 equiv.) and crown ether **S12** (162 mL, 0.44 mmol, 1.00 equiv.) were added and the mixture was refluxed overnight. The solvent was removed under reduced pressure and the residue was taken up in CH<sub>2</sub>Cl<sub>2</sub> (50 mL). The solution was washed with water and brine and dried over MgSO<sub>4</sub>. The solvent was removed under reduced pressure and the residue was purified by column chromatography (SiO<sub>2</sub>, CH<sub>2</sub>Cl<sub>2</sub> → CH<sub>2</sub>Cl<sub>2</sub>/ACN 2.6:1, R<sub>f</sub> ~ 0.3 in CH<sub>2</sub>Cl<sub>2</sub>) yielding **NDIC7** as a greenish brown solid (170 mg, 0.25 mmol, 58%).

**<sup>1</sup>H NMR** (700 MHz, CDCl<sub>3</sub>): δ = 1.01 (t, *J* = 7.4 Hz, 3H, a), 1.44 – 1.51 (m, 2H, b), 1.72 – 1.78 (m, 2H, c), 3.66 – 3.74 (m, 16H, CH<sub>2</sub>-O), 3.83 – 3.86 (m, 4H, j), 4.19 – 4.21 (m, 4H, i), 4.21 – 4.24 (m, 2H, d), 6.47 (d, *J* = 2.2 Hz, 2H, g), 6.86 (t, *J* = 2.2 Hz, 1H, h), 8.80 (s, 4H, e,f) ppm.

**<sup>13</sup>C NMR** (176 MHz, CDCl<sub>3</sub>): δ = 14.0, 20.5, 30.3, 41.0, 68.3, 69.8, 70.8, 70.9, 71.3, 71.4, 103.6, 108.3, 126.9, 127.1, 131.2, 131.5, 136.1, 160.9, 162.9, 163.0 ppm. **HRMS (MeOH)**: *m/z* calcd. for [C<sub>36</sub>H<sub>40</sub>N<sub>2</sub>O<sub>11</sub>]<sup>+</sup>: 699.2529 [M+Na]<sup>+</sup>, found: 699.2507; 715.2269 [M+K]<sup>+</sup>, found: 715.2252.

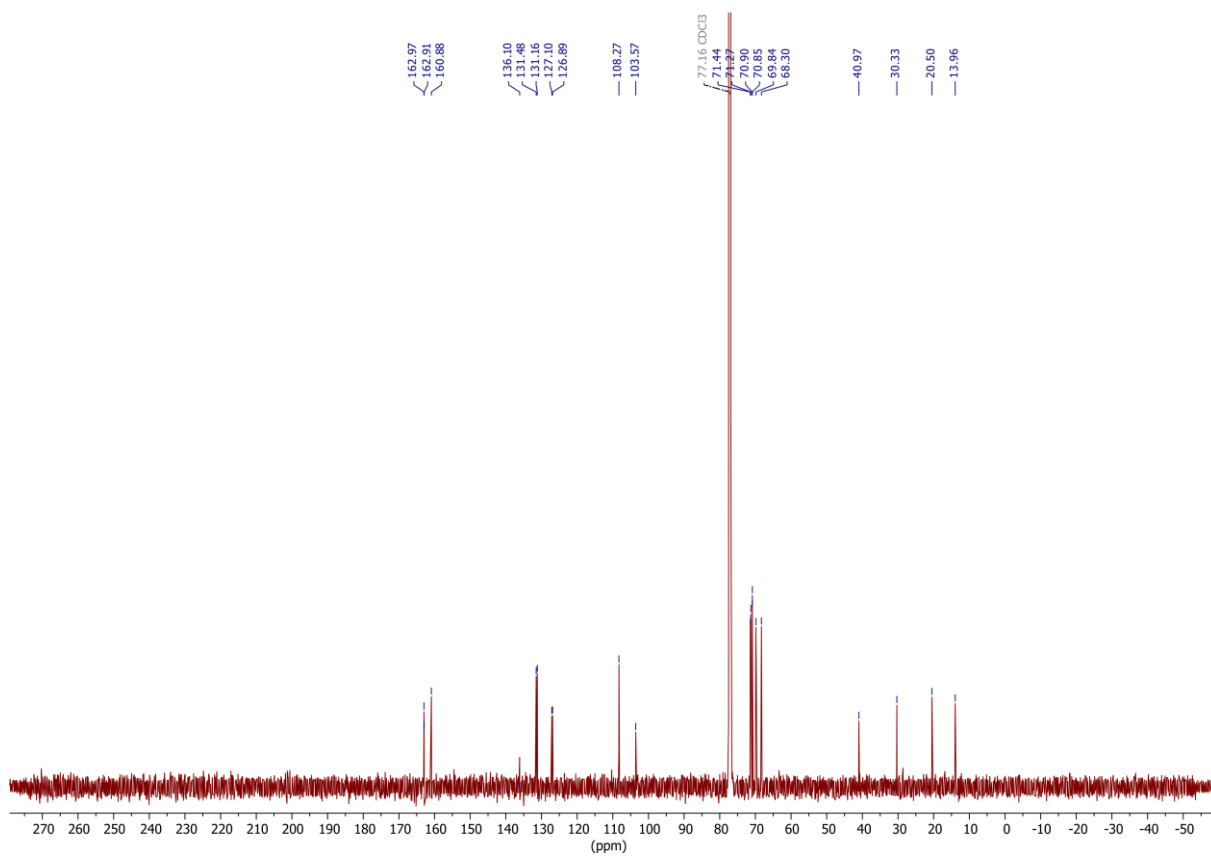
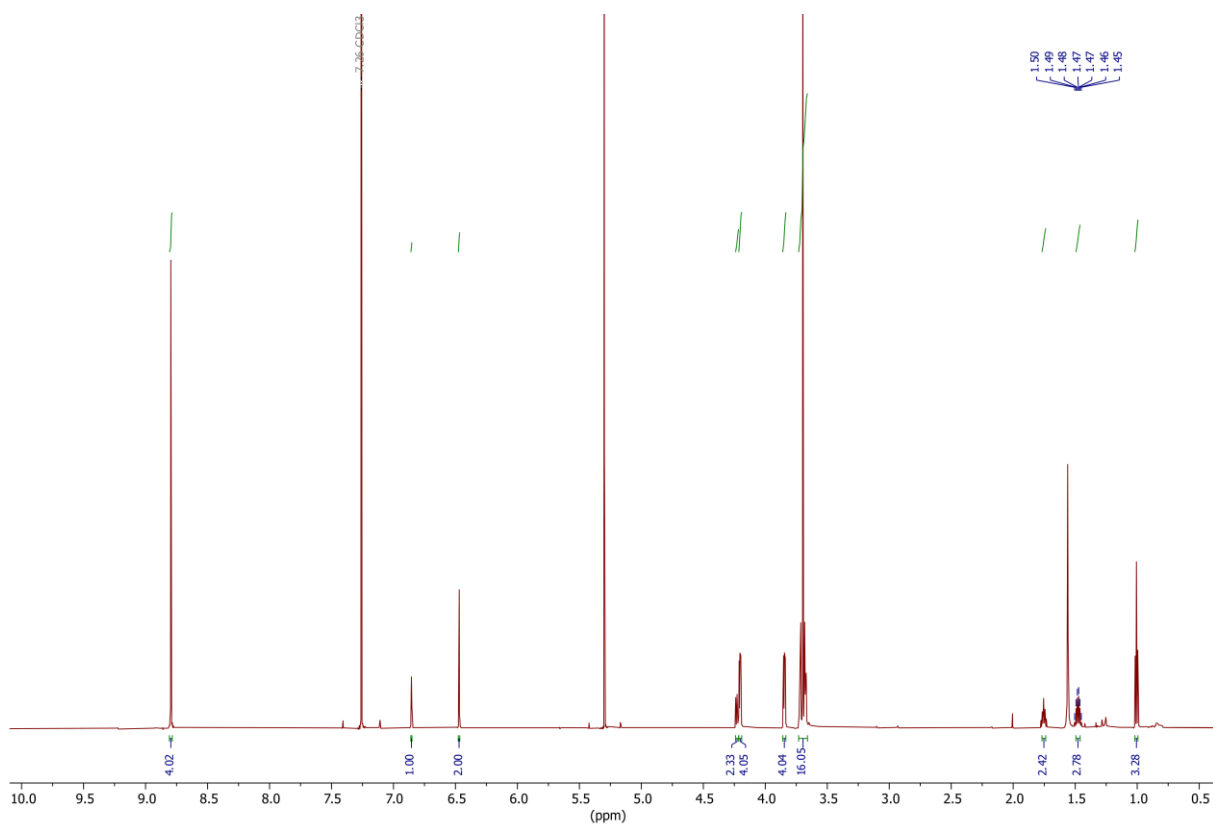
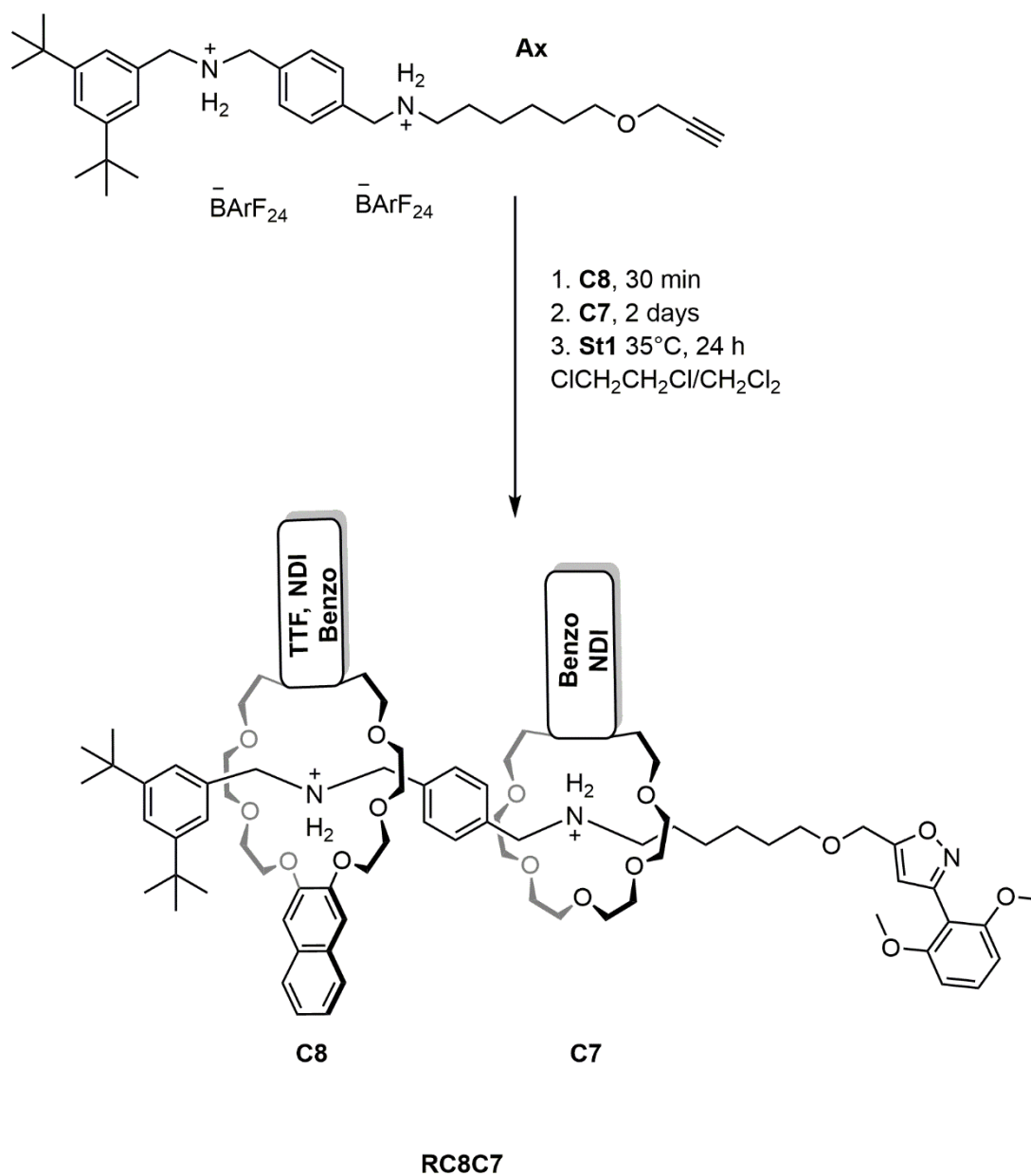


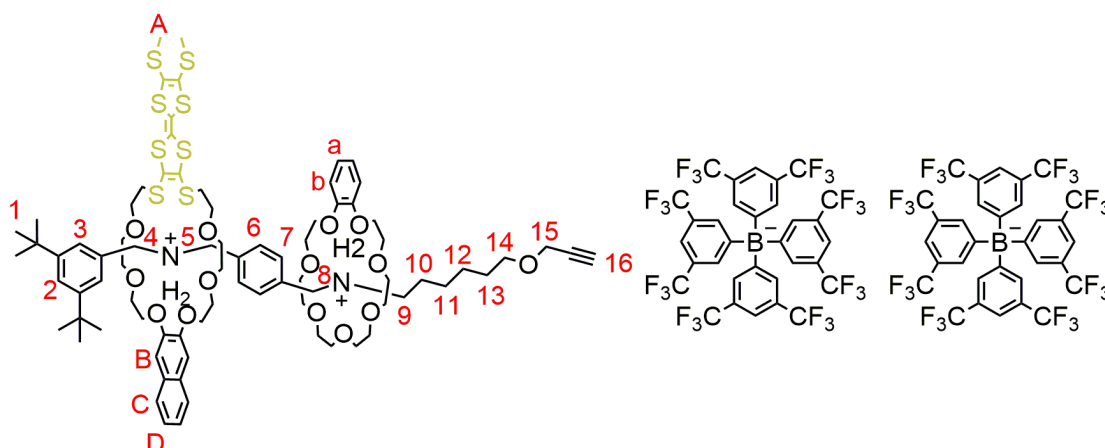
**Fig. S7** <sup>1</sup>H (top) and <sup>13</sup>C (bottom) NMR spectra (700/176 MHz, CDCl<sub>3</sub>, 298 K) of wheel NDIC7.

#### 1.4. Synthesis of (pseudo)[3]rotaxanes



**Scheme S3** General synthesis procedure for hetero[3]rotaxanes **RC8C7**.

### Pseudo[3]rotaxane PRTTFC8BC7



### PRTTFC8BC7

The axle **Ax** (50 mg, 23  $\mu\text{mol}$ , 1.00 equiv.) and macrocycle **TTFC8** (15 mg, 20  $\mu\text{mol}$ , 0.90 equiv.) were dissolved in  $\text{ClCH}_2\text{CH}_2\text{Cl}$  (2 mL) and stirred for 30 min, then macrocycle **BC7** (49 mg, 136  $\mu\text{mol}$ , 6.00 equiv.) was added. After 2 days, the mixture was purified by column chromatography ( $\text{SiO}_2$ ,  $\text{CH}_2\text{Cl}_2$ ,  $R_f \sim 0.9$  in  $\text{CH}_2\text{Cl}_2$ ) to obtain the desired product **PRTTFC8BC7** (16 mg, 5  $\mu\text{mol}$ , 24%) as an orange oil.

**$^1\text{H NMR}$**  (700 MHz,  $\text{CD}_2\text{Cl}_2$ )  $\delta$  = 1.23 – 1.25 (s, 18H, 1), 1.25 – 1.32 (m, 4H, 11,12), 1.32 – 1.38 (m, 2H, 10), 1.41 – 1.47 (m, 2H, 13), 2.40 (s, 6H, A), 2.41 – 2.43 (t,  $J$  = 2.4 Hz, 1H, 16), 3.11 – 3.24 (m, 8H, O- $\text{CH}_2$ - $\text{CH}_2$ ), 3.29 – 3.52 (m, 20H, O- $\text{CH}_2$ - $\text{CH}_2$ , 9,14), 3.53 – 3.63 (m, 8H, O- $\text{CH}_2$ - $\text{CH}_2$ ), 3.66 – 3.75 (m, 4H, O- $\text{CH}_2$ - $\text{CH}_2$ ), 3.77 – 3.87 (m, 4H, O- $\text{CH}_2$ - $\text{CH}_2$ ), 3.92 – 3.97 (m, 2H, 8), 4.00 – 4.05 (m, 4H, O- $\text{CH}_2$ - $\text{CH}_2$ ), 4.06 (d,  $J$  = 2.4 Hz, 2H, 15), 4.08 – 4.11 (m, 2H, O- $\text{CH}_2$ - $\text{CH}_2$ ), 4.11 – 4.17 (m, 2H, O- $\text{CH}_2$ - $\text{CH}_2$ ), 4.70 – 4.78 (m, 4H, 4,5), 6.81 – 6.85 (m, 2H, b), 6.88 – 6.92 (m, 4H, B, 6/7), 6.94 – 6.98 (m, 2H, a), 7.17 – 7.23 (m, 4H, 6/7,  $\text{NH}_2$ ), 7.31 – 7.37 (m, 2H, D), 7.42 (d,  $J$  = 1.8 Hz, 2H, 3), 7.50 (t,  $J$  = 1.8 Hz, 1H, 2), 7.56 ( $s_{\text{br}}$ , 8H,  $\text{BArF}_{24}$ ), 7.58 – 7.61 (m, 2H, C), 7.70 – 7.77 ( $s_{\text{br}}$ , 16H,  $\text{BArF}_{24}$ ), 7.82 – 7.90 (s, 2H,  $\text{NH}_2$ ) ppm.  **$^{13}\text{C NMR}$**  (176 MHz,  $\text{CD}_2\text{Cl}_2$ )  $\delta$  = 19.4, 26.0, 26.9, 27.0, 29.5, 29.6, 31.4, 35.3, 37.2, 47.6, 50.3, 53.1, 58.3, 68.4, 68.9, 70.0, 70.1, 70.1, 70.8, 71.0, 71.2, 71.3, 71.7, 71.8, 74.1, 80.5, 108.2, 108.3, 112.2, 114.5, 117.9, 122.0, 122.7, 123.7, 124.2, 124.8, 125.8, 126.7, 127.3, 128.0, 128.6, 129.3, 130.2, 130.6, 132.7, 134.5, 135.2, 146.9, 147.0, 152.8, 162.2 ppm. **HRMS ( $\text{CH}_2\text{Cl}_2$ ):** m/z calcd. for  $[\text{C}_{80}\text{H}_{114}\text{N}_2\text{O}_{14}\text{S}_8]^{++}$ : 791.3012  $[\text{M}]^{++}$ , found: 791.3034.

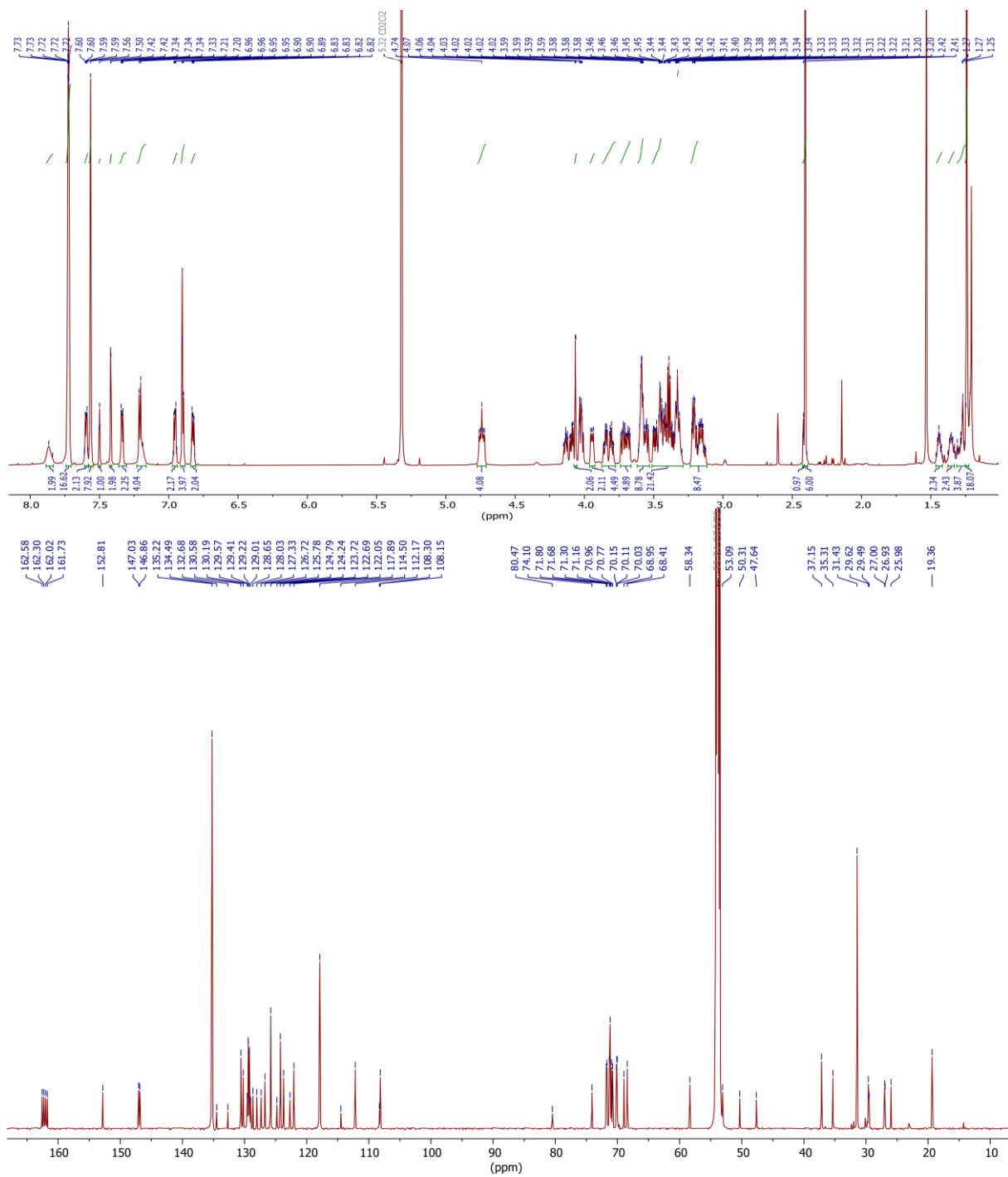


**Fig. S8**  $^1\text{H}$  (top) and  $^{13}\text{C}$  (bottom) NMR spectra (700/176 MHz,  $\text{CD}_2\text{Cl}_2$ , 298 K) of pseudo[3]rotaxane **PRTTFC8BC7**.

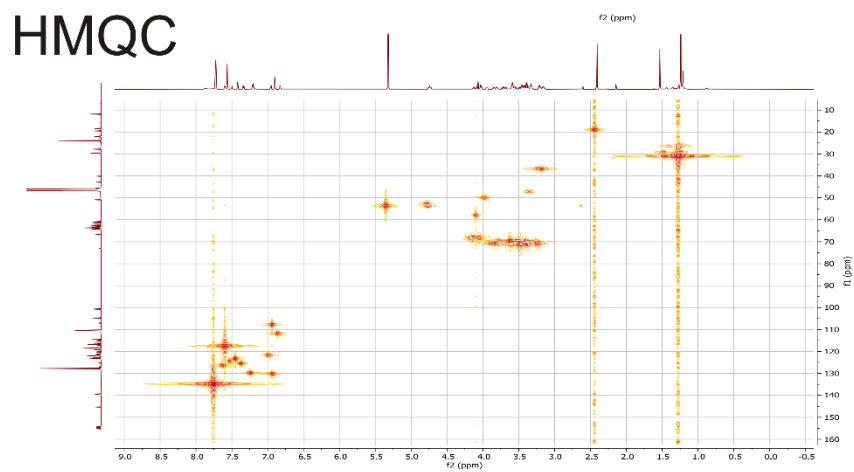
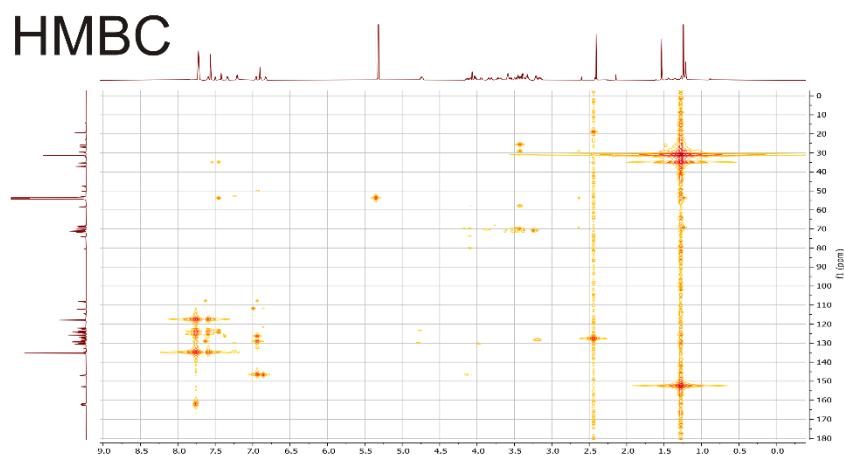
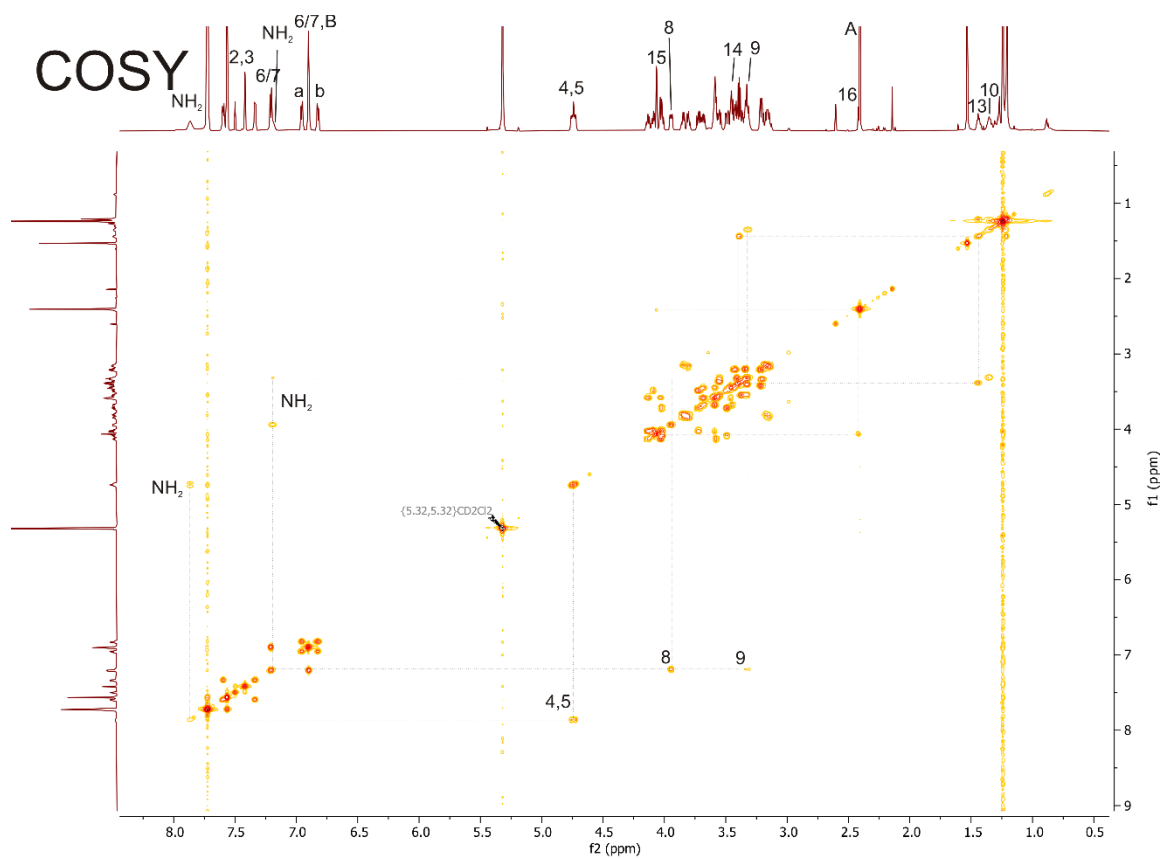
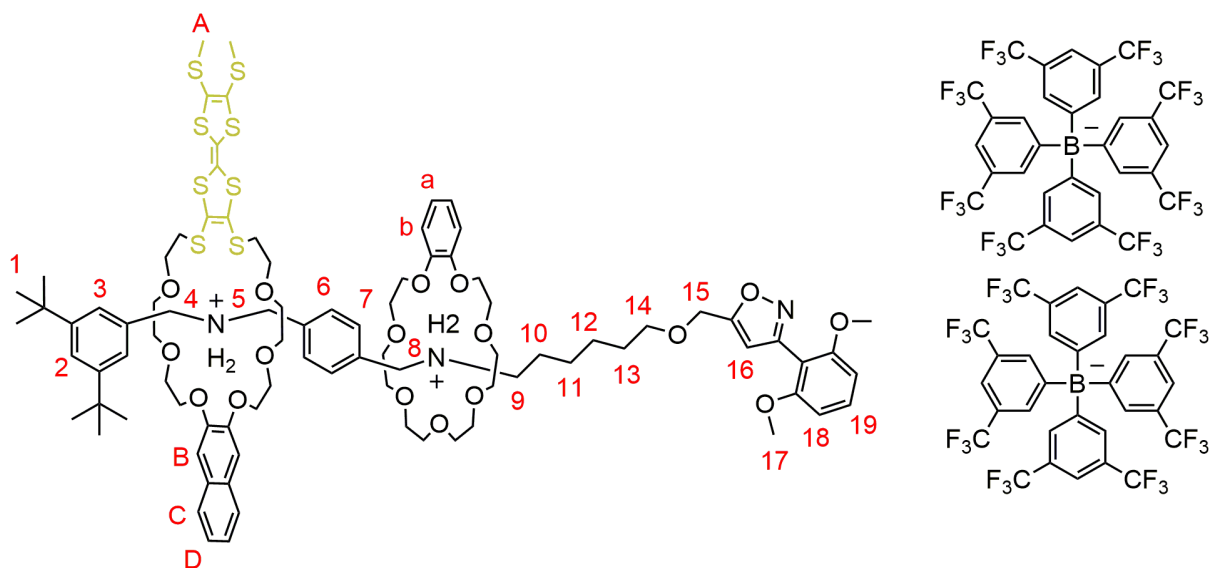


**Fig. S9** COSY (top), HMBC (center) and HMQC (bottom) NMR spectra (700/176 MHz, CD<sub>2</sub>Cl<sub>2</sub>, 298 K) of pseudo[3]rotaxane **PRTTFC8BC7**.

## RTTFC8BC7

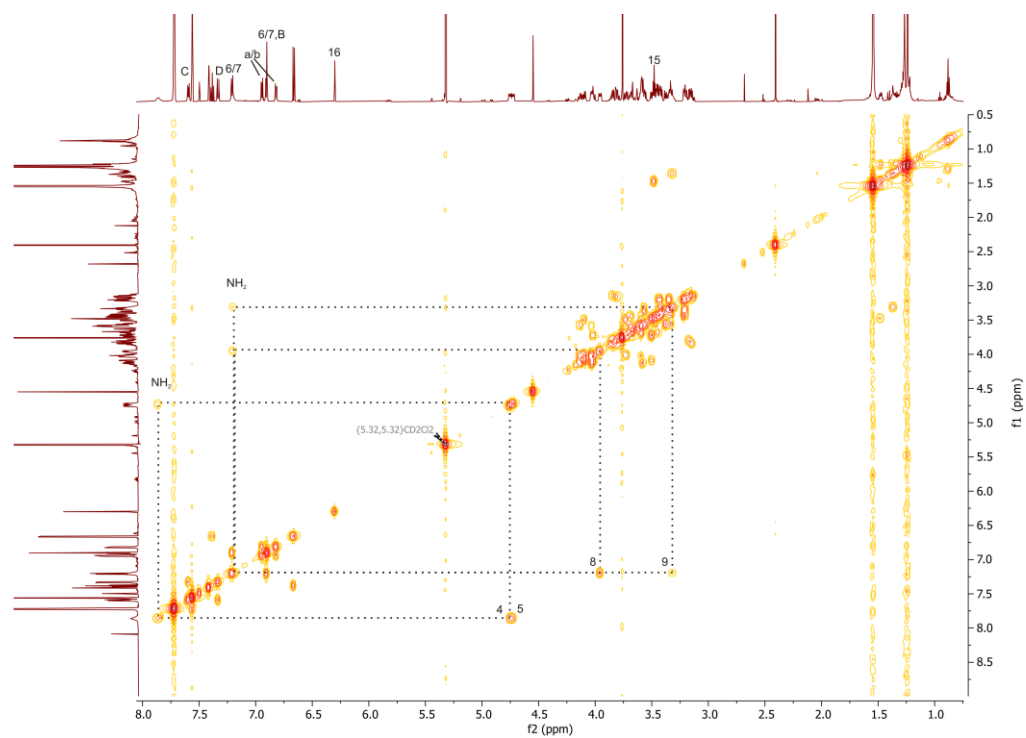


Axle **Ax** (60.0 mg, 27  $\mu\text{mol}$ , 1.00 equiv.) and **TTFC8** (18 mg, 24  $\mu\text{mol}$ , 0.90 equiv.) were dissolved in 1,2-dichloroethane (3 mL) and stirred for 30 min, then **BC7** (58 mg, 163  $\mu\text{mol}$ , 6.00 equiv.) were added and stirred at 35° C. After 2 days, N-oxide **St1** (7 mg, 41  $\mu\text{mol}$ , 1.50 equiv.) was added to the mixture and stirred for an additional 18 h at 35° C. The crude product was purified by preparative thin-layer chromatography ( $\text{SiO}_2$ ,  $\text{CH}_2\text{Cl}_2$ ,  $R_f \sim 0.3$  in  $\text{CH}_2\text{Cl}_2$ ). The product was obtained as an orange oil (12 mg, 3.6  $\mu\text{mol}$ , 15%).

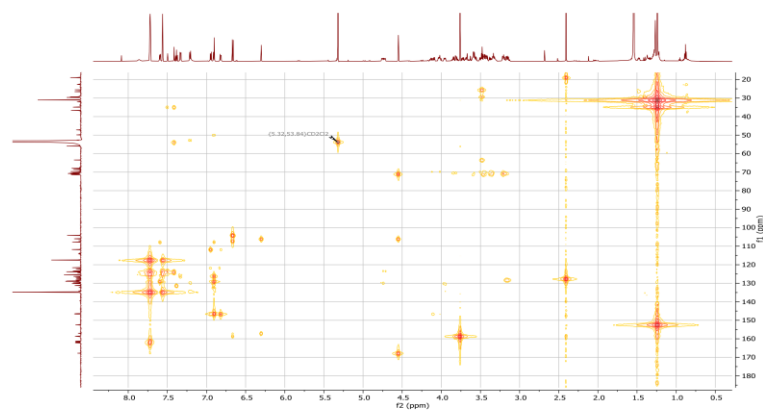
**$^1\text{H NMR}$**  (700 MHz,  $\text{CD}_2\text{Cl}_2$ )  $\delta$  = 1.23 – 1.25 (s, 18H, 1), 1.34 – 1.39 (m, 6H, 10,11,12), 1.45 – 1.50 (m, 4H, 13), 2.40 – 2.41 (s, 6H, A), 3.11 – 3.23 (m, 8H, O- $\text{CH}_2$ - $\text{CH}_2$ ), 3.28 – 3.39 (m, 10H, 9, O- $\text{CH}_2$ - $\text{CH}_2$ ), 3.40 – 3.52 (m, 14H, 14, O- $\text{CH}_2$ - $\text{CH}_2$ ), 3.54 – 3.64 (m, 10H, O- $\text{CH}_2$ - $\text{CH}_2$ ), 3.66 – 3.71 (m, 4H, O- $\text{CH}_2$ - $\text{CH}_2$ ), 3.71 – 3.75 (m, 3H, O- $\text{CH}_2$ - $\text{CH}_2$ ), 3.75 – 3.76 (s, 6H, 17), 3.76 – 3.83 (m, 3H, O- $\text{CH}_2$ - $\text{CH}_2$ ), 3.83 – 3.88 (m, 3H, O- $\text{CH}_2$ - $\text{CH}_2$ ), 3.93 – 3.98 (m, 2H, 8), 3.99 – 4.05 (m, 4H, O- $\text{CH}_2$ - $\text{CH}_2$ ), 4.08 – 4.16 (m, 4H, O- $\text{CH}_2$ - $\text{CH}_2$ ), 4.55 (s, 2H, 15), 4.70 – 4.77 (m, 4H, 4,5), 6.29 – 6.31 (s, 1H, 16), 6.65 – 6.68 (d,  $J$  = 8.5 Hz, 2H, 18), 6.80 – 6.84 (m, 2H, a/b), 6.89 – 6.92 (m, 4H, 7,B), 6.93 – 6.97 (m, 2H, a/b), 7.17 – 7.24 (m, 4H, 6,  $\text{NH}_2$ ), 7.32 – 7.34 (m, 2H, D), 7.36 – 7.41 (t,  $J$  = 8.5 Hz, 1H, 19), 7.41 – 7.42 (d,  $J$  = 1.8 Hz, 2H, 3), 7.49 – 7.50 (t,  $J$  = 1.8 Hz, 1H, 2), 7.55 – 7.57 (s<sub>br</sub>, 8H,  $\text{BArF}_{24}$ ), 7.58 – 7.61 (m, 2H, C), 7.71 – 7.73 (s<sub>br</sub>, 16H,  $\text{BArF}_{24}$ ), 7.81 – 7.90 (s<sub>br</sub>, 2H,  $\text{NH}_2$ ) ppm.  **$^{13}\text{C NMR}$**  (176 MHz,  $\text{CD}_2\text{Cl}_2$ )  $\delta$  = 14.3, 19.4, 23.1, 25.9, 26.9, 27.0, 29.8, 30.1, 31.4, 32.3, 35.3, 37.1, 47.6, 50.3, 53.1, 56.3, 63.9, 68.4, 68.9, 70.0, 70.1, 70.8, 71.0, 71.1, 71.2, 71.3, 71.4, 71.6, 71.8, 104.5, 106.4, 107.4, 108.2, 112.2, 114.2, 114.5, 117.9, 122.0, 122.7, 123.7, 124.2, 124.8, 125.8, 126.7, 127.3, 128.0, 128.6, 129.3, 130.2, 130.6, 131.7, 132.7, 134.5, 135.2, 146.8, 147.0, 152.8, 157.4, 159.0, 162.1, 168.2 ppm. **HRMS (acetonitrile):**  $m/z$  calcd. for  $[\text{C}_{89}\text{H}_{123}\text{N}_3\text{O}_{17}\text{S}_8]^{++}$ : 881.3319  $[\text{M}]^{++}$ , found: 881.3325.



COSY



HMBC



HMQC

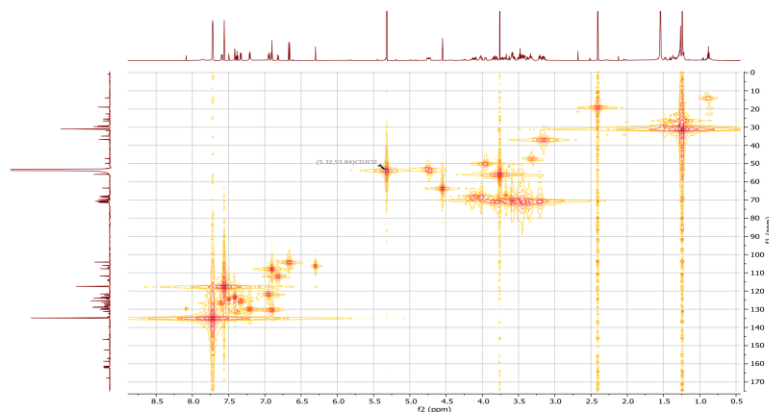
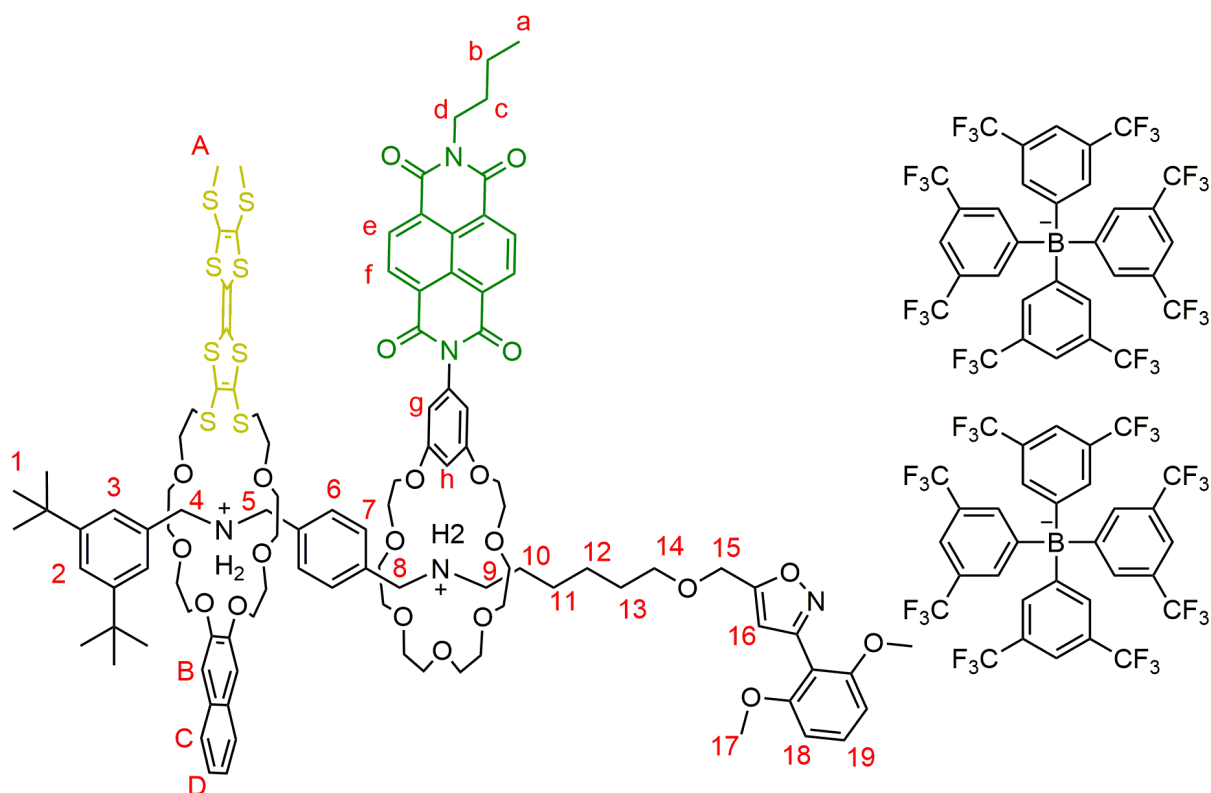


**Fig. S11** COSY (top), HMBC (center) and HMQC (bottom) NMR spectra (700/176 MHz,  $\text{CD}_2\text{Cl}_2$ , 298 K) of [3]rotaxane **RTTFC8BC7**.

### [3]rotaxane RTTFC8NDIC7



### RTTFC8NDIC7

The axle **Ax** (60 mg, 27  $\mu\text{mol}$ , 1.00 equiv.) and **TTFC8** (18 mg, 24  $\mu\text{mol}$ , 0.90 equiv.) were dissolved in  $\text{CH}_2\text{Cl}_2$  (3 mL) and stirred for 30 min. **NDIC7** (110 mg, 163  $\mu\text{mol}$ , 6.00 equiv.) was added and stirred for another 2 days. Finally, N-oxide **St1** (7 mg, 41  $\mu\text{mol}$ , 1.50 equiv.) was added to the mixture and stirred for an additional 24 h at 35° C. The crude product was purified via preparative thin-layer chromatography ( $\text{SiO}_2$ ,  $\text{CH}_2\text{Cl}_2/\text{EtOH}$  50:1,  $R_f \sim 0.25$  in  $\text{CH}_2\text{Cl}_2/\text{EtOH}$  100:1) The product was obtained as a greenish brown oil (27 mg, 7  $\mu\text{mol}$ , 29%).

**$^1\text{H NMR}$**  (700 MHz,  $\text{CD}_2\text{Cl}_2$ )  $\delta$  = 1.00 (t,  $J$  = 7.4 Hz, 3H, a), 1.27 (s, 18H, 1), 1.34 – 1.38 (m, 4H, 11,12), 1.42 – 1.45 (m, 2H, 10), 1.45 – 1.49 (m, 2H, b), 1.58 – 1.62 (m, 2H, 13), 1.74 – 1.76 (m, 2H, c), 2.40 (s, 6H, A), 2.96 – 3.03 (m, 4H, O- $\text{CH}_2\text{-CH}_2$ ), 3.07 – 3.19 (m, 10H, O- $\text{CH}_2\text{-CH}_2$ , 9), 3.26 – 3.30 (m, 2H, O- $\text{CH}_2\text{-CH}_2$ ), 3.32 – 3.35 (m, 2H, O- $\text{CH}_2\text{-CH}_2$ ), 3.38 – 3.42 (m, 2H, O- $\text{CH}_2\text{-CH}_2$ ), 3.46 – 3.50 (m, 4H, O- $\text{CH}_2\text{-CH}_2$ ), 3.50 – 3.56 (m, 10H, O- $\text{CH}_2\text{-CH}_2$ , 14), 3.58 – 3.67 (m, 16H, O- $\text{CH}_2\text{-CH}_2$ ), 3.67 – 3.69 (m, 4H, O- $\text{CH}_2\text{-CH}_2$ ), 3.70 – 3.71 (s, 6H, 17), 3.73 – 3.77 (m, 6H, O- $\text{CH}_2\text{-CH}_2$ , 8), 3.79 – 3.90 (m, 8H, O- $\text{CH}_2\text{-CH}_2$ ), 4.04 – 4.08 (m, 2H, O- $\text{CH}_2\text{-CH}_2$ ), 4.16 – 4.22 (m, 6H, O- $\text{CH}_2\text{-CH}_2$ , d), 4.22 – 4.28 (m, 6H, O- $\text{CH}_2\text{-CH}_2$ ), 4.53 (s, 2H, 15), 4.71 – 4.74 (m, 2H, 4/5), 4.90 – 4.94 (m, 2H, 4/5), 6.23 (s, 1H, 16), 6.43 (t,  $J$  = 2.3 Hz, 1H, h), 6.56 (d,  $J$  = 8.4 Hz, 18H), 6.61 (d,  $J$  = 2.2 Hz, 2H, g), 6.94 – 6.97 (m, 4H, B, 6/7), 7.27 – 7.37 (m, 5H, D, 19,  $\text{NH}_2$ ), 7.36 – 7.38 (m, 2H, 6/7), 7.44 (d,  $J$  = 1.8 Hz, 2H, 3), 7.54 (t,  $J$  = 1.8 Hz, 1H, 2), 7.56 (s<sub>br</sub>, 8H,  $\text{BArF}_{24}$ ), 7.60 – 7.64 (m, 2H, C), 7.72 (s<sub>br</sub>, 16H,  $\text{BArF}_{24}$ ), 7.99 (s<sub>br</sub>, 2H,  $\text{NH}_2$ ),

8.69 – 8.77 (m, 4H, e,f) ppm.  $^{13}\text{C}$  NMR (176 MHz,  $\text{CD}_2\text{Cl}_2$ )  $\delta$  = 8.9, 14.0, 14.3, 19.3, 20.8, 23.1, 25.2, 26.1, 26.2, 26.7, 26.8, 26.9, 27.6, 29.5, 29.8, 29.9, 29.9, 30.1, 30.5, 31.4, 31.6, 32.0, 32.3, 33.5, 34.5, 35.4, 37.2, 41.1, 47.1, 48.4, 51.1, 56.2, 63.8, 67.8, 68.0, 68.9, 70.0, 70.2, 70.6, 70.8, 70.9, 71.3, 71.4, 71.9, 103.7, 104.4, 106.5, 107.2, 108.0, 108.2, 108.6, 109.2, 114.7, 117.9, 122.7, 123.5, 124.2, 124.8, 125.8, 126.1, 126.5, 126.7, 126.9, 127.3, 127.4, 127.7, 128.0, 128.8, 129.0, 129.2, 129.4, 129.5, 129.7, 130.1, 130.3, 130.5, 130.6, 130.7, 131.1, 131.4, 131.5, 133.1, 133.5, 135.2, 138.5, 146.6, 152.9, 157.2, 158.9, 159.7, 159.9, 161.7, 162.0, 162.3, 162.6, 163.1, 163.3, 168.0 ppm. **HRMS (acetonitrile):**m/z calcd. for  $[\text{C}_{107}\text{H}_{135}\text{N}_5\text{O}_{21}\text{S}_8]^{++}$ : 1041.3719  $[\text{M}]^{++}$ , found: 1041.3729.

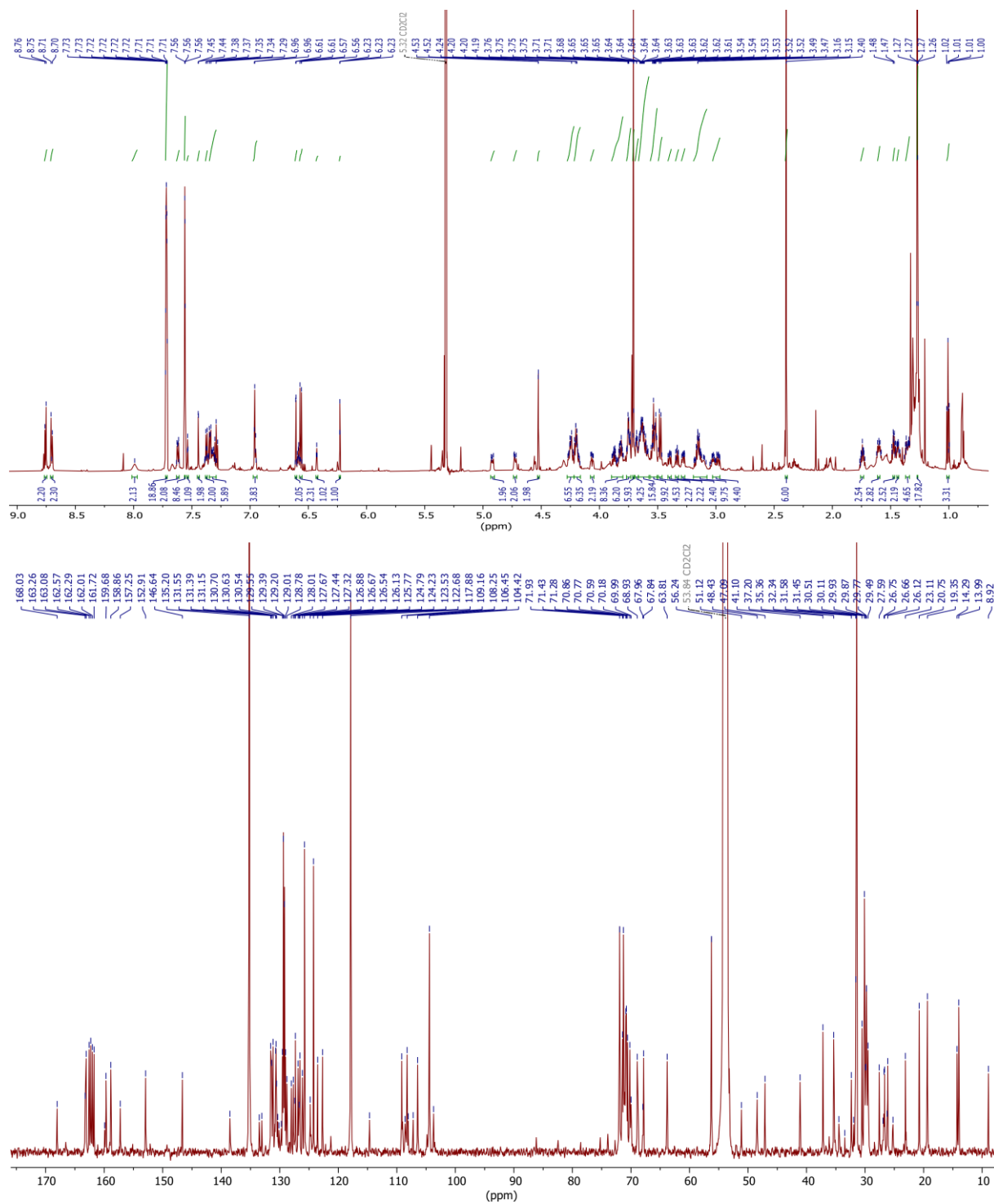


**Fig. S12** <sup>1</sup>H (top) and <sup>13</sup>C (bottom) NMR spectra (700/176 MHz, CD<sub>2</sub>Cl<sub>2</sub>, 298 K) of [3]rotaxane RTTFC8NDIC7

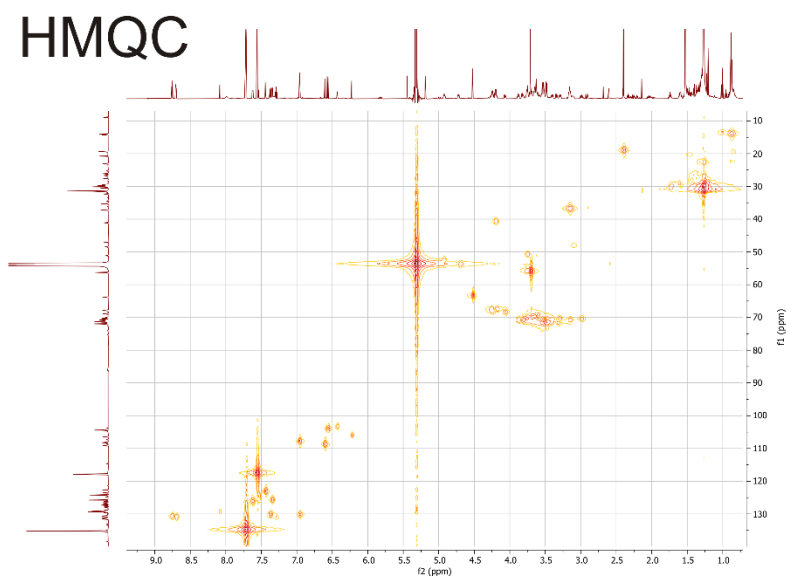
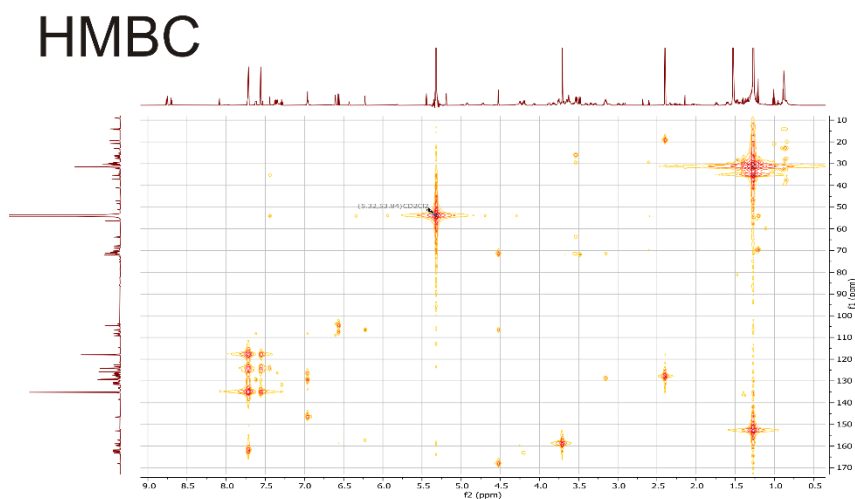
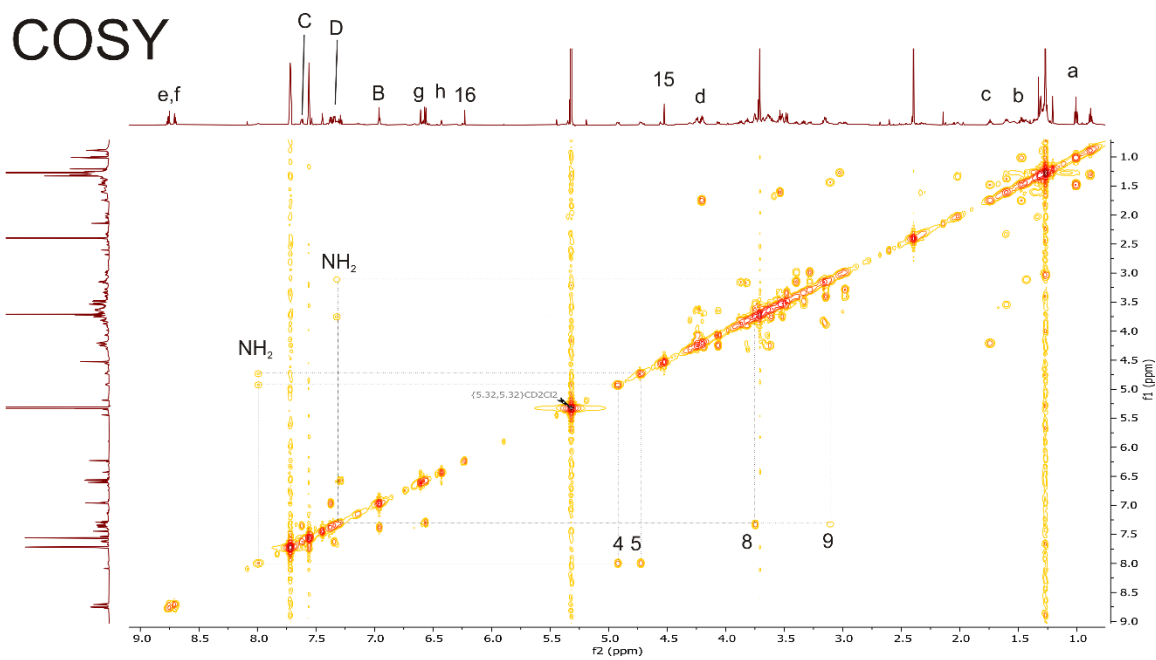


**Fig. S13** COSY (top), HMBC (center) and HMQC (bottom) NMR spectra (700/176 MHz, CD<sub>2</sub>Cl<sub>2</sub>, 298 K) of [3]rotaxane **RTTFC8NDIC7**

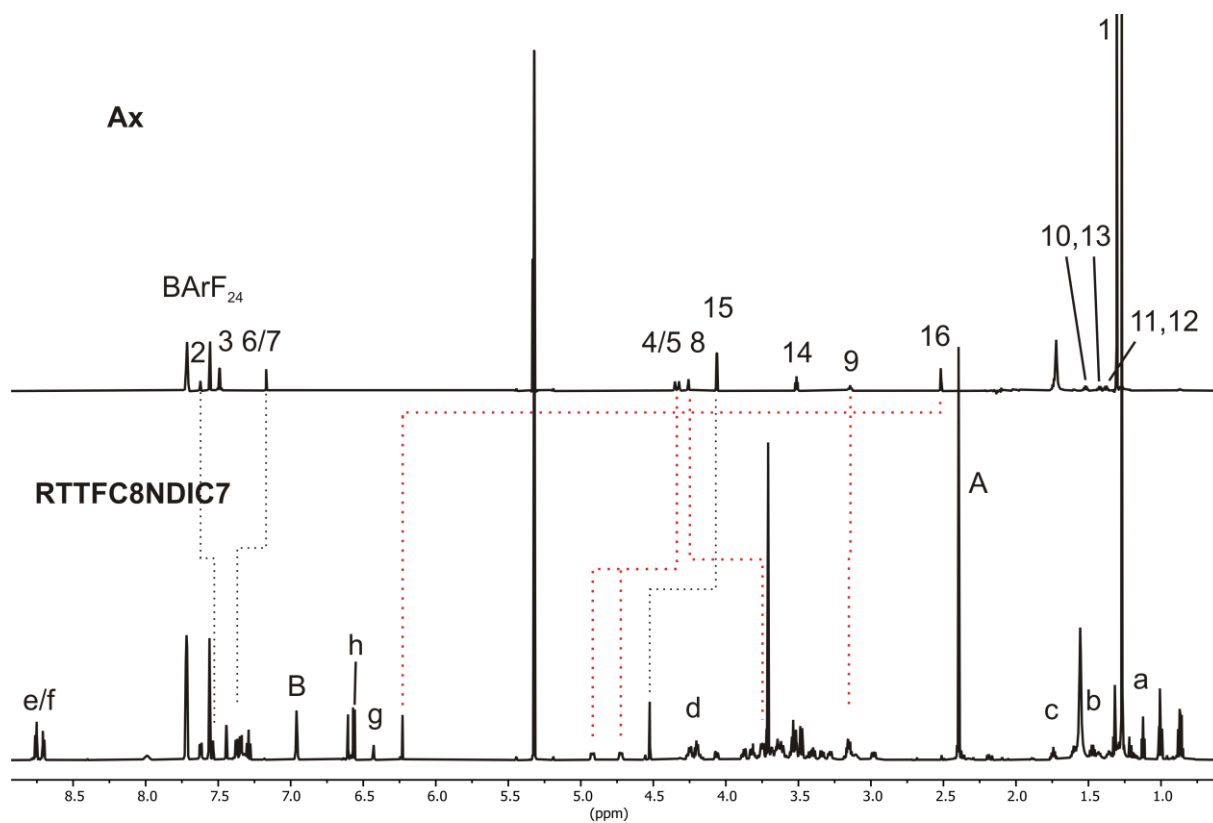


**Fig. S14** [3]rotaxane **RTTFC8NDIC7** (bottom) and axle **Ax** (top) NMR spectra (700 MHz,  $\text{CD}_2\text{Cl}_2$ , 298 K).



Hz, 1H, 2), 7.55 (s<sub>br</sub>, 8H, BArF<sub>24</sub>), 7.58 - 7.62 (m, 2H, J), 7.71 (s<sub>br</sub>, 16H, BArF<sub>24</sub>), 8.00 (s<sub>br</sub>, 2H, NH<sub>2</sub>), 8.67 – 8.80 (m, 4H, E,F) ppm. **<sup>13</sup>C NMR** (176 MHz, CD<sub>2</sub>Cl<sub>2</sub>) δ = 1.2, 14.0, 14.3, 20.7, 25.9, 27.0, 27.1, 29.7, 30.1, 30.5, 31.3, 31.4, 32.3, 35.3, 41.2, 47.7, 50.3, 52.4, 57.2, 63.8, 68.4, 68.4, 68.8, 69.5, 70.0, 70.9, 71.1, 71.2, 71.6, 71.7, 71.8, 77.6, 77.7, 77.9, 104.4, 106.2, 106.7, 107.0, 108.1, 108.9, 112.1, 117.9, 122.0, 122.7, 123.9, 124.2, 124.9, 125.8, 126.7, 126.9, 127.3, 127.6, 128.1, 129.3, 130.3, 130.4, 130.7, 131.3, 131.5, 132.6, 134.7, 135.2, 137.9, 146.8, 147.0, 152.8, 157.9, 158.5, 160.6, 162.1, 163.3, 164.8, 168.9 ppm. **HRMS (acetonitrile):** m/z calcd. for [C<sub>105</sub>H<sub>133</sub>N<sub>5</sub>O<sub>23</sub>]<sup>++</sup>: 916.4707 [M]<sup>++</sup>, found: 916.4714

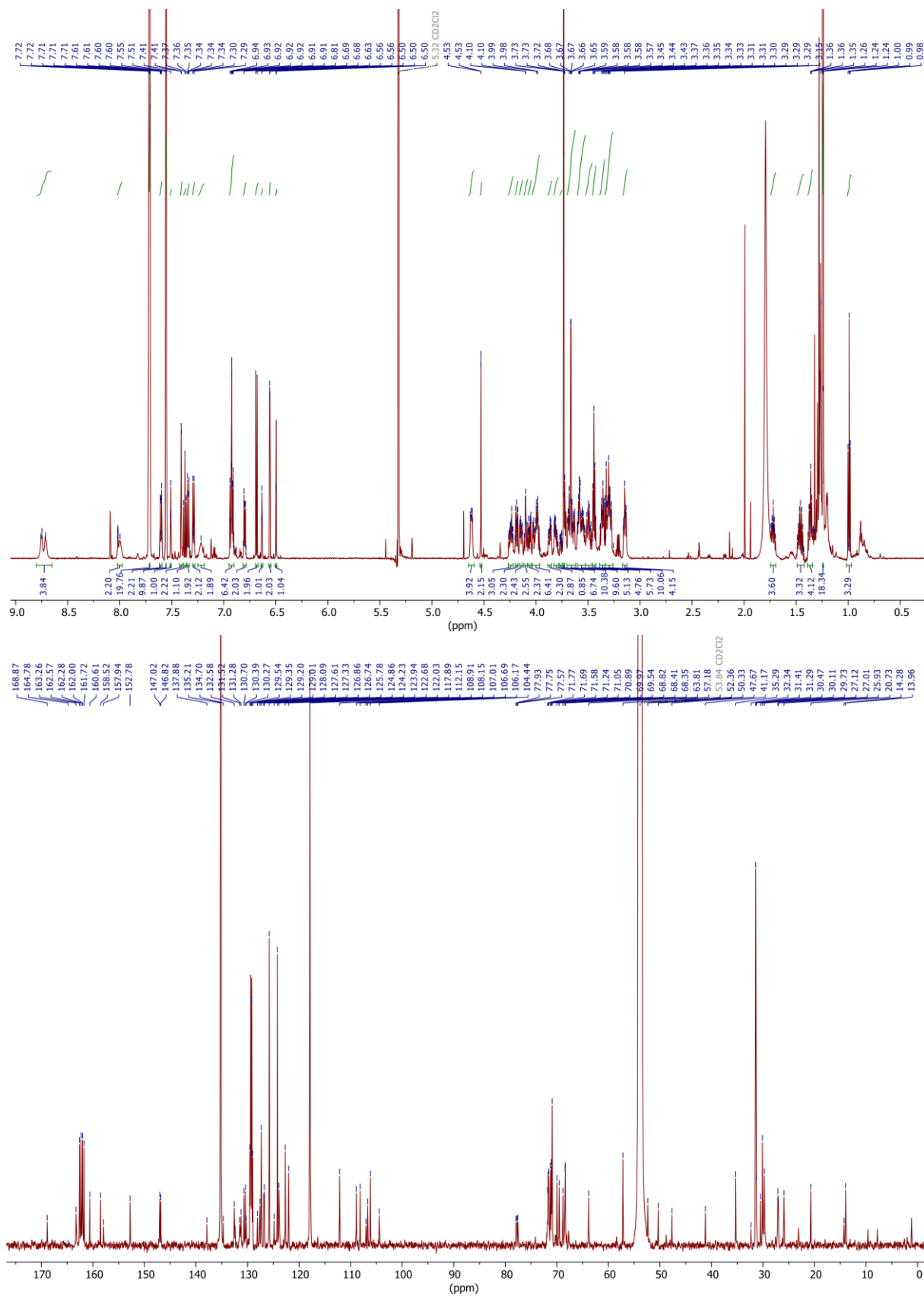
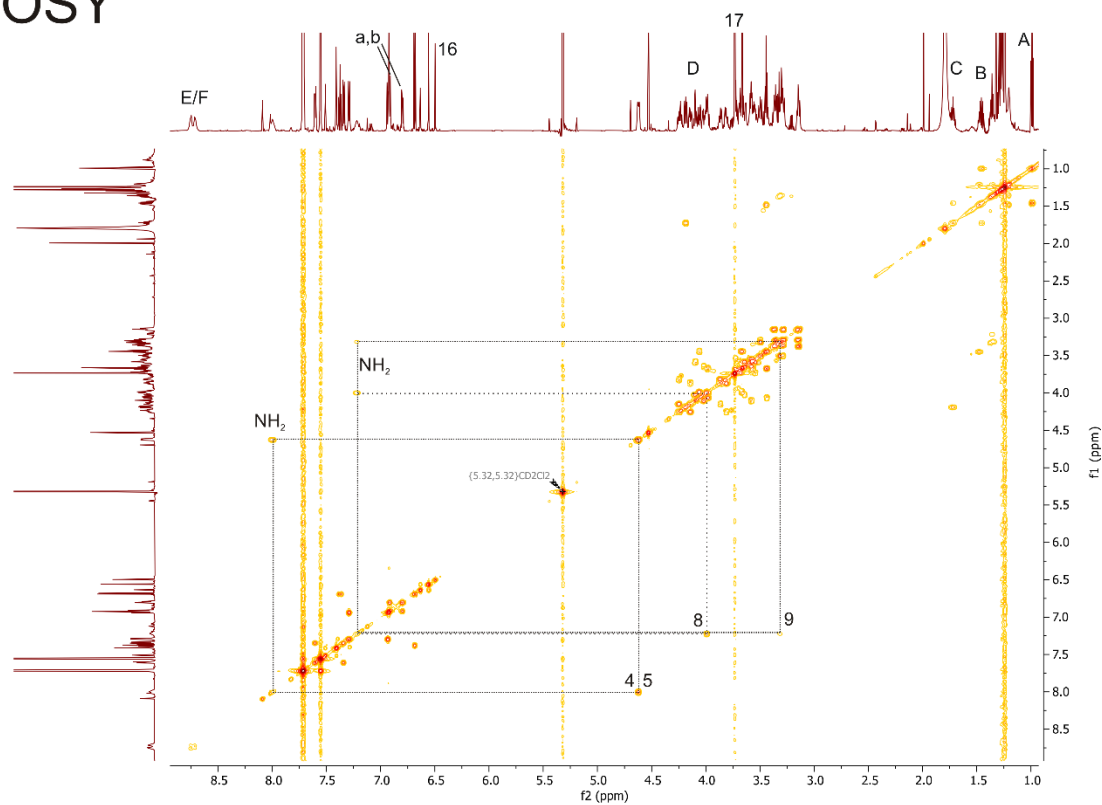
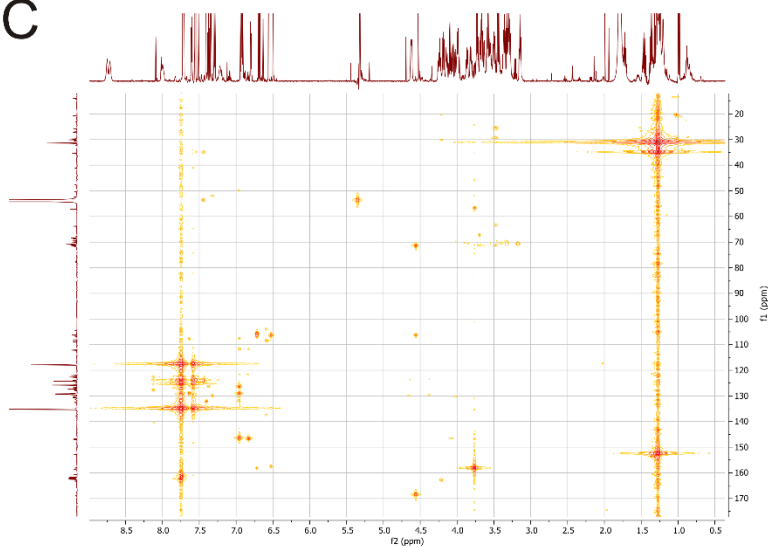


**Fig. S15** <sup>1</sup>H (top) and <sup>13</sup>C (bottom) NMR spectra (700/176 MHz, CD<sub>2</sub>Cl<sub>2</sub>, 298 K) of [3]rotaxane **RNDIC8BC7**.

# COSY



# HMBC



# HMQC

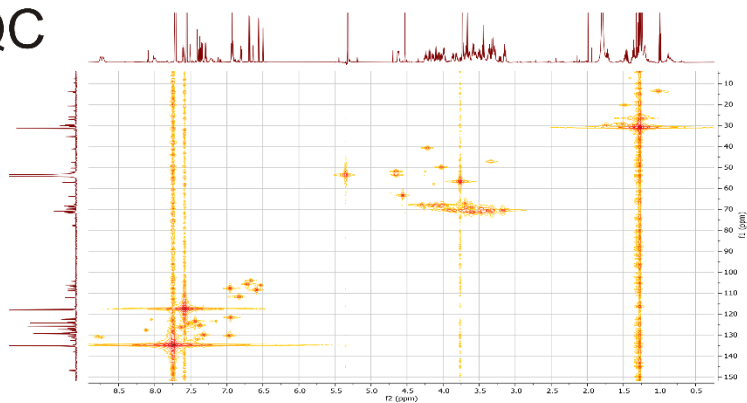


**Fig. S16** COSY (top), HMBC (center) and HMQC (bottom) NMR spectra (700/176 MHz,  $\text{CD}_2\text{Cl}_2$ , 298 K) of [3]rotaxane **RNDIC8BC7**.

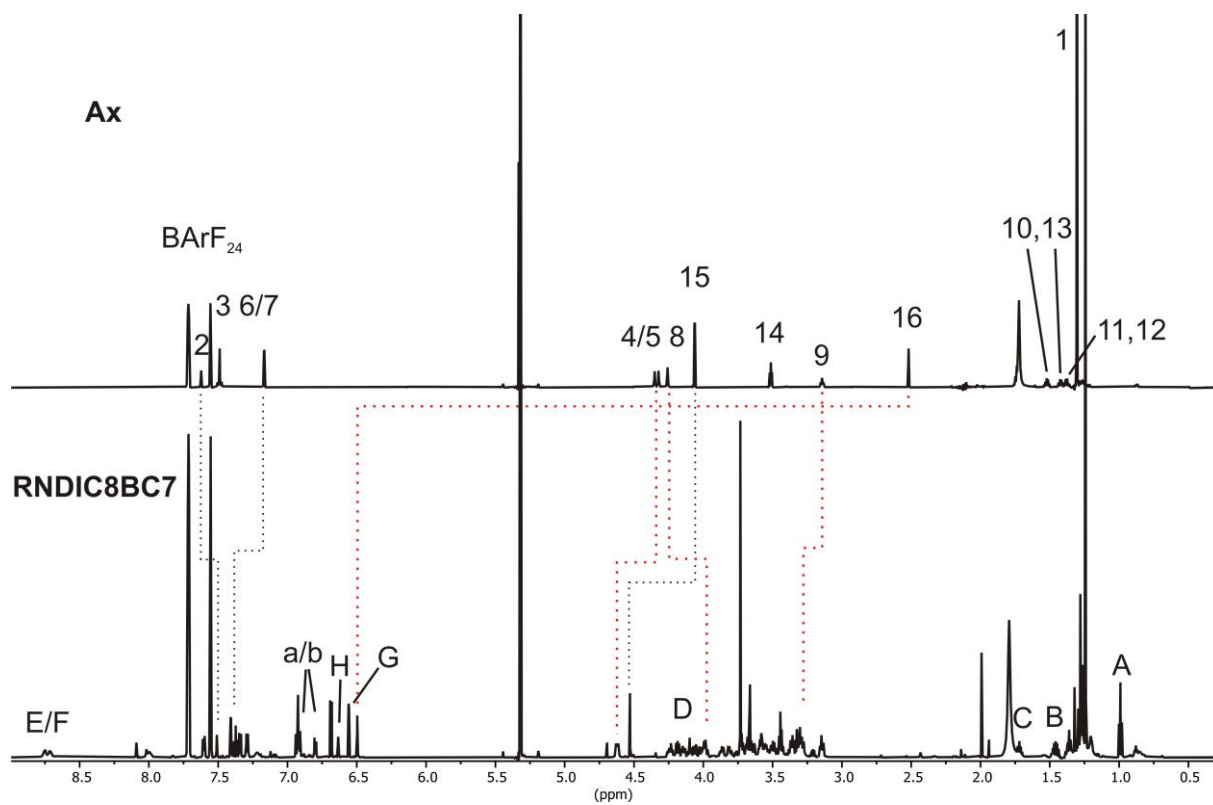


**Fig. S17** [3]rotaxane **RNDIC8BC7** (bottom) and axle **Ax** (top) NMR spectra (700 MHz,  $\text{CD}_2\text{Cl}_2$ , 298 K).



70.8, 71.1, 71.2, 71.5, 71.9, 72.0, 103.9, 104.6, 106.6, 107.1, 109.1, 112.9, 117.9, 122.0, 122.7, 123.8, 124.2, 124.3, 125.8, 126.9, 127.3, 127.6, 129.3, 130.4, 130.6, 131.2, 131.4, 131.6, 132.7, 133.9, 135.2, 138.6, 147.9, 152.5, 157.3, 158.8, 159.8, 162.2, 163.1, 163.2, 168.0 ppm. **HRMS (acetonitrile):** m/z calcd. for  $[C_{101}H_{131}N_5O_{23}]^{++}$ : 891.4629  $[M]^{++}$ , found: 891.4639.

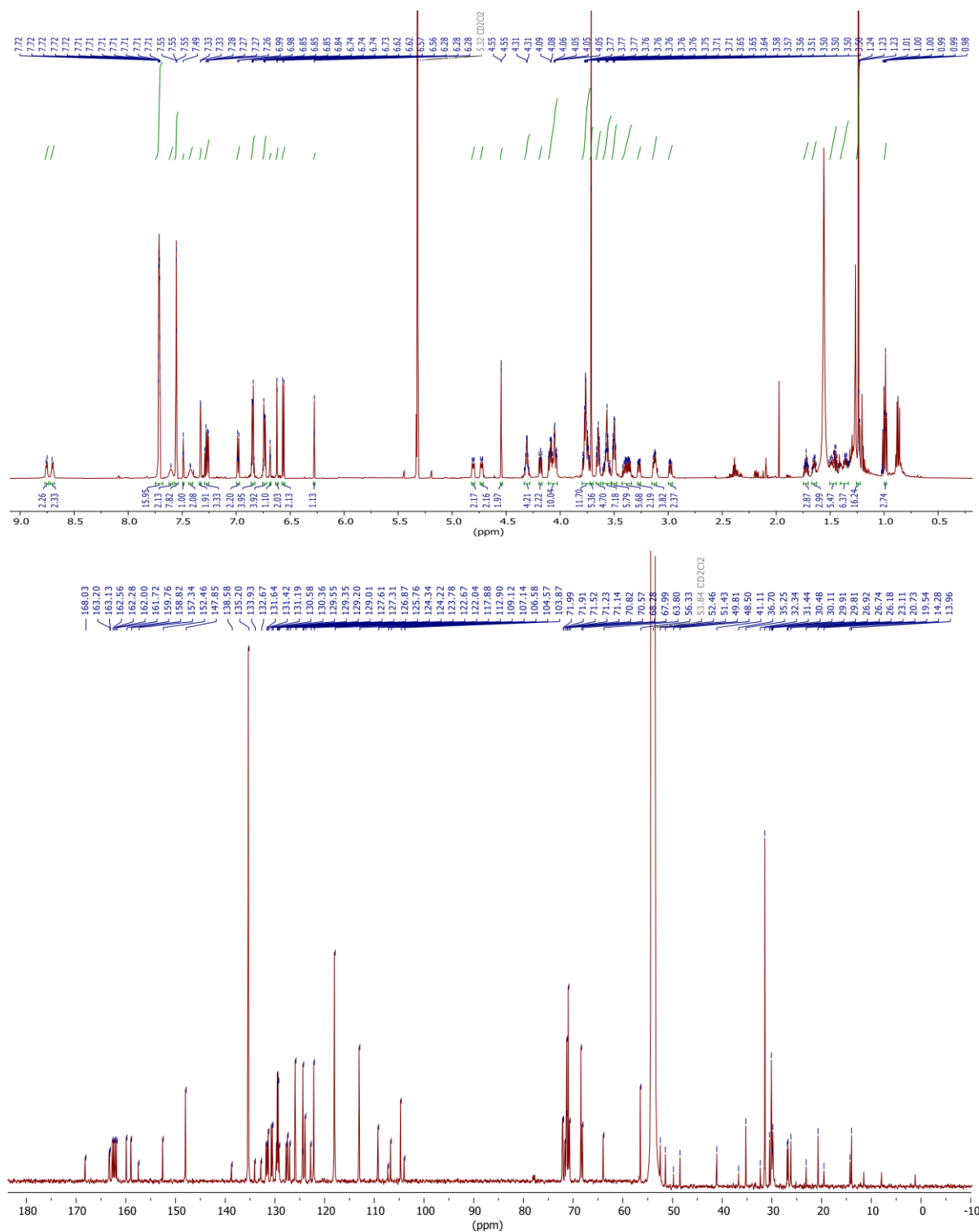
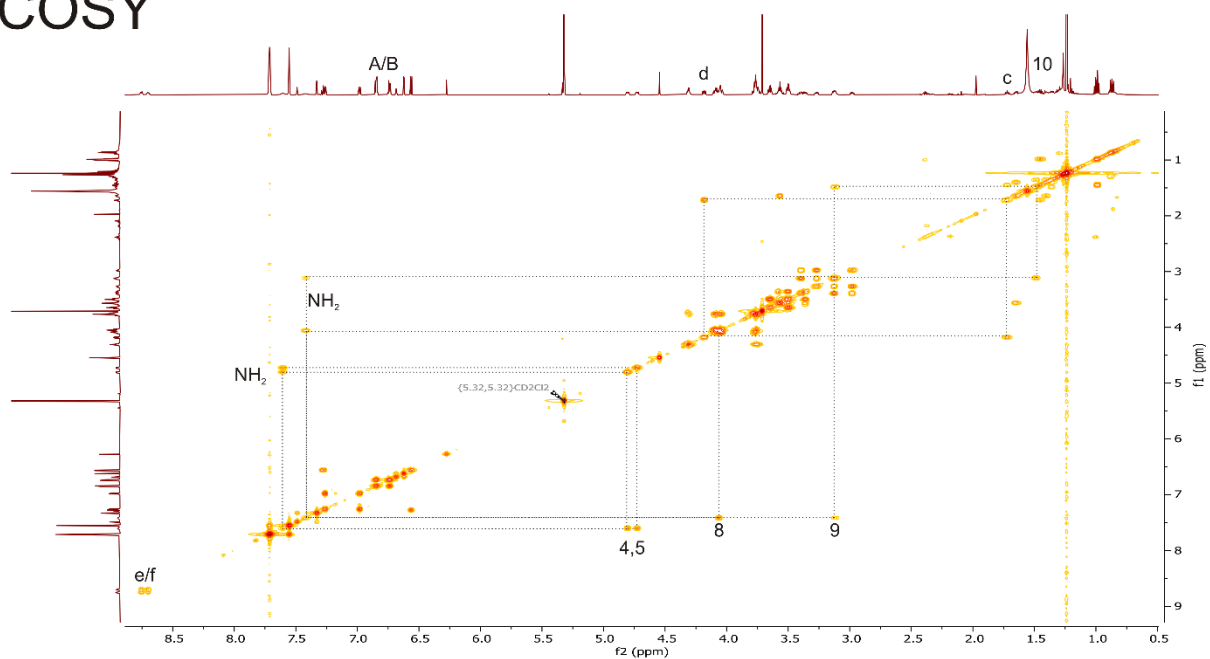
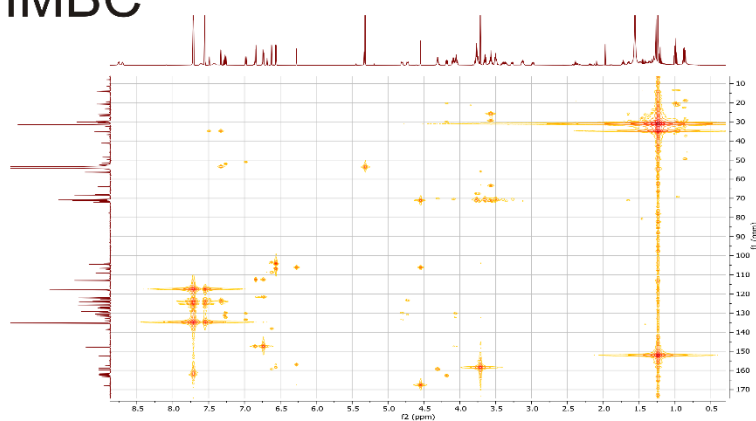


**Fig. S18**  $^1H$  (top) and  $^{13}C$  (bottom) NMR spectra (700/176 MHz,  $CD_2Cl_2$ , 298 K) of [3]rotaxane **RDBC8NDIC7**.

# COSY



# HMBC



# HMQC

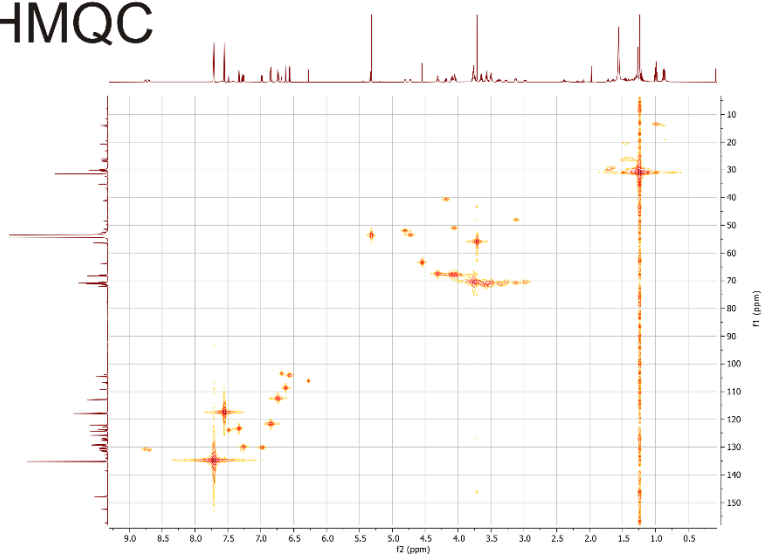


**Fig. S19** COSY (top), HMBC (center) and HMQC (bottom) NMR spectra (700/176 MHz, CD<sub>2</sub>Cl<sub>2</sub>, 298 K) of [3]rotaxane **RDBC8NDIC7**.

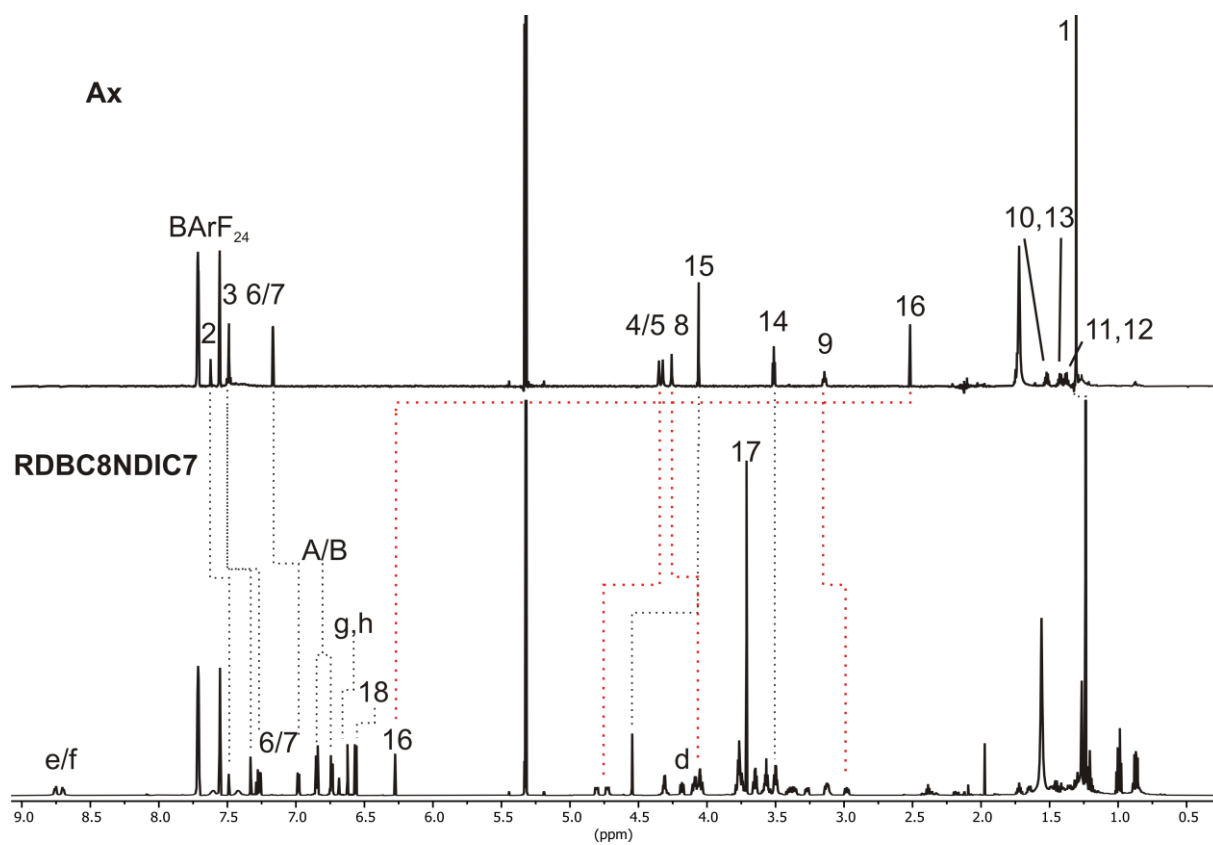


**Fig. S20** [3]rotaxane **RDBC8NDIC7** (bottom) and axle **Ax** (top) NMR spectra (700 MHz,  $\text{CD}_2\text{Cl}_2$ , 298 K).

## 2. Isothermal titration calorimetry

ITC titrations were carried out in dry 1,2-dichloroethane (DCE) at 298 K on a TAM III microcalorimeter (Waters GmbH, TA Instruments, Eschborn, Germany). In a typical experiment, an 800  $\mu\text{L}$  solution of crown ether was placed in the sample cell at a concentration of 1.1 mM, and 260  $\mu\text{L}$  of a solution of the ammonium salt (8.0 mM) were put into the syringe. The titrations consisted of 32 consecutive injections of 8  $\mu\text{L}$  each with a 20 min interval between injections. Heats of dilution were determined by titration of ammonium salt solutions into the sample cell containing blank solvent and were subtracted from each data set. The heat flow generated in the sample cell is measured as a differential signal between sample and reference cell. Hence, an exothermic event results in a positive and an endothermic in a negative heat flow. The data were analysed using the instrument's internal software package and fitted with a 1:1 binding model. Each titration was conducted at least three times and the measured values for  $K$  and  $\Delta H$  were averaged.

Instead of divalent axle **Ax**, two monovalent model compounds **A1** and **A2** were titrated to the five macrocycles (Figure S21) of this study. Hexafluorophosphate  $\text{PF}_6^-$  was used as counter ion, as the binding constants are too high with  $\text{BARF}_{24}^-$  anions to be determined with ITC. Earlier studies showed that the binding constant is roughly 15 – 20 times higher with  $\text{BARF}_{24}^-$ -anions and that trends are similar for both counterions.<sup>3</sup>

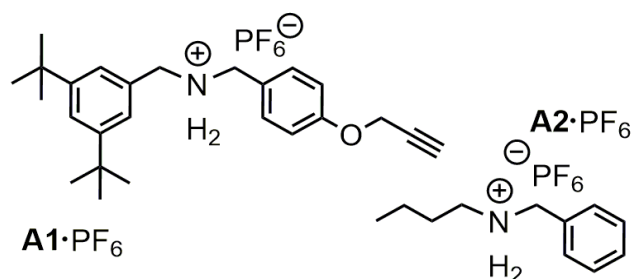


**Fig. S21** Chemical structures of the monovalent model ammonium axles used to determine thermodynamic binding data for all five macrocycles.

**Table S1.** Thermodynamic binding data of different crown ether/secondary ammonium axle complexes obtained by ITC titrations in 1,2-dichloroethane at 298 K.

axle	macrocycle	$K_a / 10^3 \text{ M}^{-1}$	$\Delta G^\circ / \text{kJ/mol}$	$\Delta H^\circ / \text{kJ/mol}$	$T\Delta S^\circ / \text{kJ/mol}$
<b>A2</b> ·PF <sub>6</sub>	<b>BC7</b> <sup>[a]</sup>	1200 ± 100	-34.6 ± 0.2	-63.0 ± 0.5	-28.3 ± 0.7
	<b>NDIC7</b>	7.0 ± 1.0	-22.1 ± 0.2	-51.2 ± 2.0	-29.2 ± 2.2
<b>A2</b> ·PF <sub>6</sub>	<b>DBC8</b> <sup>[a]</sup>	480 ± 70	-32.4 ± 0.3	-60.4 ± 1.5	-28.0 ± 1.8
	<b>NDIC8</b> <sup>[a]</sup>	13 ± 1	-23.4 ± 0.2	-48.1 ± 1.0	-24.7 ± 1.2
	<b>TTFC8</b> <sup>[a]</sup>	7.0 ± 1.0	-22.1 ± 0.2	-50.3 ± 1.0	-28.3 ± 1.2
<b>A1</b> ·PF <sub>6</sub>	<b>DBC8</b> <sup>[a]</sup>	1300 ± 100	-34.8 ± 0.3	-60.9 ± 2.0	-26.1 ± 2.3
	<b>NDIC8</b> <sup>[a]</sup>	49 ± 6	-26.7 ± 0.3	-46.6 ± 2.0	-19.9 ± 2.3
	<b>TTFC8</b> <sup>[a]</sup>	33 ± 3	-25.7 ± 0.2	-51.5 ± 0.9	-25.9 ± 1.1

<sup>[a]</sup> Taken from a previous report.<sup>3</sup>

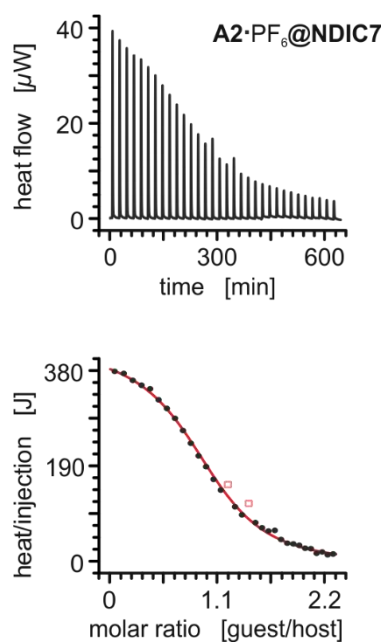


**Fig. S22** Titration plots (heat flow versus time and heat/volume versus guest/host ratio) obtained from ITC experiments at 298 K in 1,2-dichloroethane: vial: **NDIC7**, syringe: axle **A2**·PF<sub>6</sub>. Points marked with non-filled squares were not considered in the fitting process. Titration plots for the other combinations are part of a previous report.<sup>3</sup>

### 3. Heteropseudo[3]rotaxane $^1\text{H}$ NMR experiments

Equimolar solutions of divalent axle **Ax** and macrocycles gave complex  $^1\text{H}$  NMR spectra. When a crown ether is bound to ammonium units, the methylene protons ( $\text{H}_4$ ,  $\text{H}_5$ ,  $\text{H}_8$  and  $\text{H}_9$ ) exhibit unambiguous cross coupling signals in the COSY spectrum to the corresponding ammonium protons. The characteristic shifts of these methylene protons were used to identify the pseudorotaxane species present in solution and the integrals of these signals were used to calculate the ratio of the species, which is given in percent of all identified pseudorotaxane species. Due to imprecise integration, the given percentages have experimental errors of 5%.

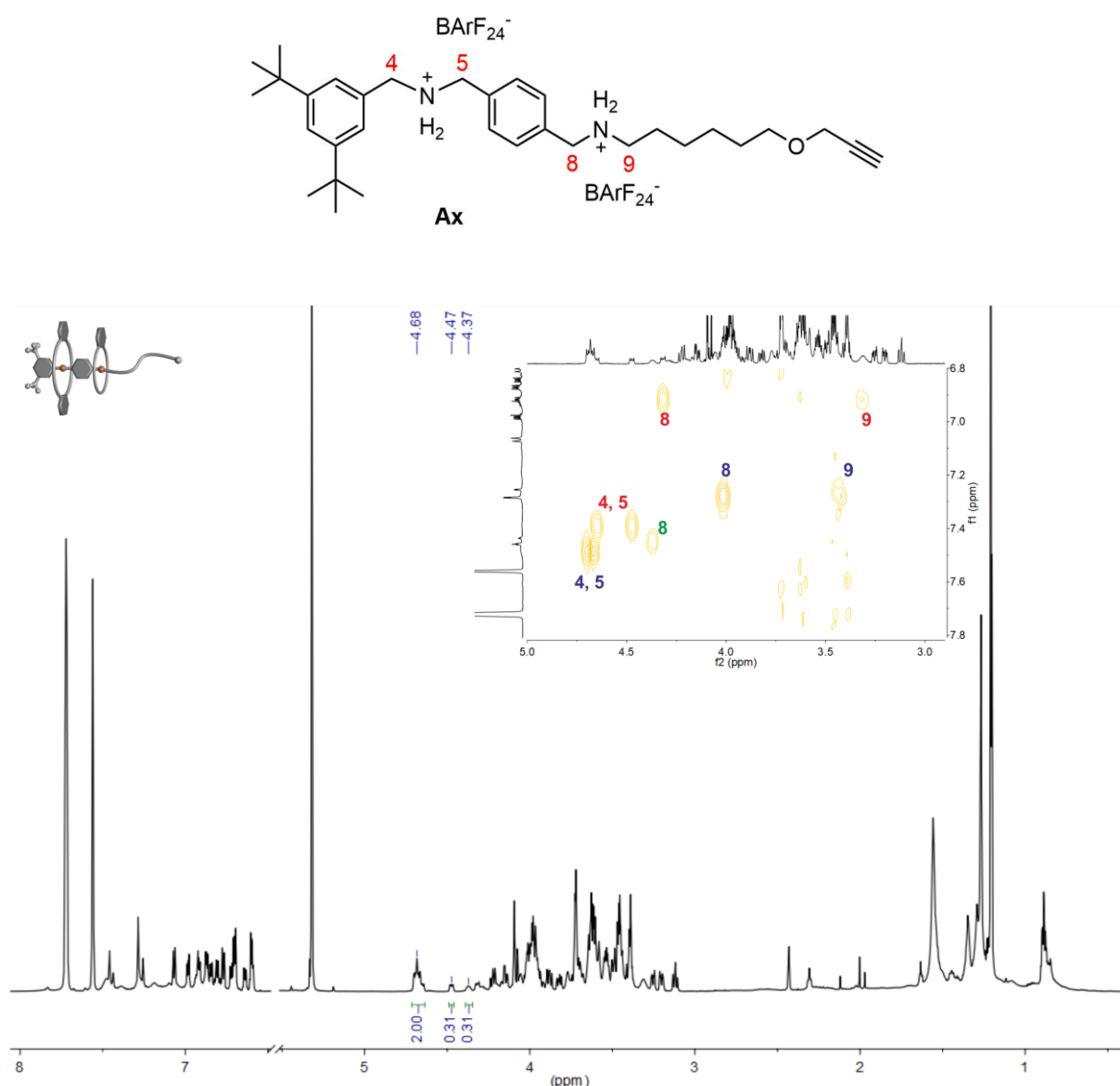


**Fig. S23**  $^1\text{H}$  NMR and partial COSY spectra (700 MHz,  $\text{CD}_2\text{Cl}_2$ , 298 K, 5 mM) of an equimolar solution of **Ax**, **DBC8** and **BC7** 16 d after mixing. Signals of protons corresponding to the heteropseudo[3]rotaxane **PRDBC8BC7** (58%) are labeled in blue, those corresponding to the homopseudo[3]rotaxane **PRDBC8DBC8** (21%) in red and those of the pseudo[2]rotaxane **PRBC7** (21%) in green.

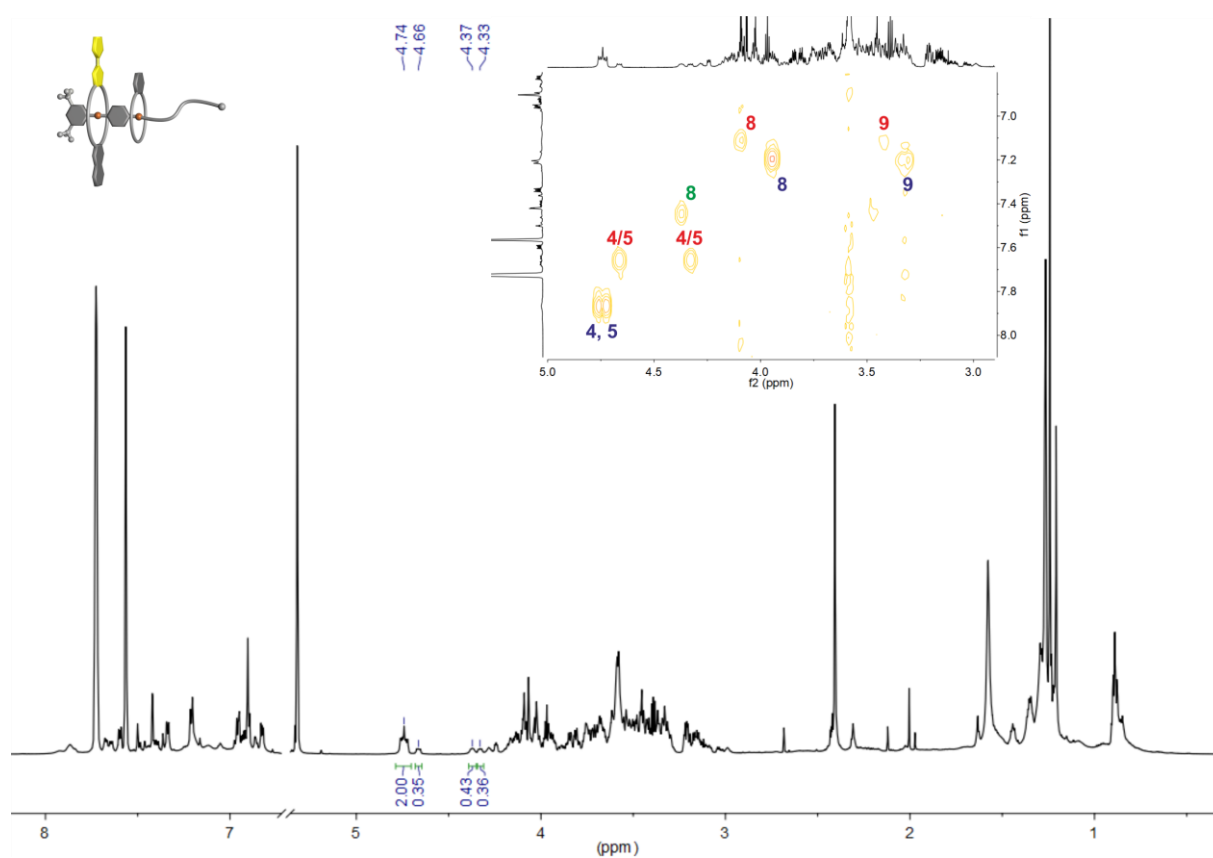


**Fig. S24** <sup>1</sup>H NMR and partial COSY spectra (700 MHz, CD<sub>2</sub>Cl<sub>2</sub>, 298 K, 5 mM) of an equimolar solution of **Ax**, **TTFC8** and **BC7** 16 d after mixing. Signals of protons corresponding to the heteropseudo[3]rotaxane **PRTTFC8BC7** (56%) are labeled in blue, those corresponding to the homopseudo[3]rotaxane **PRTTFC8TTFC8** (20%) in red and those of the pseudo[2]rotaxane **PRBC7** (24%) in green.

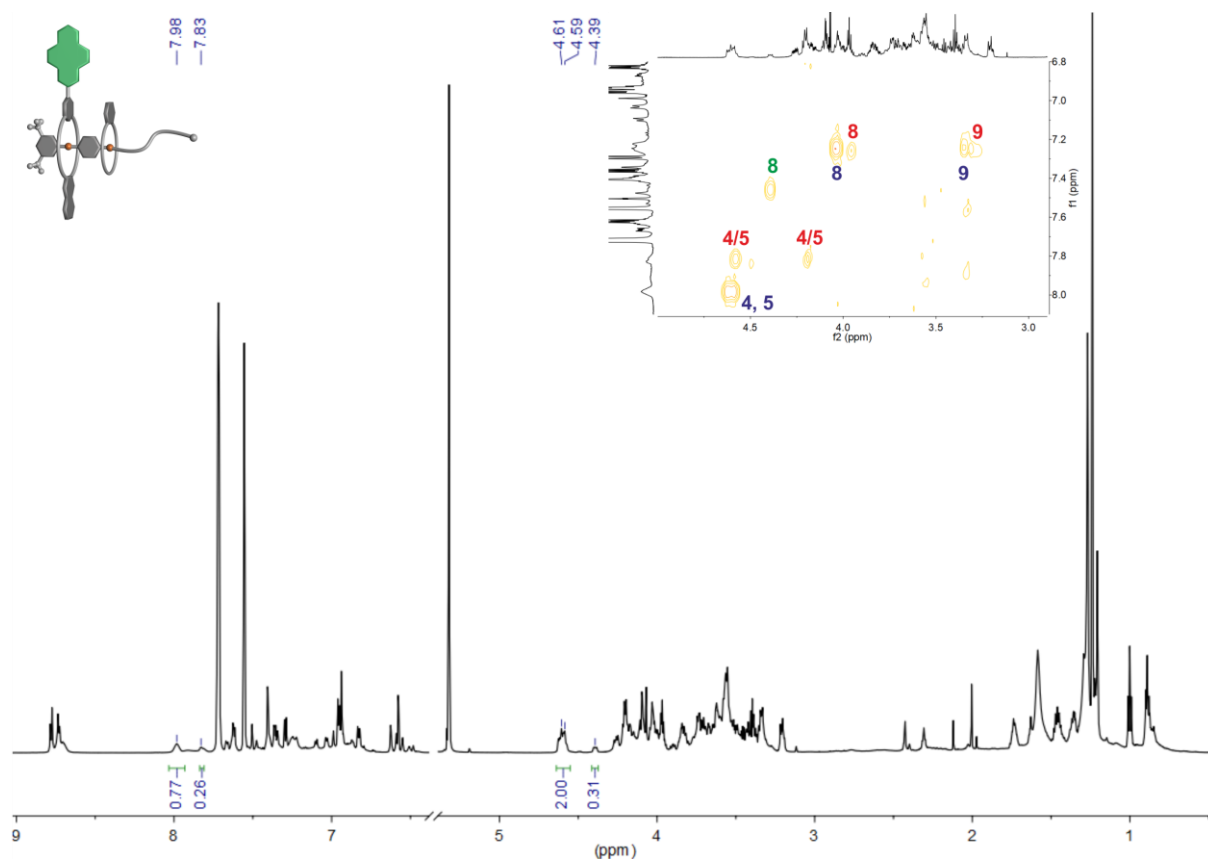


**Fig. S25** <sup>1</sup>H NMR and partial COSY spectra (700 MHz, CD<sub>2</sub>Cl<sub>2</sub>, 298 K, 5 mM) of an equimolar solution of **Ax**, **NDIC8** and **BC7** 16 d after mixing. Signals of protons corresponding to the heteropseudo[3]rotaxane **PRNDIC8BC7** (57%) are labeled in blue, those corresponding to the homopseudo[3]rotaxane **PRNDIC8NDIC8** (19%) in red and those to the pseudo[2]rotaxane **PRBC7** (24%) in green. The methylene protons of **PRNDIC8NDIC8** overlap with **PRNDIC8BC7** and crown ether signals, therefore, the integrals of the ammonium protons were used to calculate the ratios.

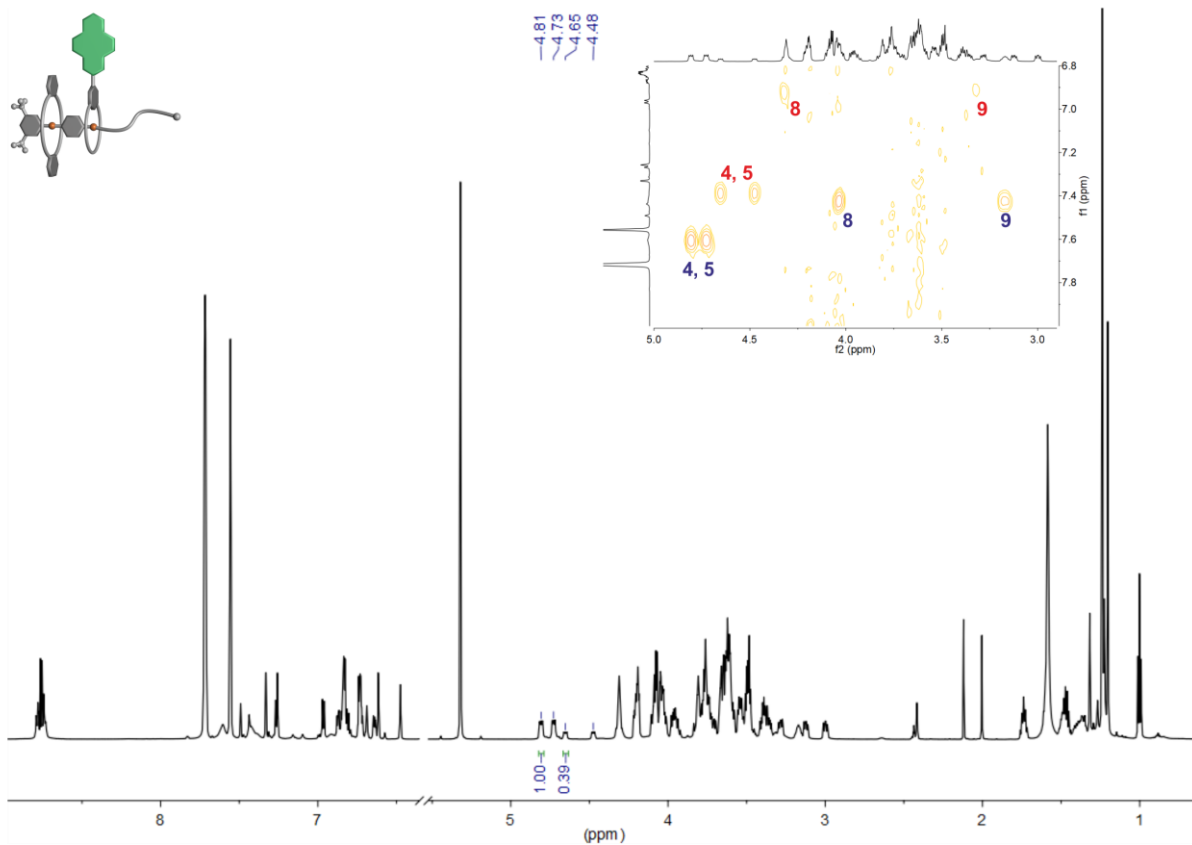


**Fig. S26** <sup>1</sup>H NMR and partial COSY spectra (700 MHz, CD<sub>2</sub>Cl<sub>2</sub>, 298 K, 5 mM) of an equimolar solution of **Ax**, **DBC8** and **NDIC7** 16 d after mixing. Signals of protons corresponding to the heteropseudo[3]rotaxane **PRDBC8NDIC7** (72%) are labeled in blue and those corresponding to the homopseudo[3]rotaxane **PRDBC8DBC8** (28%) in red.

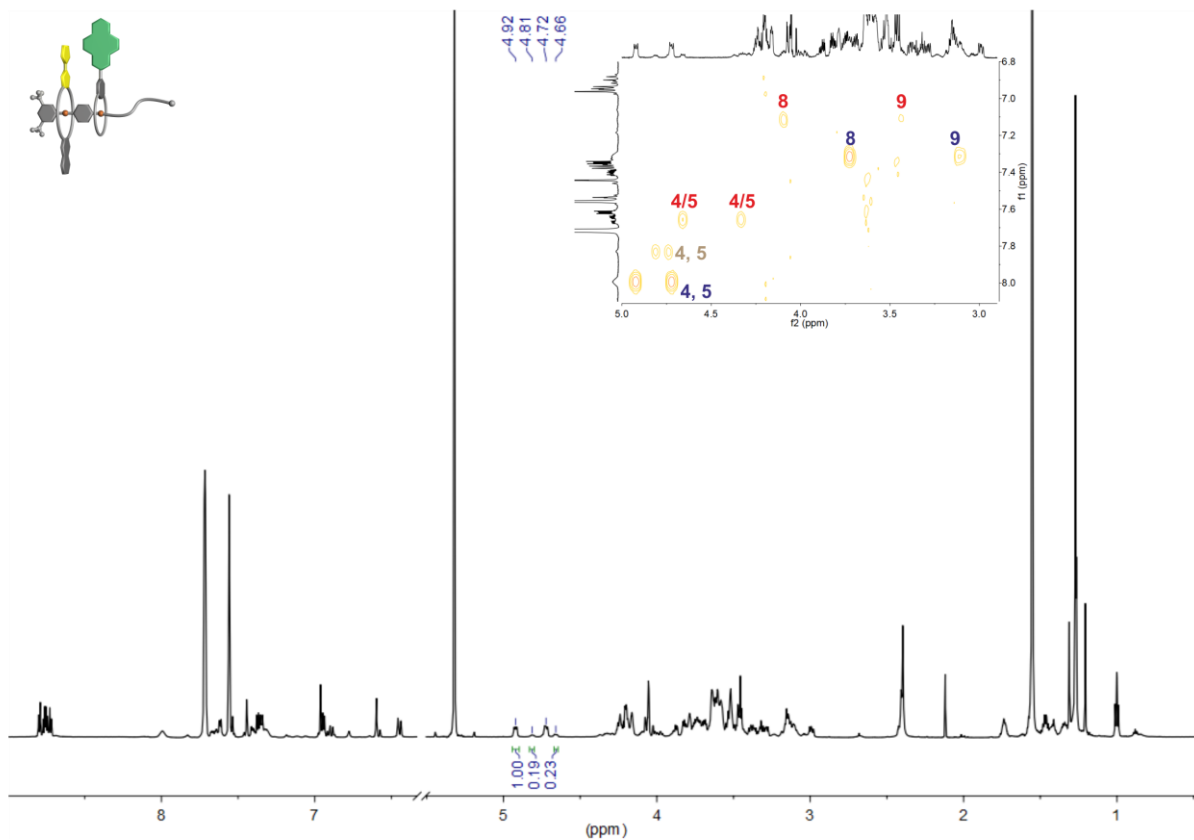


**Fig. S27** <sup>1</sup>H NMR and partial COSY spectra (700 MHz, CD<sub>2</sub>Cl<sub>2</sub>, 298 K, 5 mM) of an equimolar solution of **Ax**, **TTFC8** and **NDIC7** 16 d after mixing. Signals of protons corresponding to the heteropseudo[3]rotaxane **PRTTFC8NDIC7** (70%) are labeled in blue, those corresponding to the homopseudo[3]rotaxane **PRTTFC8TTFC8** (16%) in red and those to the pseudo[2]rotaxane **PRTTFC8** (13%) in brown.

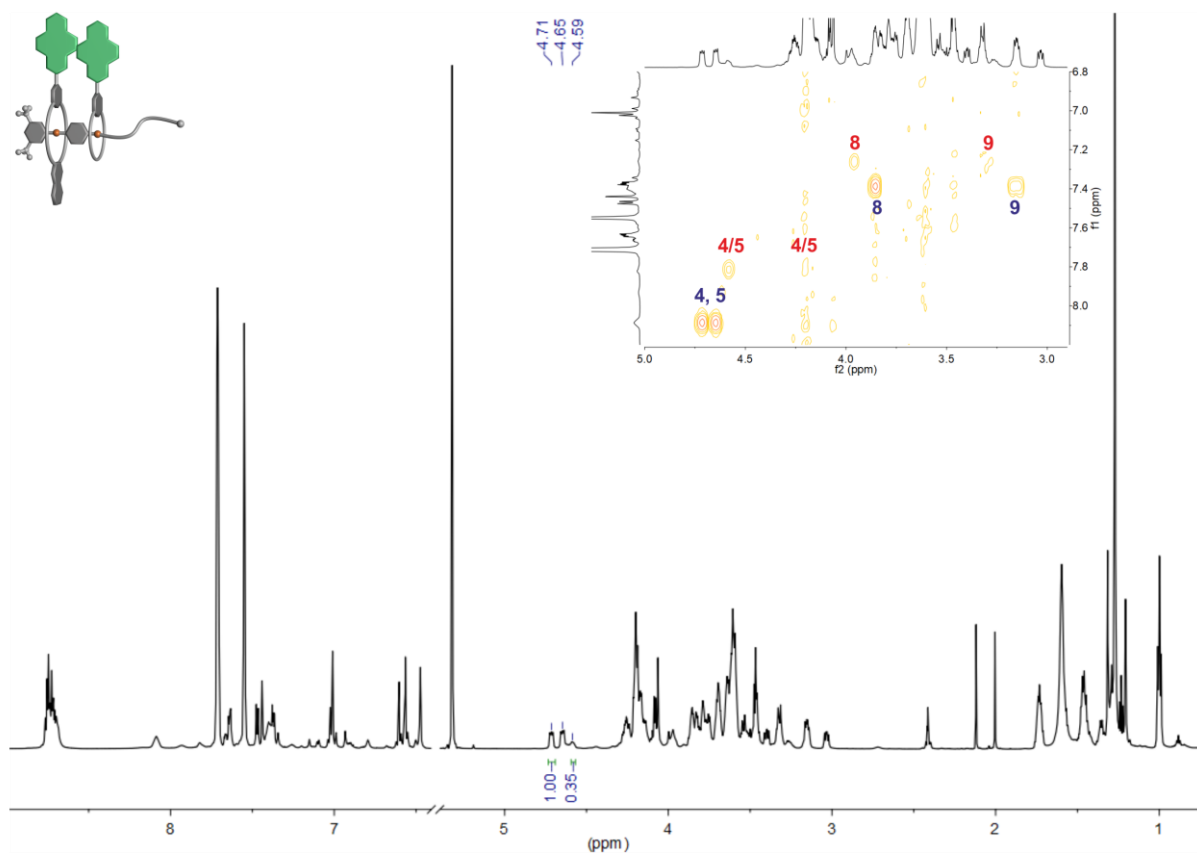


**Fig. S28** <sup>1</sup>H NMR and partial COSY spectra (700 MHz, CD<sub>2</sub>Cl<sub>2</sub>, 298 K, 5 mM) of an equimolar solution of **Ax**, **NDIC8** and **NDIC7** 16 d after mixing. Signals of protons corresponding to the Heteropseudo[3]rotaxane **PRNDIC8NDIC7** (74%) are labeled in blue and those corresponding to the Homopseudo[3]rotaxane **PRNDIC8NDIC8** (26%) in red.

## 4. Tandem mass spectrometry

A Synapt G2-S HDMS (Waters Co., Milford, MA, USA) instrument with a quadrupole-time-of-flight high-resolution mass analyser was used to perform electrospray ionization tandem mass spectrometry. One of the following ionization conditions were used: a) For pseudorotaxane mixtures in dichloromethane or acetonitrile: flow rate  $8 \mu\text{L min}^{-1}$ , capillary voltage 1.5 or 2.5 kV, sample cone voltage 34 V, source offset 54 V, source temperature  $100 \text{ }^\circ\text{C}$ , desolvation temperature  $220 \text{ }^\circ\text{C}$ , nebulizer gas 3.0 bar, desolvation gas flow  $450 \text{ L h}^{-1}$ . b) For sample solutions of the isolated rotaxane in acetonitrile: flow rate  $8 \mu\text{L min}^{-1}$ , capillary voltage 2.5 kV, sample cone voltage 80 V, source offset 54 V, source temperature  $100 \text{ }^\circ\text{C}$ , desolvation temperature  $220 \text{ }^\circ\text{C}$ , nebulizer gas 2.5 bar, desolvation gas flow  $700 \text{ L h}^{-1}$ .

For collision-induced dissociation (CID) experiments of mass-selected ions,  $\text{N}_2$  was used as the collision gas. Fragmentation experiments were conducted in the trap cell of the Synapt G2-S HDMS instrument with collision energies of 3 – 55 V. For the isolated rotaxane, 5 V steps were used and for the pseudorotaxane mixtures 3 V steps. Data acquisition and processing was carried out using MassLynx™ (version 4.1).

For plotting of the survival yield curves the spectra were centroided. For each spectrum at different collision voltages, the intensity of the ion with the selected mass was divided by the total ion intensity (only fragments with an intensity above 1% were considered) and then plotted against the collision voltage. Fitting was done with applying a sigmoidal Boltzmann function using Origin Pro 2020 to obtain the 50% survival yield voltages.

For time-dependent measurements, a solution of the axle **Ax** and one kind of crown[8] ether was prepared and stirred for 1 h (10 mM, 1,2-dichloroethane,  $20 \text{ }^\circ\text{C}$ ). One kind of crown[7] ether was added to yield an equimolar solution of 5 mM. The pseudorotaxane equilibrium in solution was monitored by HRMS. Prior to each measurement the sample was diluted to a concentration of  $2.5 \mu\text{M}$  using dichloromethane. The absolute intensities of the ions do not necessarily correlate with the concentrations of the species in solution, as the ionization efficiencies of the involved species may differ significantly. Especially, all ions involving **BC7** ionize very efficiently at the conditions used in the experiment. For a better visibility of the signals of interest the mass range of these ions ( $m/z < 450$ ) is not shown. Nevertheless, a good qualitative picture may be derived from these experiments.

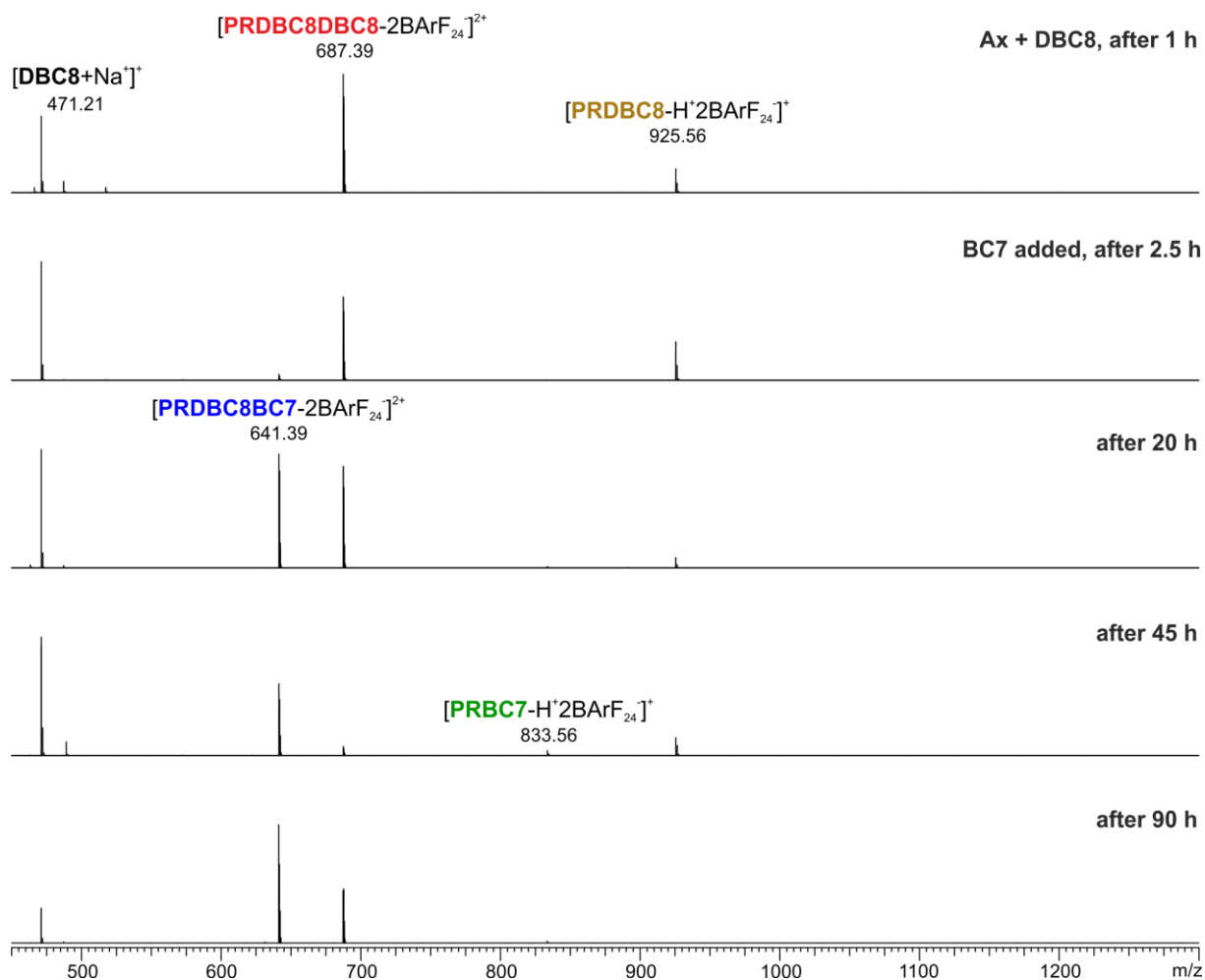


**Figure S29** ESI-Q-TOF-HRMS spectra of a solution containing **Ax**, **DBC8** and **BC7** at different times. Prior to each measurement the solution was diluted to 2.5  $\mu\text{M}$  using dichloromethane. Signals belonging to the heteropseudo[3]rotaxane **PRDBC8BC7** are labeled in blue, to the homopseudo[3]rotaxane **PRDBC8DBC8** in red, to the pseudo[2]rotaxane **PRDBC8** in brown and to the pseudo[2]rotaxane **PRBC7** in green.

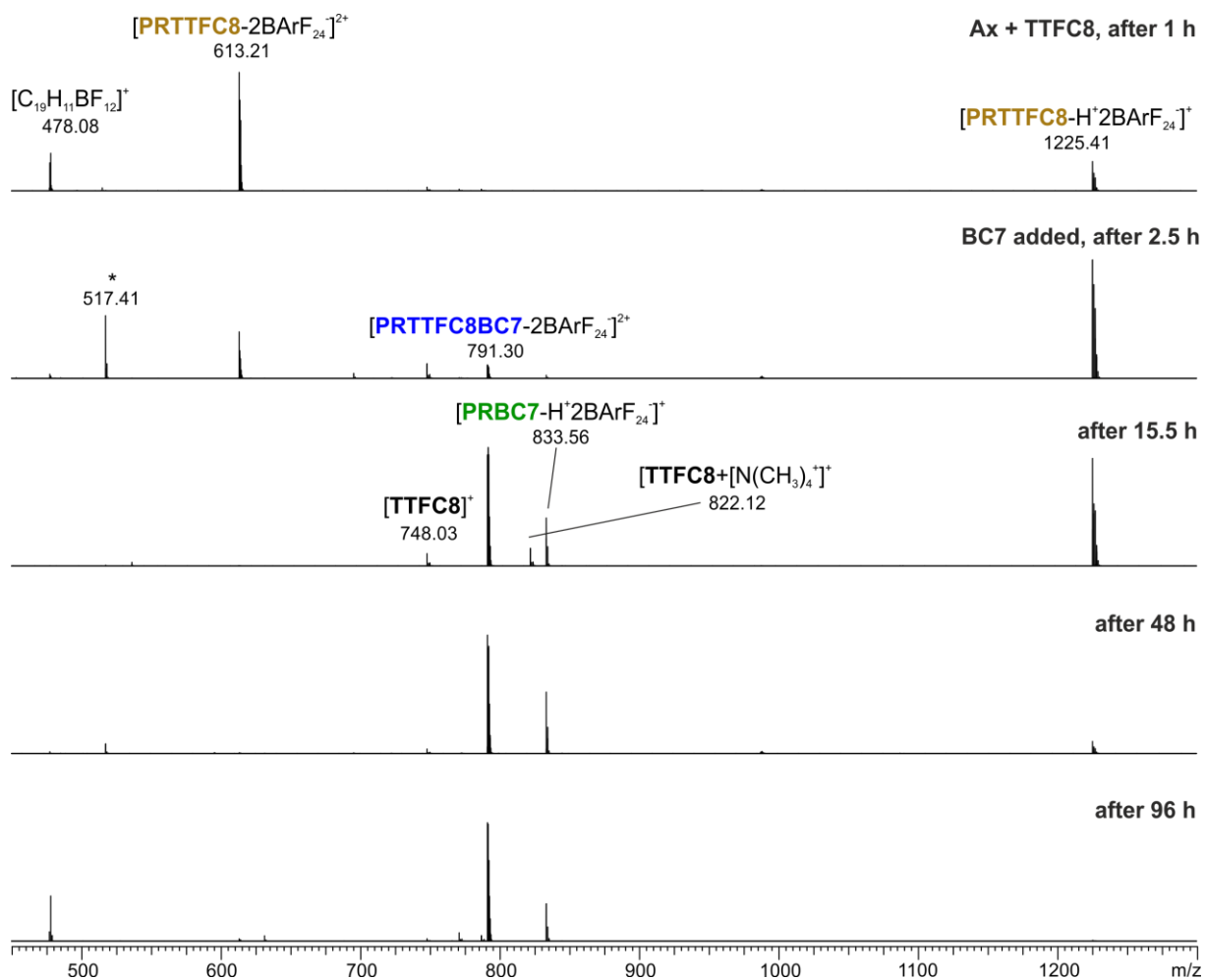


**Figure S30** ESI-Q-TOF-HRMS spectra of a solution containing **Ax**, **TTFC8** and **BC7** at different times. Prior to each measurement the solution was diluted to 2.5  $\mu\text{M}$  using dichloromethane. Signals belonging to the heteropseudo[3]rotaxane **PRTTFC8BC7** are labeled in blue, to the pseudo[2]rotaxane **PRTTFC8** in brown and to the pseudo[2]rotaxane **PRBC7** in green. The ion  $m/z$  478.08 represents a fragment of the  $\text{BArF}_{24}^-$  counterion. Peak marked with a \* are impurities present in the instrument.

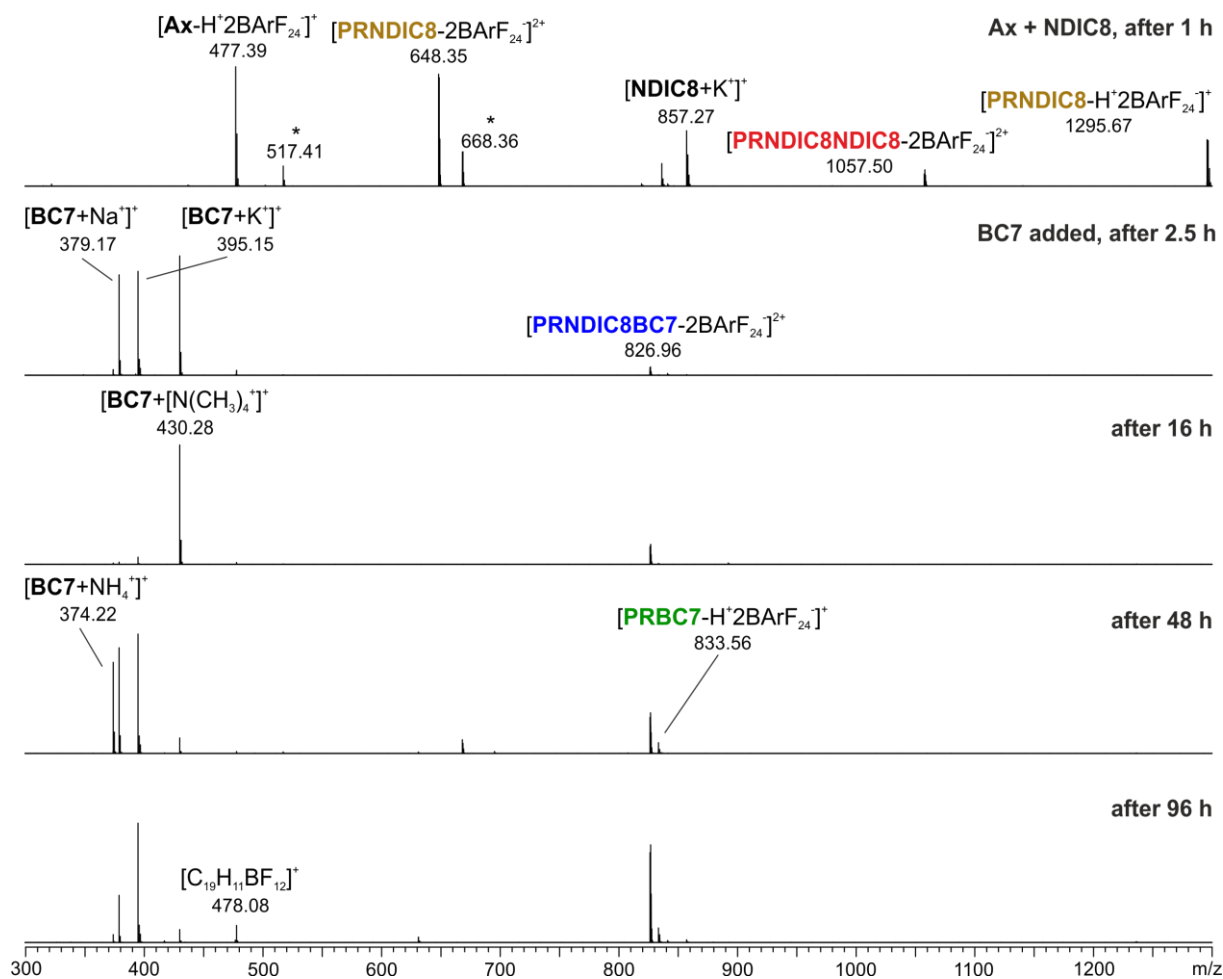


**Figure S31** ESI-Q-TOF-HRMS spectra of a solution containing **Ax**, **NDIC8** and **BC7** at different times. Prior to each measurement the solution was diluted to 2.5  $\mu\text{M}$  using dichloromethane. Signals belonging to the heteropseudo[3]rotaxane **PRNDIC8BC7** are labeled in blue, to the homopseudo[3]rotaxane **PRNDIC8NDIC8** in red, to the pseudo[2]rotaxane **PRNDIC8** in brown and to the pseudo[2]rotaxane **PRBC7** in green. The ion  $m/z$  478.08 represents a fragment of the  $\text{BArF}_{24}$ -counterion. Peaks marked with a \* are impurities present in the instrument.

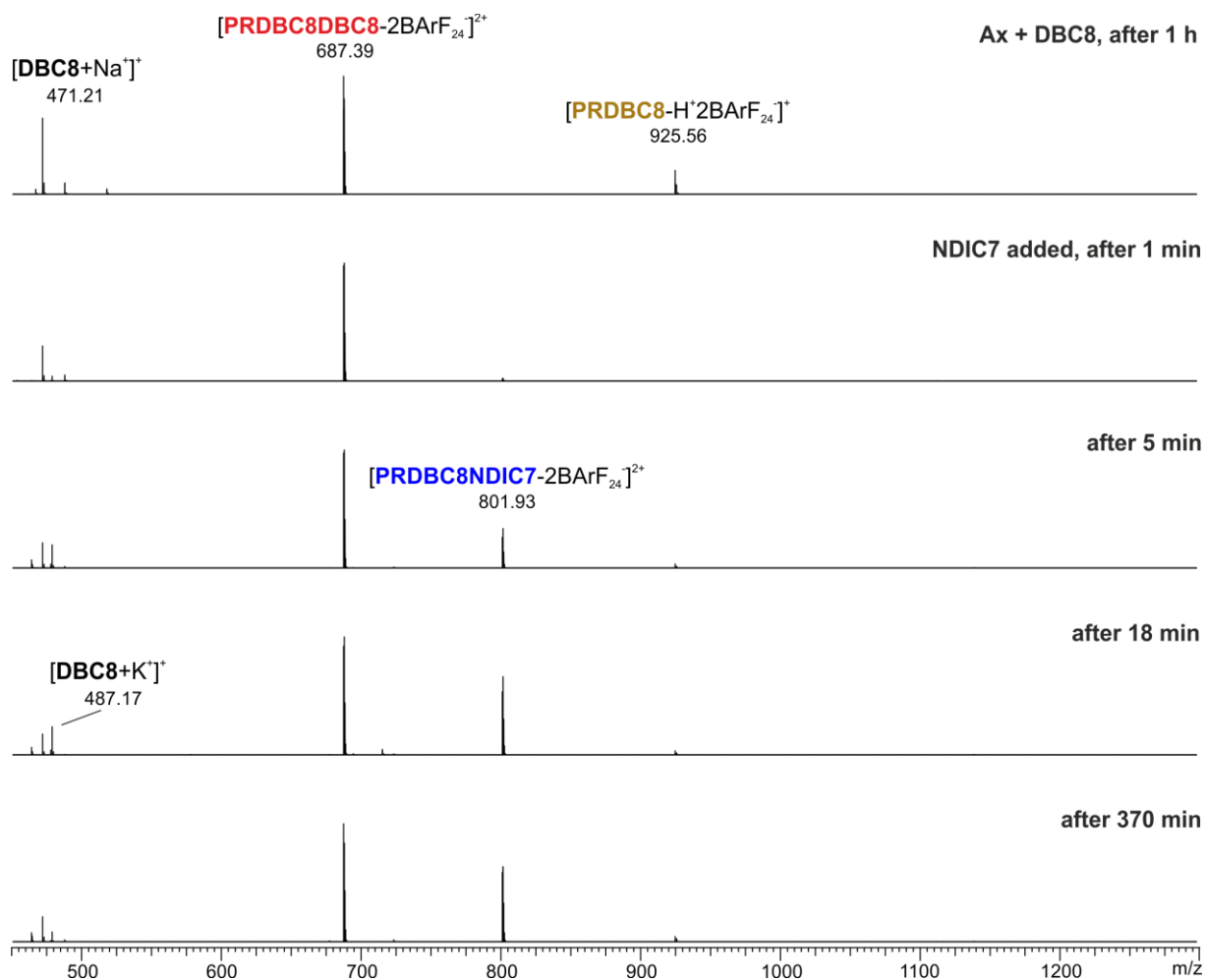


**Figure S32** ESI-Q-TOF-HRMS spectra of a solution containing **Ax**, **DBC8** and **NDIC7** at different times. Prior to each measurement the solution was diluted to 2.5  $\mu\text{M}$  using dichloromethane. Signals belonging to the heteropseudo[3]rotaxane **PRDBC8NDIC7** are labeled in blue, to the homopseudo[3]rotaxane **PRDBC8DBC8** in red and to the pseudo[2]rotaxane **PRDBC8** in brown.

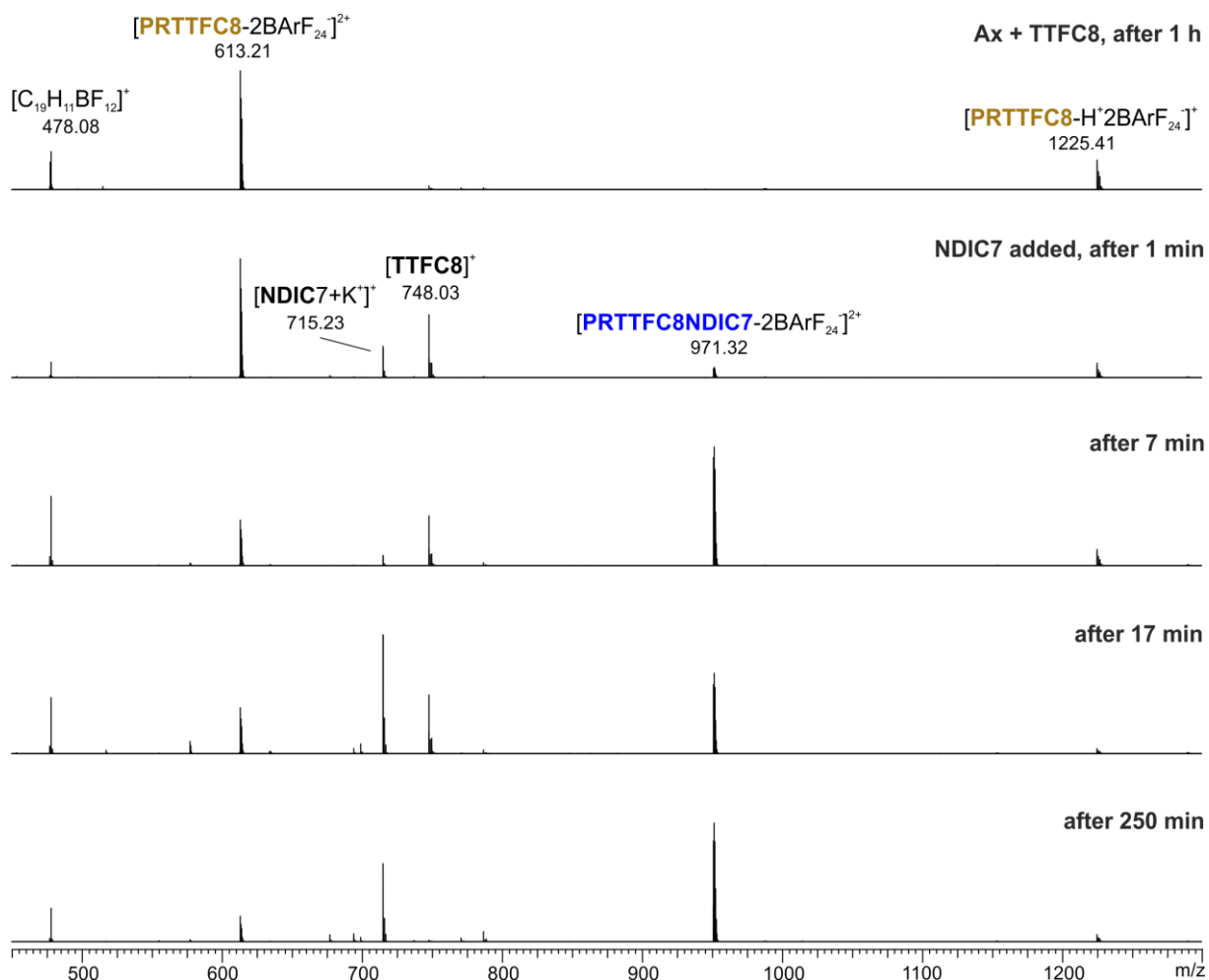


**Figure S33** ESI-Q-TOF-HRMS spectra of a solution containing **Ax**, **TTFC8** and **NDIC7** at different times. Prior to each measurement the solution was diluted to 2.5  $\mu$ M using dichloromethane. Signals belonging to the heteropseudo[3]rotaxane **PRTTFC8NDIC7** are labeled in blue and to the pseudo[2]rotaxane **PRTTFC8** in brown. The ion m/z 478.08 represents a fragment of the  $BArF_{24}$ -counterion.

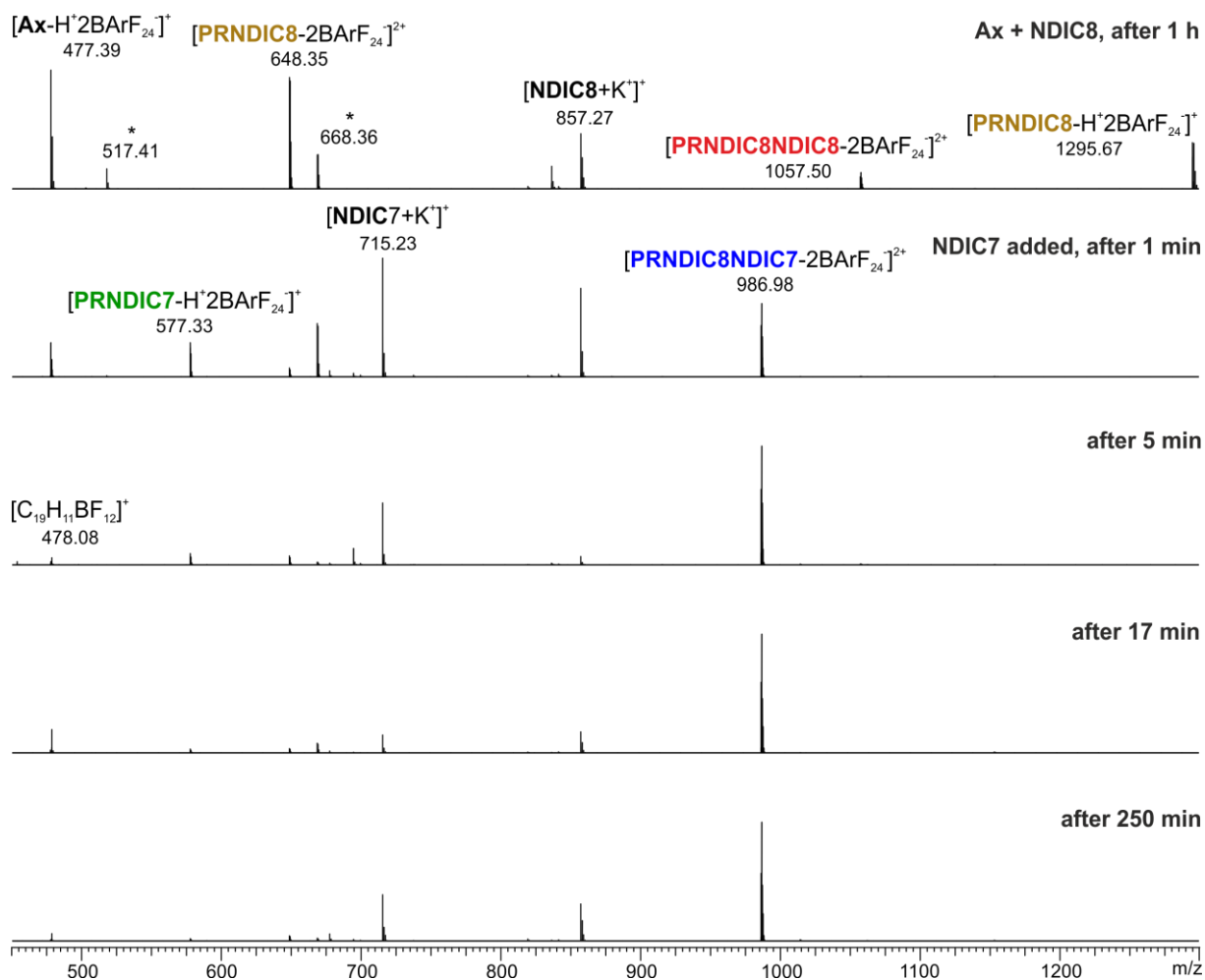


**Figure S34** ESI-Q-TOF-HRMS spectra of a solution containing **Ax**, **NDIC8** and **NDIC7** at different times. Prior to each measurement the solution was diluted to 2.5  $\mu\text{M}$  using dichloromethane. Signals belonging to the heteropseudo[3]rotaxane **PRNDIC8NDIC7** are labeled in blue, to the homopseudo[3]rotaxane **PRNDIC8NDIC8** in red, to the pseudo[2]rotaxane **PRNDIC8** in brown and to the pseudo[2]rotaxane **PRBC7** in green. The ion m/z 478.08 represents a fragment of the  $\text{BArF}_{24}$ -counterion. Peaks marked with a \* are impurities present in the instrument.

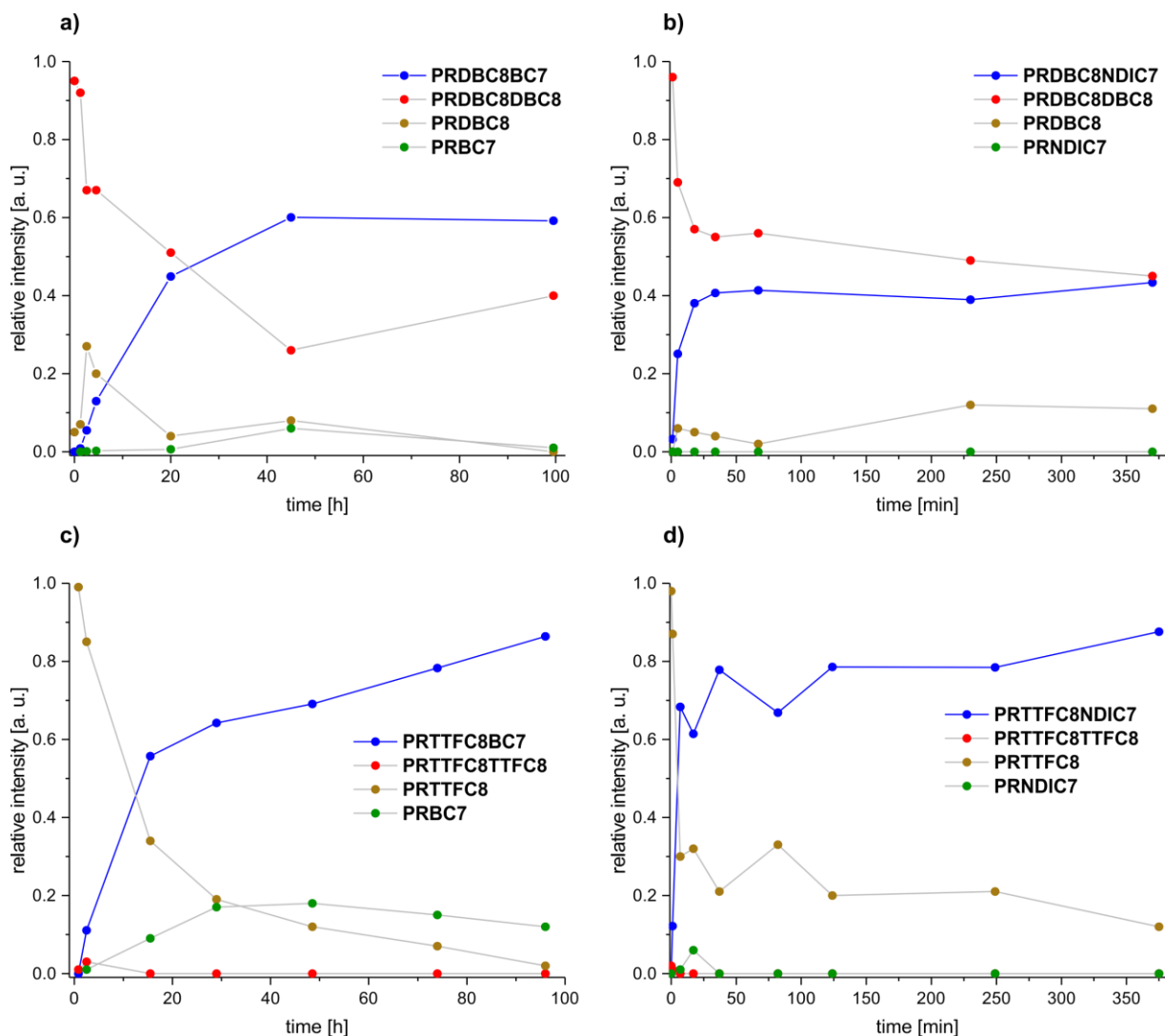


**Figure S35** Plots summarising the changes of the hetero- and homopseudo[3]rotaxanes signal intensities and those of their pseudorotaxane precursors over reaction time from equimolar solutions of **Ax**, crown[8] ether and crown[7] ether at 20 °C. The relative intensities are taken from ESI-Q-TOF-HRMS spectra. The absolute intensities of the ions are not representative for the concentrations of the species in solution, as the ionization efficiencies of the involved species differ significantly. For full spectra see above.

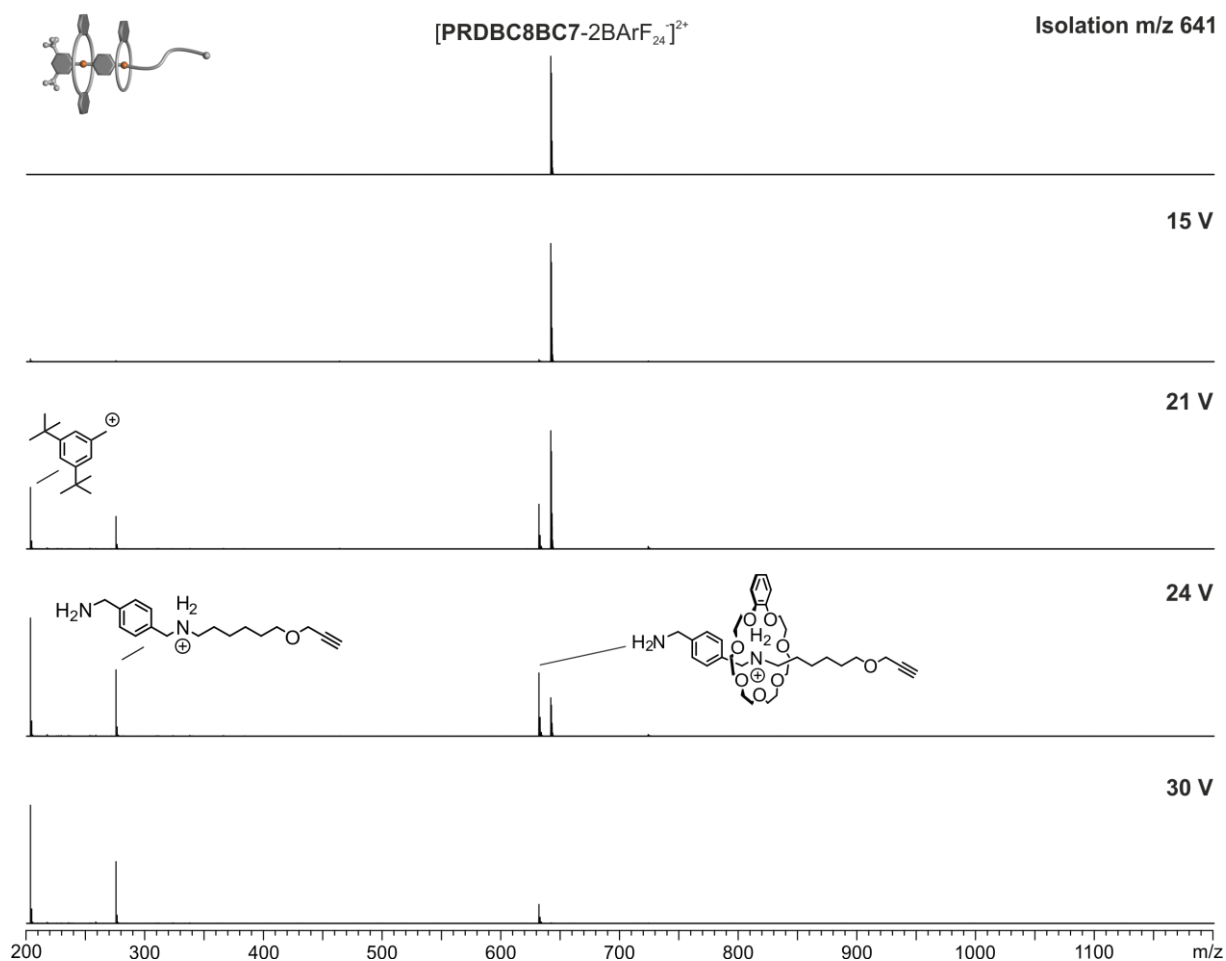


**Figure S36** CID experiment with mass-selected  $[\text{PRDBC8BC7-2BArF}_{24}^{-}]^{2+}$  ions at  $m/z$  641 obtained from a  $\text{CH}_2\text{Cl}_2$  solution (2.5  $\mu\text{M}$ ). Due to the remarkably strong binding of **BC7**, the first fragmentation at high collision voltages is the cleavage of a covalent bond in the axle rather than dissociation of the crown ether. The loss of **DBC8** upon axle cleavage at the western ammonium station evidences the desired sequence in the **PRDBC8BC7** pseudo[3]rotaxane.

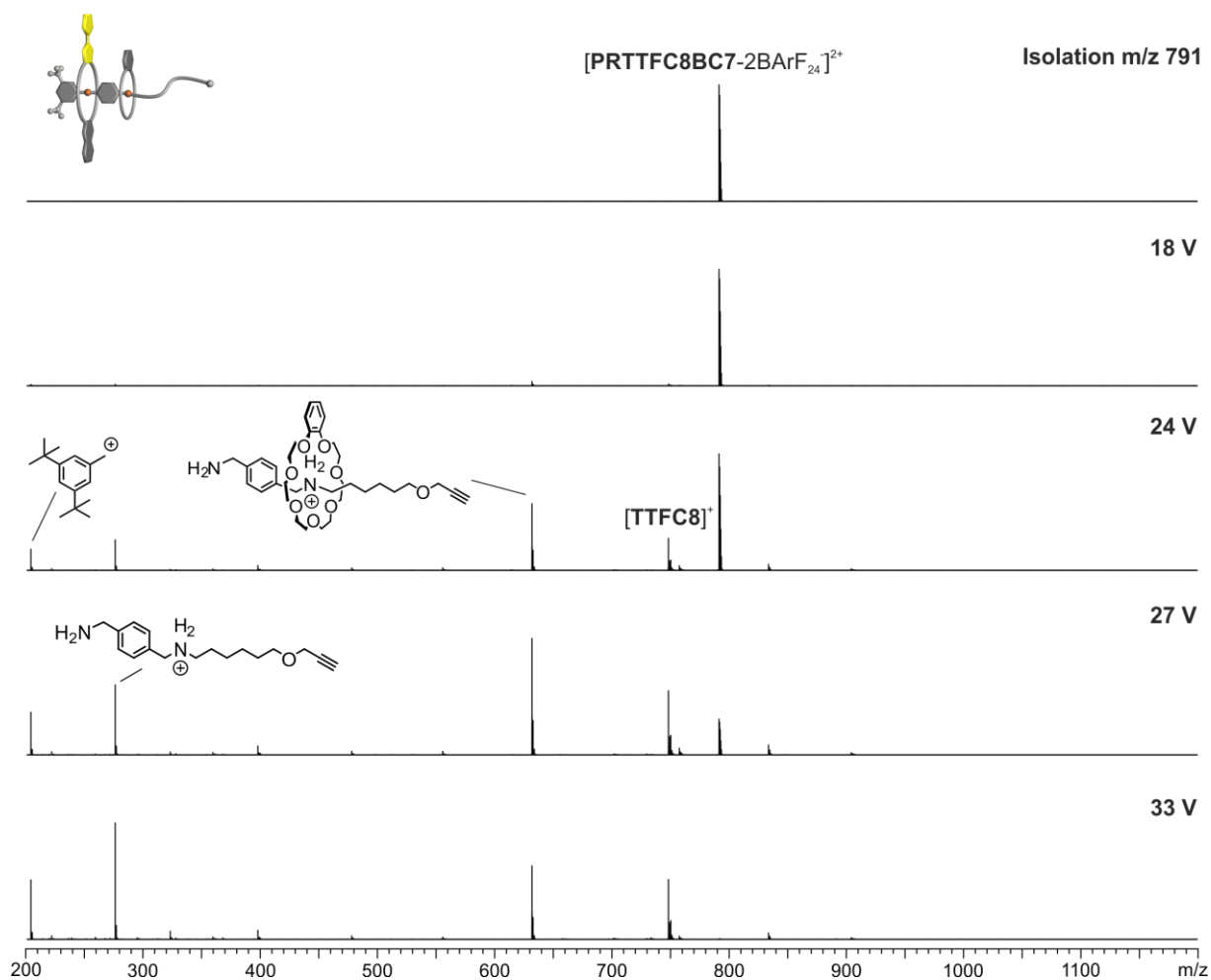


**Figure S37** CID experiment with mass-selected  $[PRTTFC8BC7-2BArF_{24}]^{2+}$  ions at  $m/z$  791 obtained from a  $CH_2Cl_2$  solution (2.5  $\mu M$ ). Due to the remarkably strong binding of **BC7**, the first fragmentation at high collision voltages is the cleavage of a covalent bond in the axle rather than dissociation of the crown ether. The loss of **TTFC8** upon cleavage of the axle at the western ammonium station evidences the desired sequence in the **PRTTFC8BC7** pseudo[3]rotaxane. The appearance of **TTFC8**<sup>+</sup> as a fragment has been observed for other mechanically interlocked structures containing **TTFC8**.<sup>1,8</sup>

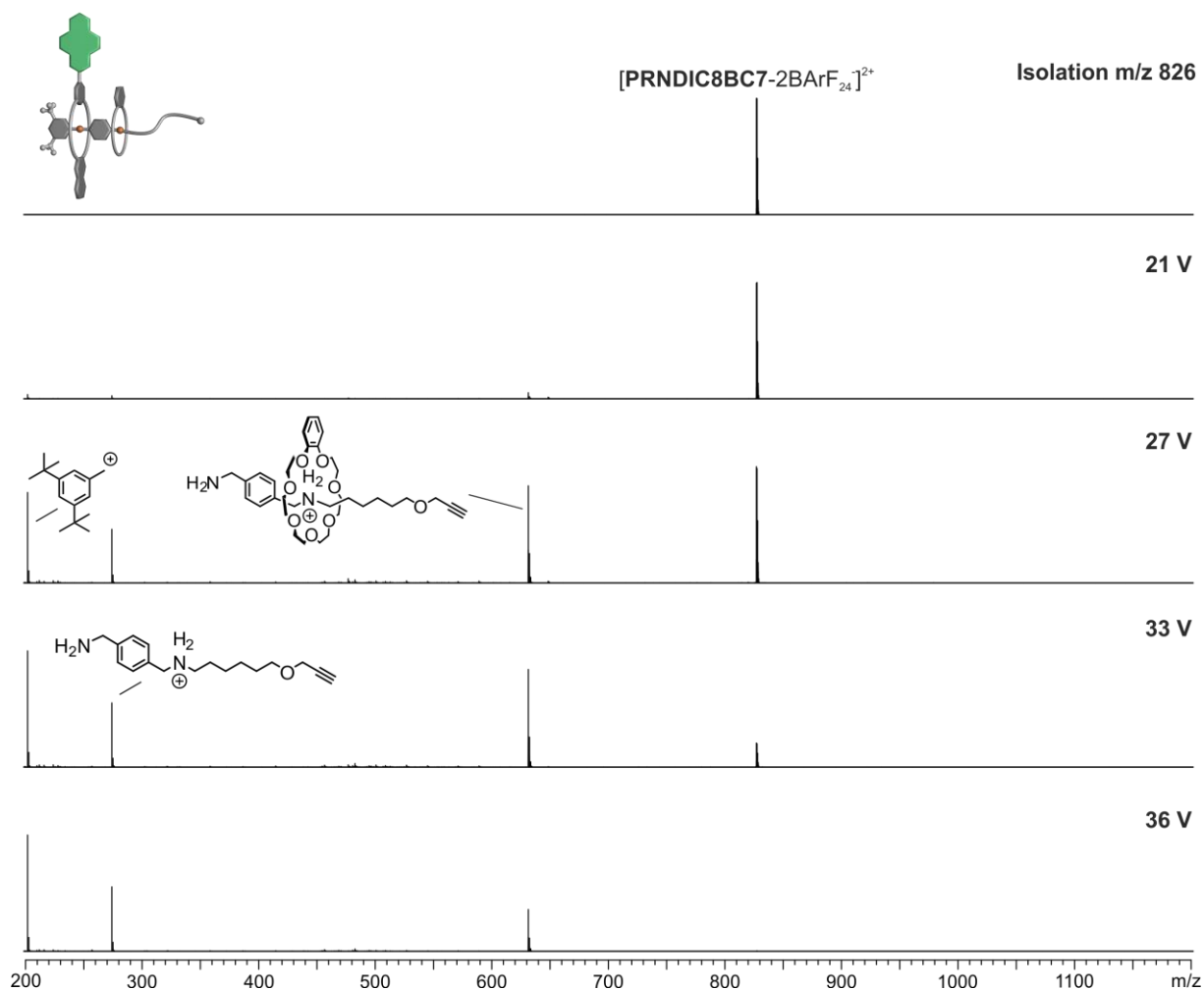


**Figure S38** CID experiment with mass-selected  $[\text{PRNDIC8BC7-2BArF}_{24}]^{2+}$  ions at  $m/z$  826 obtained from a  $\text{CH}_2\text{Cl}_2$  solution (2.5  $\mu\text{M}$ ). Due to the remarkably strong binding of **BC7**, the first fragmentation at high collision voltages is the cleavage of a covalent bond in the axle rather than dissociation of the crown ether. The loss of **NDIC8** upon cleavage of the axle at the western ammonium station evidences the desired sequence in the **PRNDIC8BC7** pseudo[3]rotaxane.

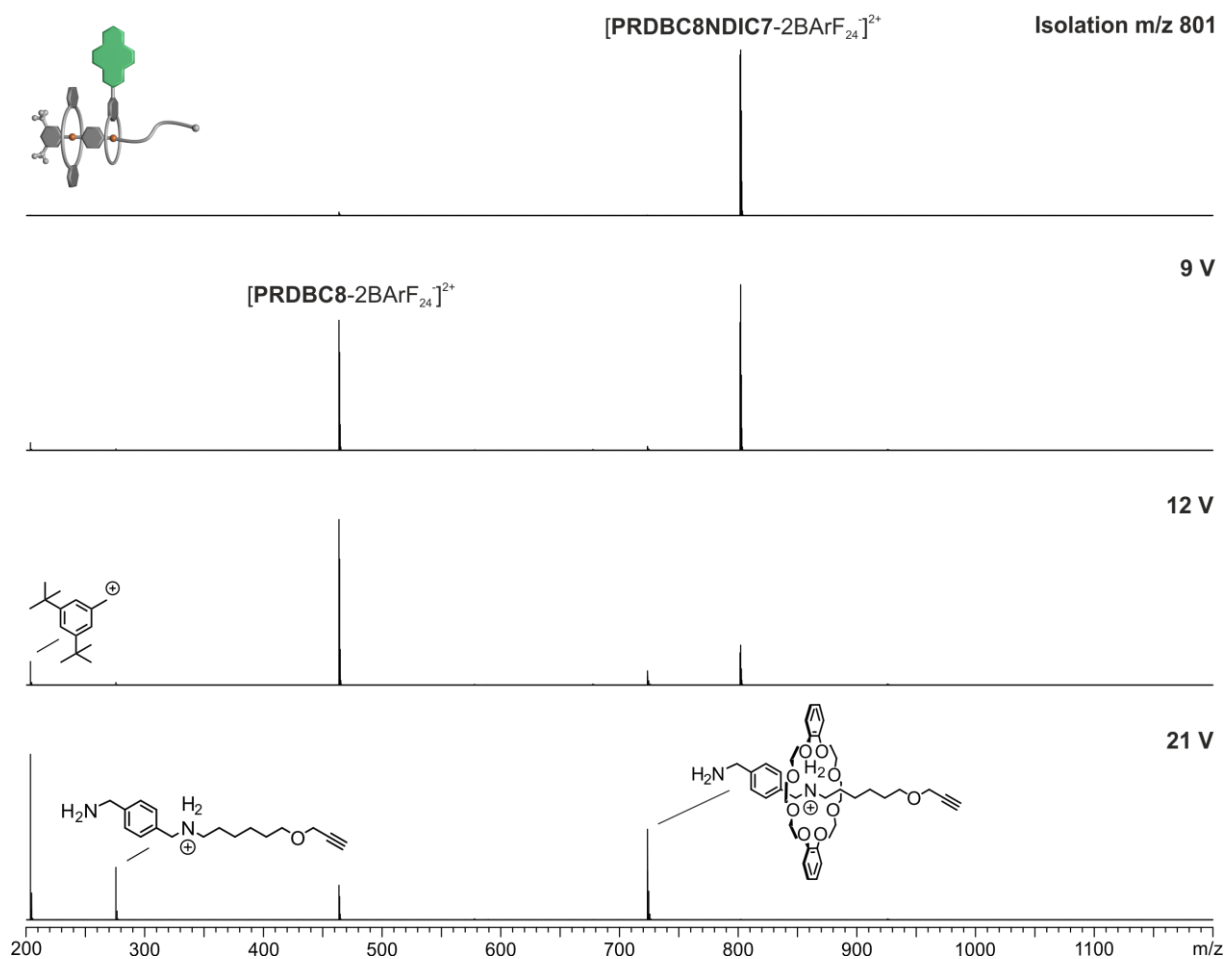


**Figure S39** CID experiment with mass-selected  $[PRDBC8NDIC7-2BArF_{24}]^{2+}$  ions at  $m/z$  801 obtained from a  $CH_2Cl_2$  solution (2.5  $\mu M$ ). The first fragmentation step at lower collision energies is the cleaving of the non-covalent bond to **NDIC7** to form the pseudo[2]rotaxane **PRDBC8**, which evidences the desired sequence in the **PRDBC8NDIC7** pseudo[3]rotaxane.

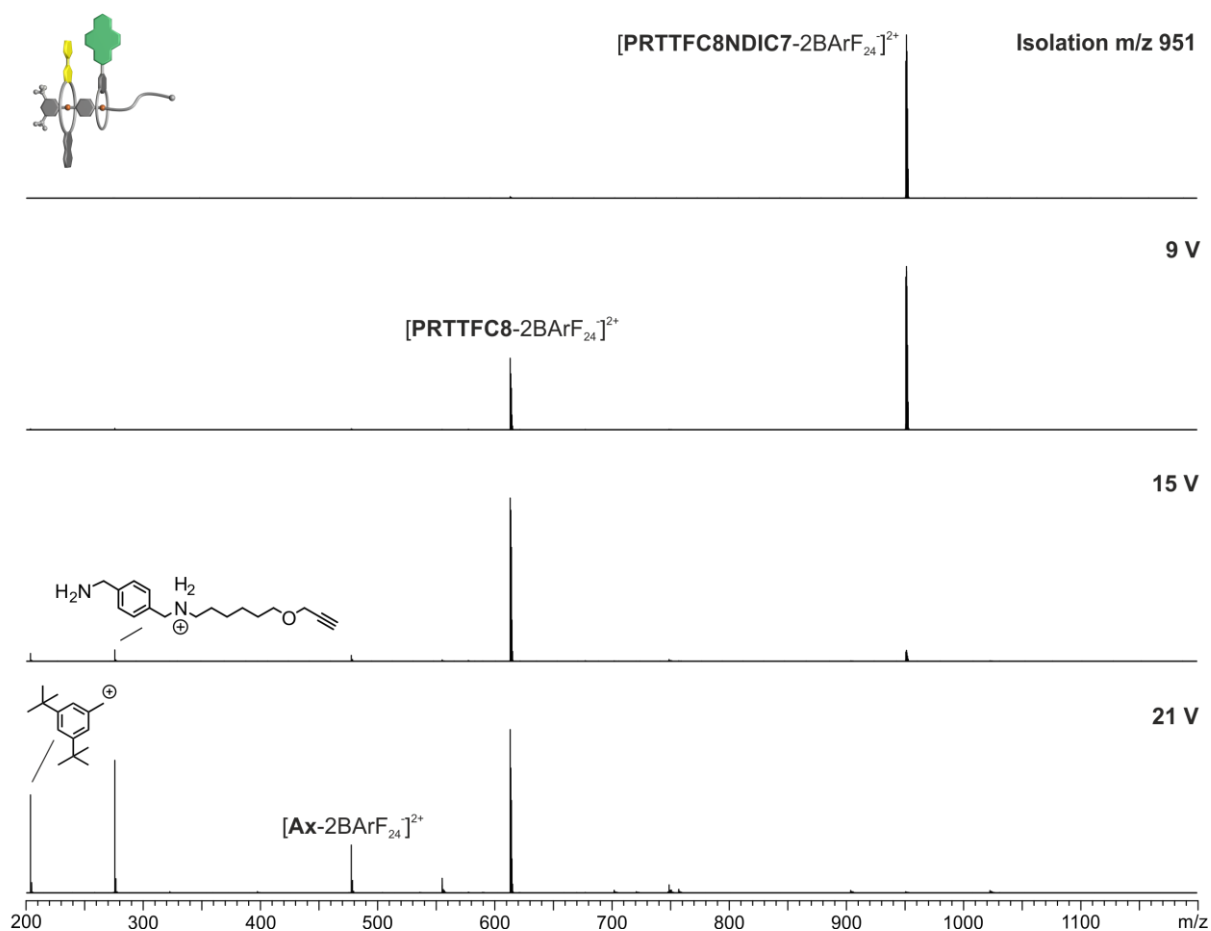


**Figure S40** CID experiment with mass-selected  $[PRTTFC8NDIC7-2BArF_{24}]^{2+}$  ions at  $m/z$  951 obtained from a  $CH_2Cl_2$  solution (2.5  $\mu M$ ). The first fragmentation step at lower collision energies is the cleavage of the non-covalent bond to **NDIC7** to form the pseudo[2]rotaxane **PRTTFC8**, which evidences the desired sequence in the **PRTTFC8NDIC7** pseudo[3]rotaxane.



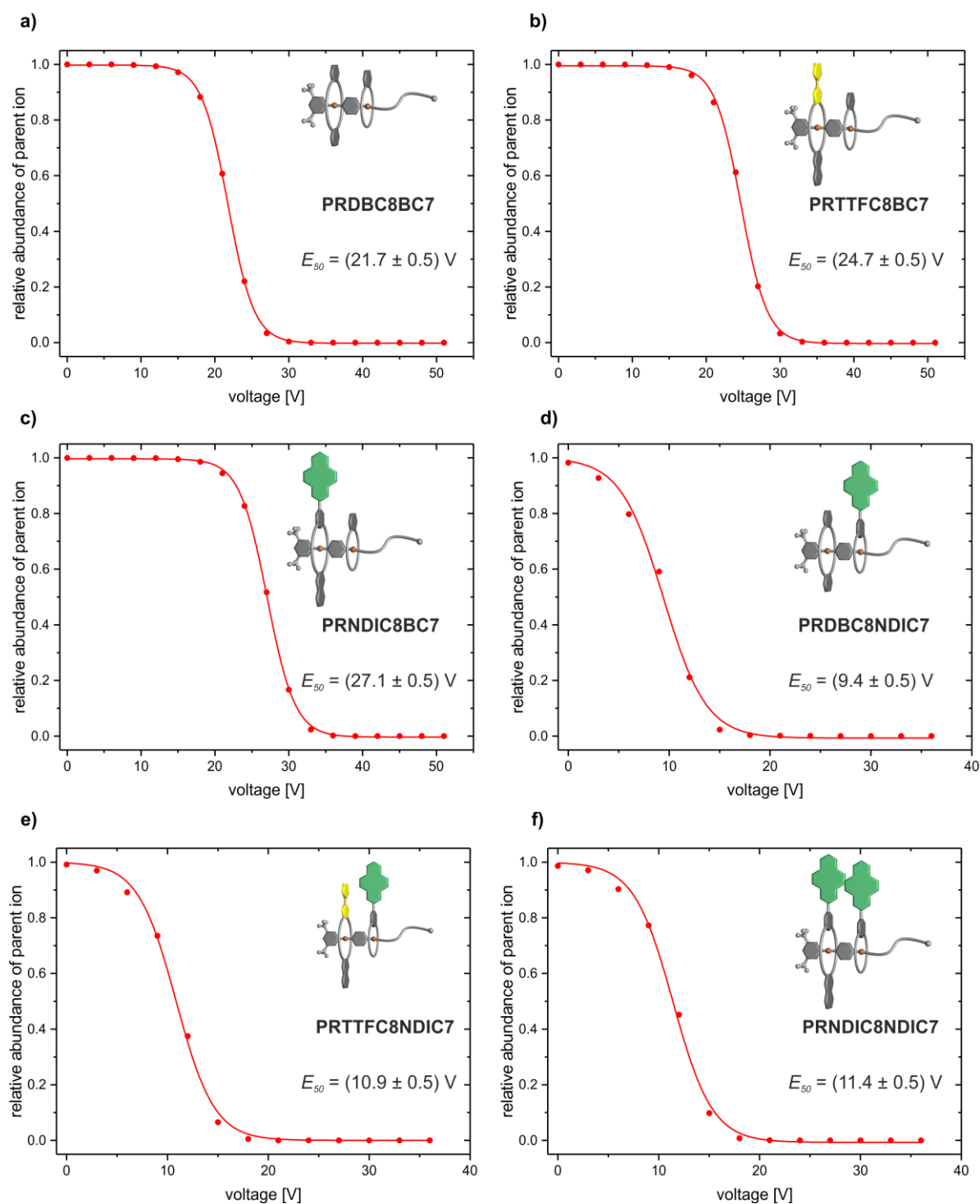


**Figure S42** Survival yield curves for the different hetero[3]pseudorotaxane under study. Dications of hetero[3]pseudorotaxanes were mass-selected and fragmented at increasing collision voltages. The solid lines represent a sigmoidal fitting to determine 50% survival yield voltages.

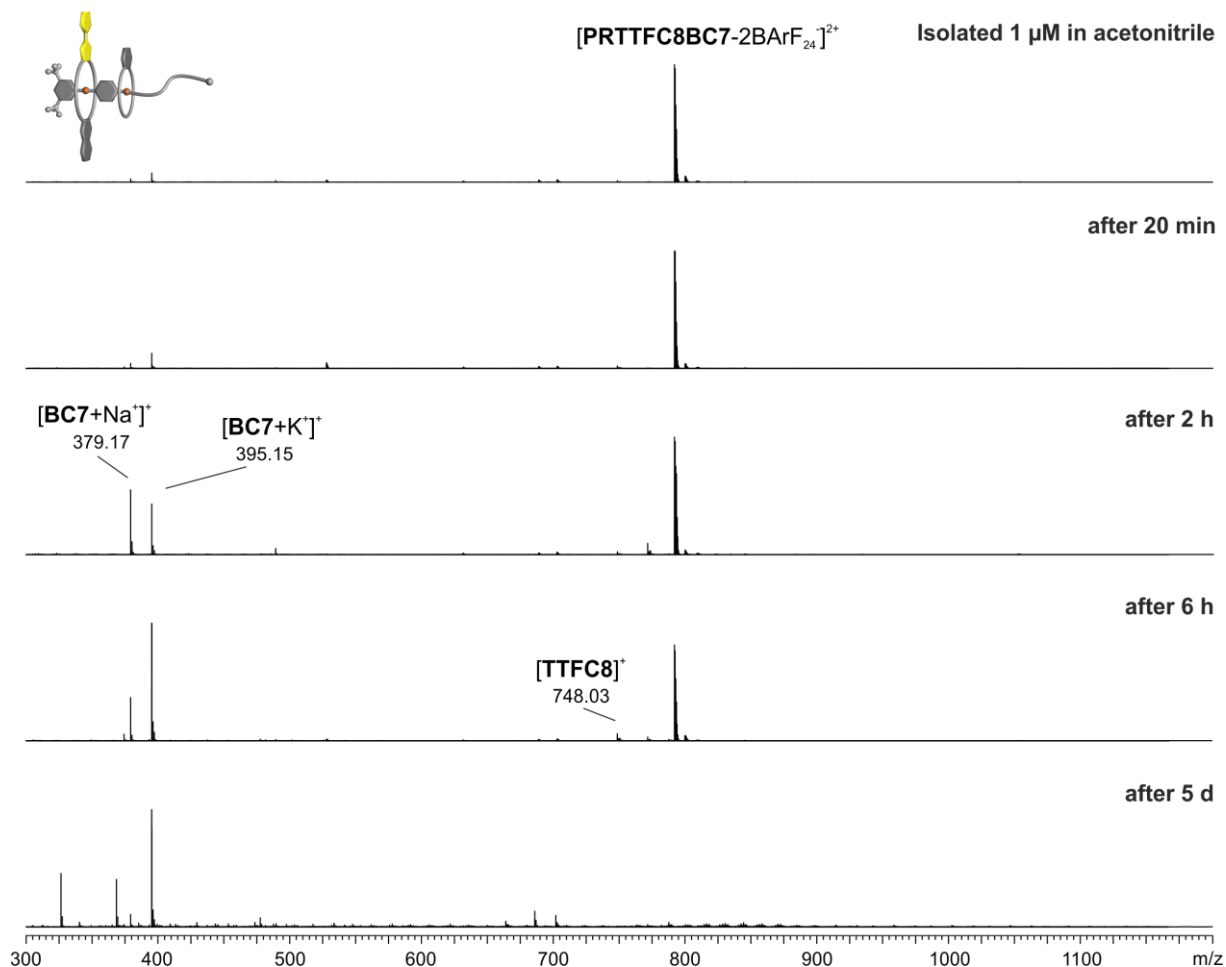


**Figure S43** ESI-Q-TOF-HRMS spectra of a **PRTTFC8BC7** solution in acetonitrile at different times (1  $\mu\text{M}$ , 25°C). The pronounced peak of **PRTTFC8BC7** after 6 h indicates the kinetic hinderance for dethreading of **BC7** and the kinetic stability of the pseudorotaxane **PRTTFC8BC7** in acetonitrile at low concentrations.

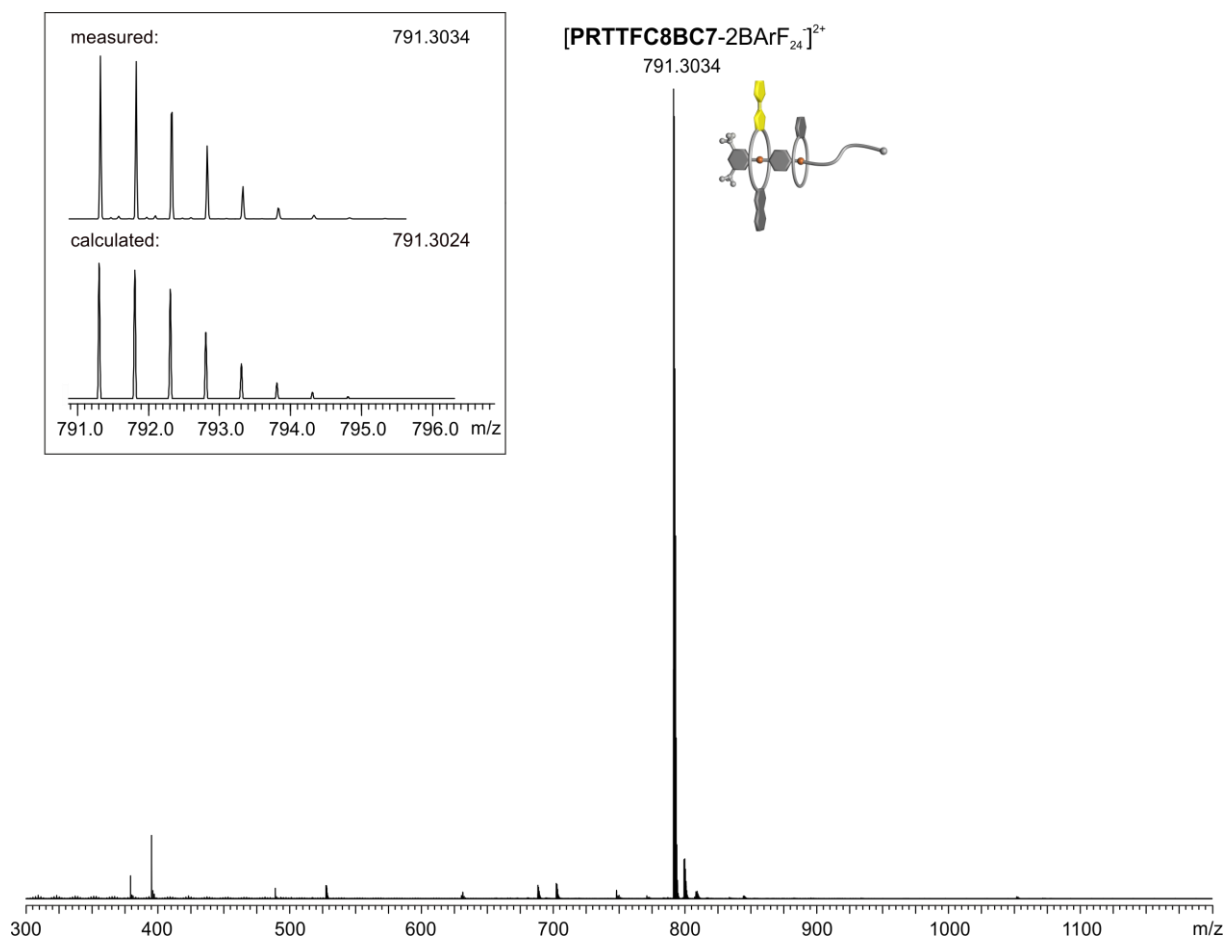


**Figure S44** ESI-Q-TOF-HRMS spectrum of **PRTTFC8BC7** (1  $\mu$ M in acetonitrile) isolated after column chromatography; inset: comparison of measured and calculated isotopic patterns.

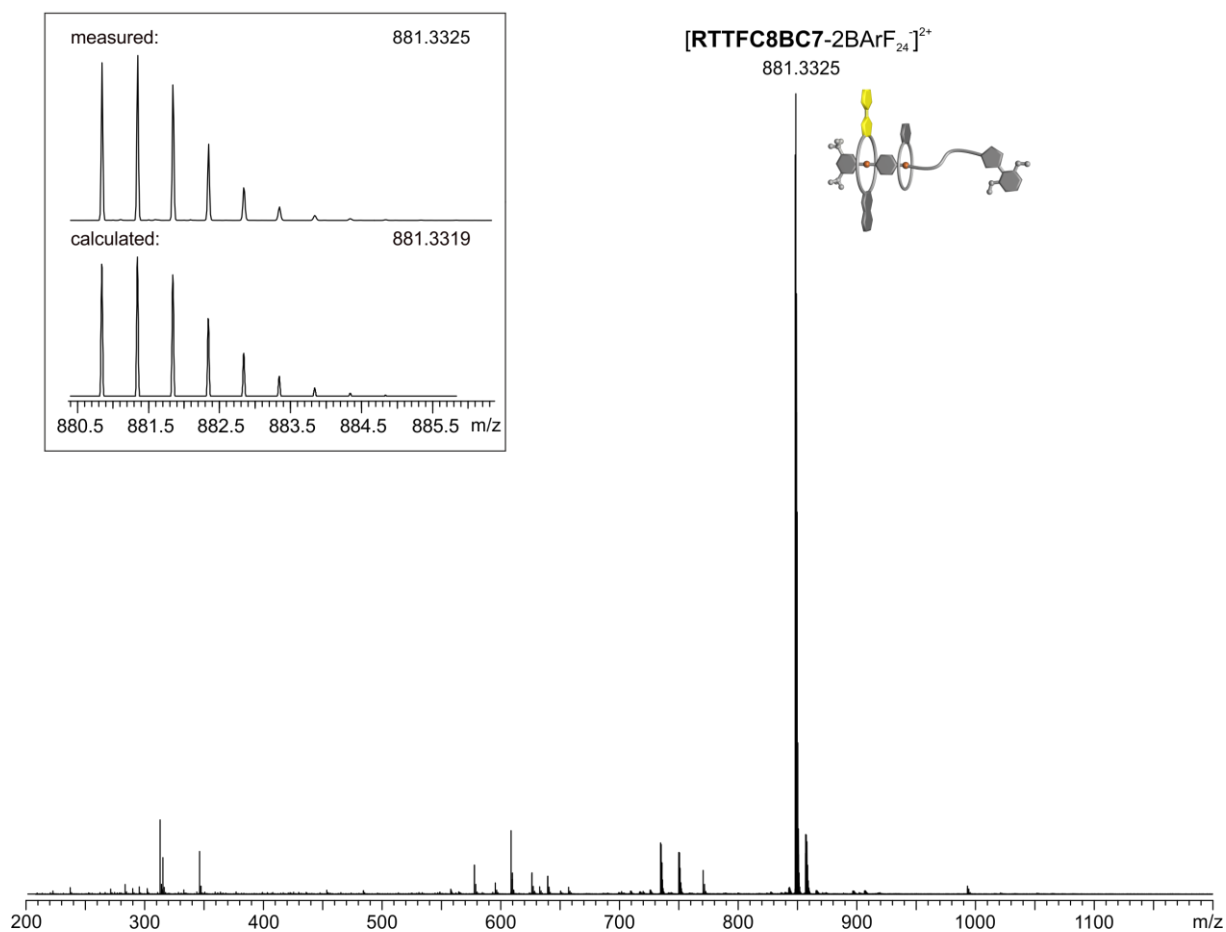


**Figure S45** ESI-Q-TOF-HRMS spectrum of **RTTFC8BC7** (1  $\mu$ M in acetonitrile); inset: comparison of measured and calculated isotopic patterns.

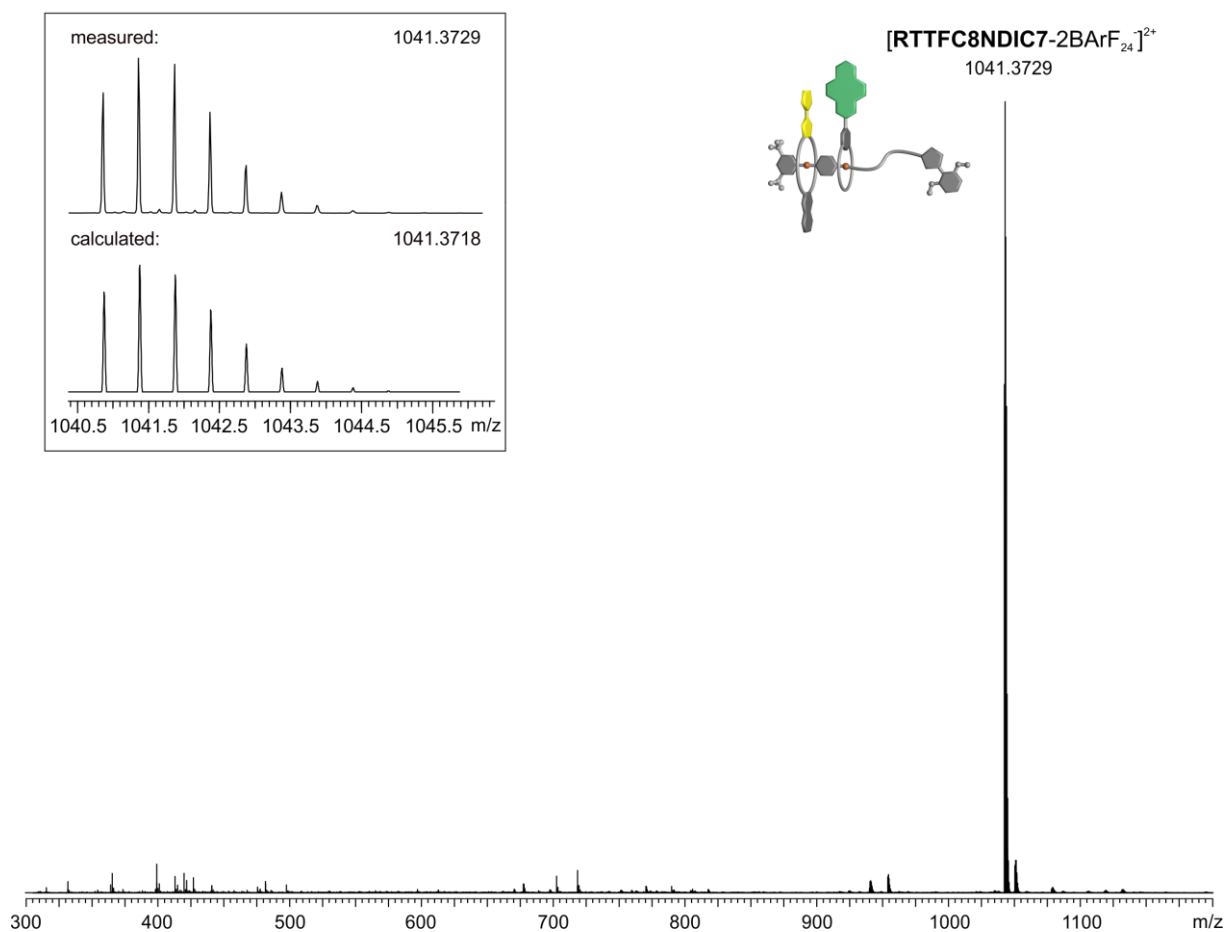


**Figure S46** ESI-Q-TOF-HRMS spectrum of **RTTFC8NDIC7** (1  $\mu$ M in acetonitrile); inset: comparison of measured and calculated isotopic patterns.

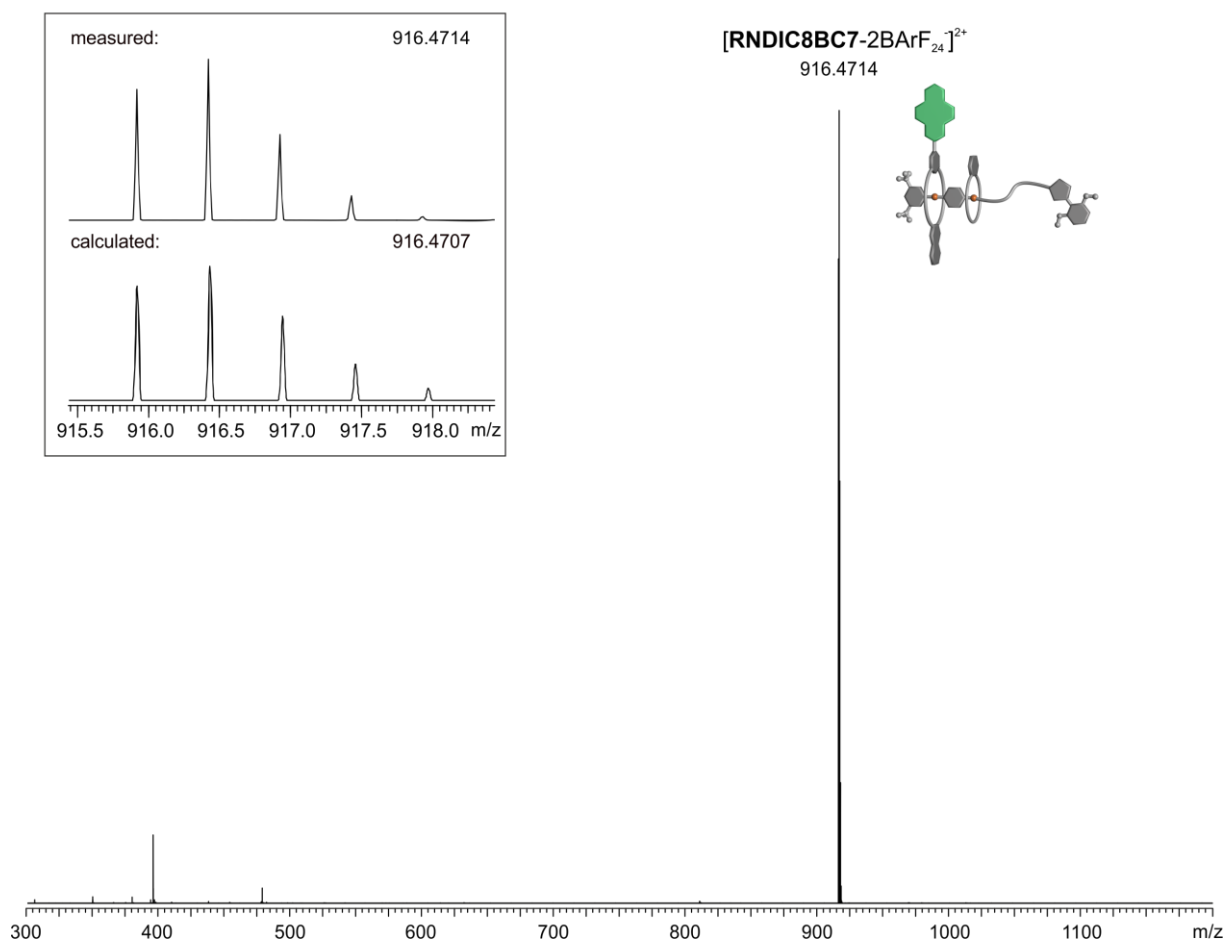


**Figure S47** ESI-Q-TOF-HRMS spectrum of **RNDIC8BC7** (1  $\mu$ M in acetonitrile); inset: comparison of measured and calculated isotopic patterns.

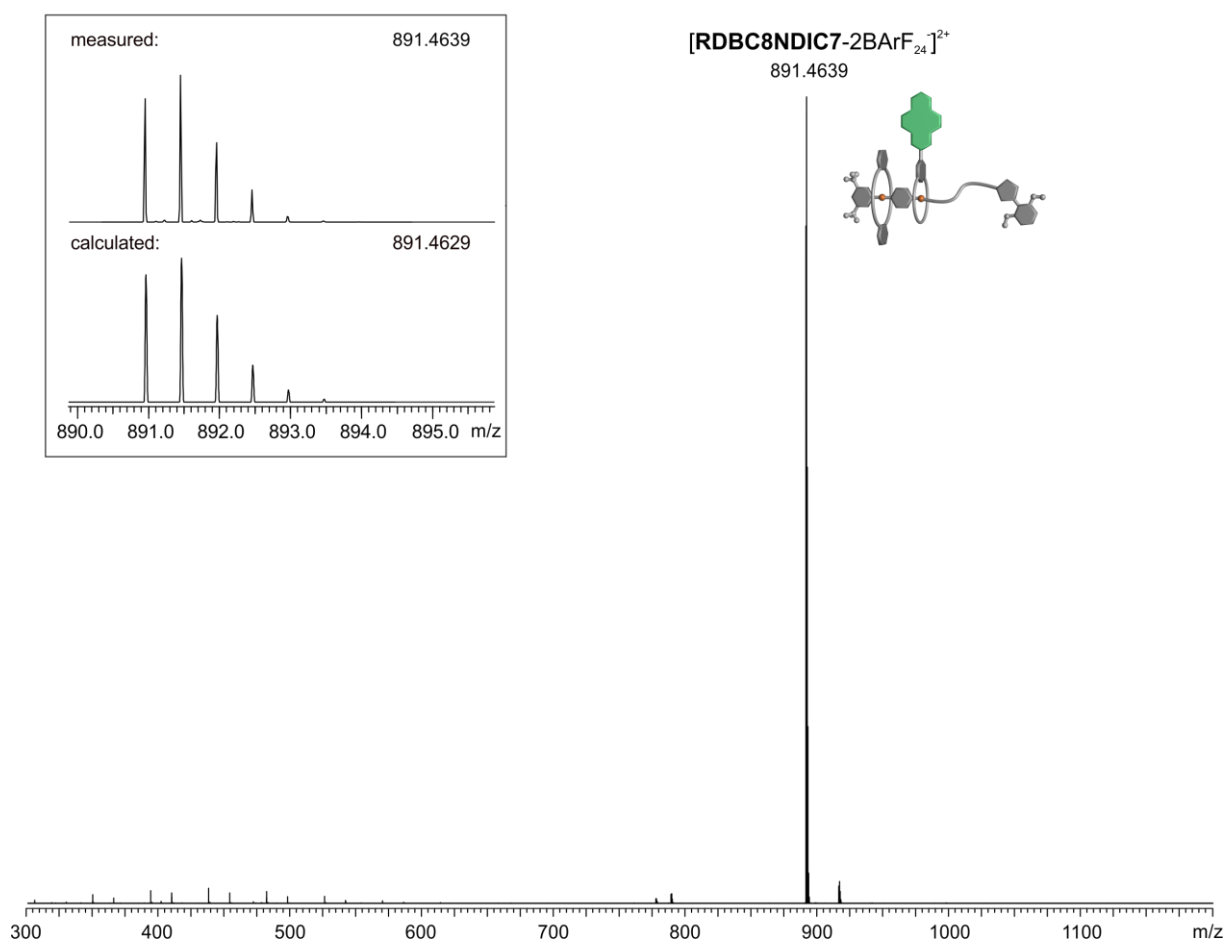


**Figure S48** ESI-Q-TOF-HRMS spectrum of **RDBC8NDIC7** (1  $\mu\text{M}$  in acetonitrile); inset: comparison of measured and calculated isotopic patterns.

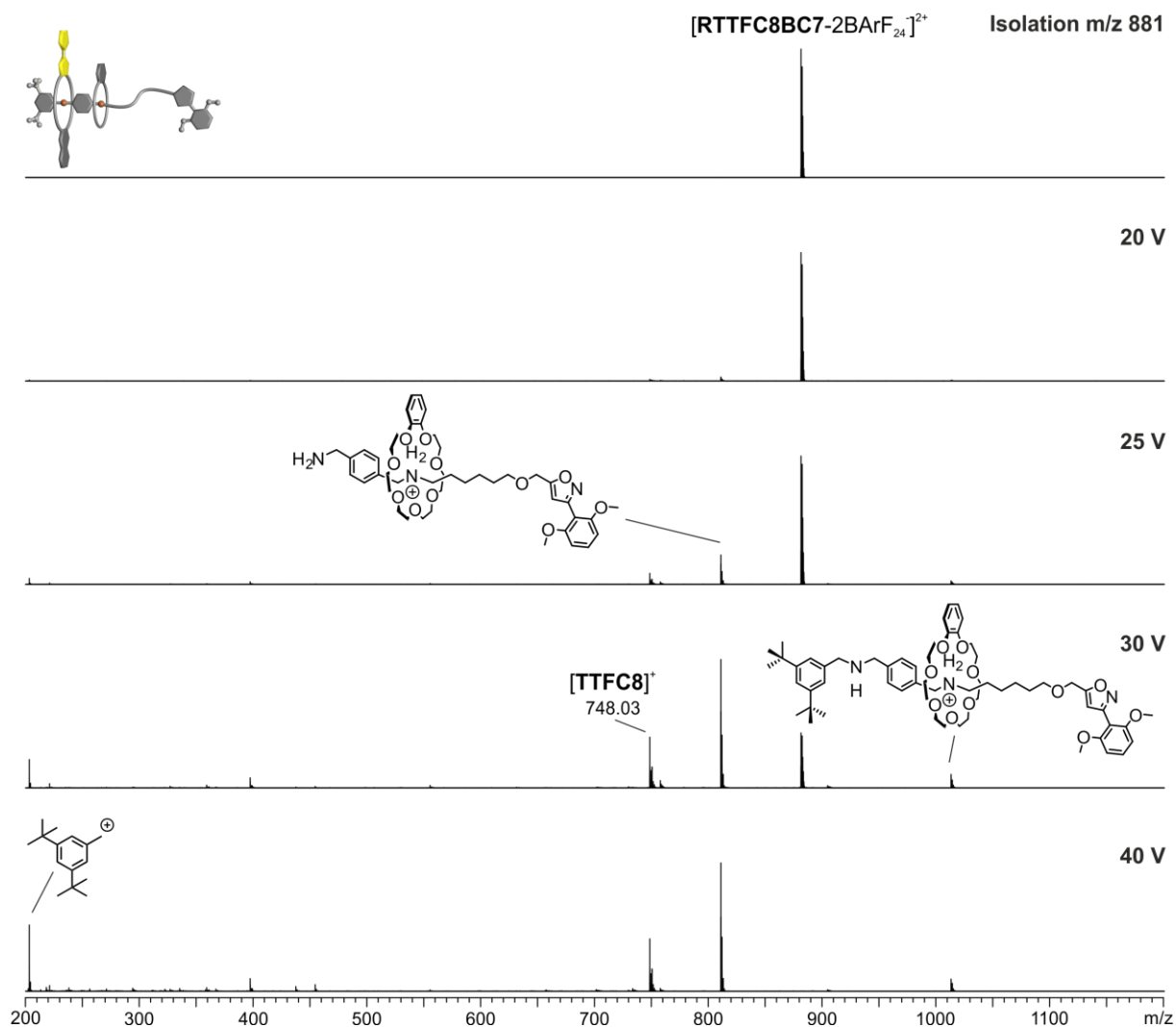


**Figure S49** CID experiment with mass-selected ions at  $m/z$  881 obtained from solution of **RTTFC8BC7** (1  $\mu\text{M}$  in acetonitrile). Higher voltages are necessary to induce fragmentation of **RTTFC8BC7** and as major fragments oxidized **TTFC8** and axle fragments are observed.

This is diagnostic for a mechanically interlocked structure.<sup>8,9</sup> The small amount of [2]rotaxane fragment at  $m/z$  1012 is formed by the opening and loss of **TTFC8** at high collision energies. The loss of **TTFC8** upon cleavage of the axle at the western ammonium station proves the desired sequence in the **RTTFC8BC7** [3]rotaxane.

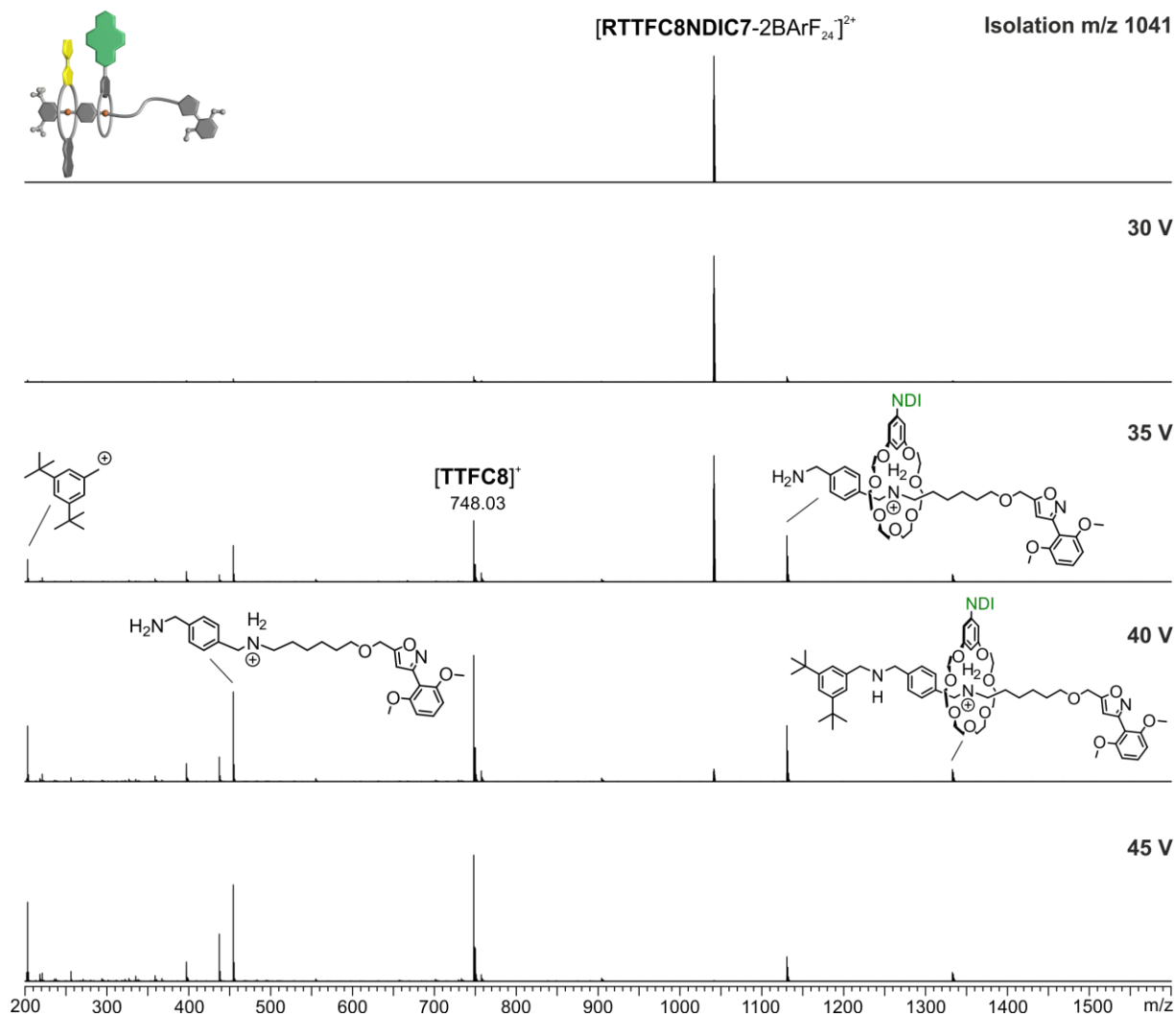


**Figure S50** CID experiment with mass-selected ions at  $m/z$  1041 obtained from solution of **RTTFC8NDIC7** ( $1 \mu\text{M}$  in acetonitrile). Higher voltages are necessary to induce fragmentation of **RTTFC8NDIC7** and as major fragments oxidized **TFC8** and axle fragments are observed. This is diagnostic for a mechanically interlocked structure.<sup>8,9</sup> The small amount of [2]rotaxane fragment at  $m/z$  1332 is formed by the opening and loss of **TFC8** at high collision energies. The loss of **TFC8** upon cleavage of the axle at the western ammonium station proves the desired sequence in the **RTTFC8NDIC7** [3]rotaxane.

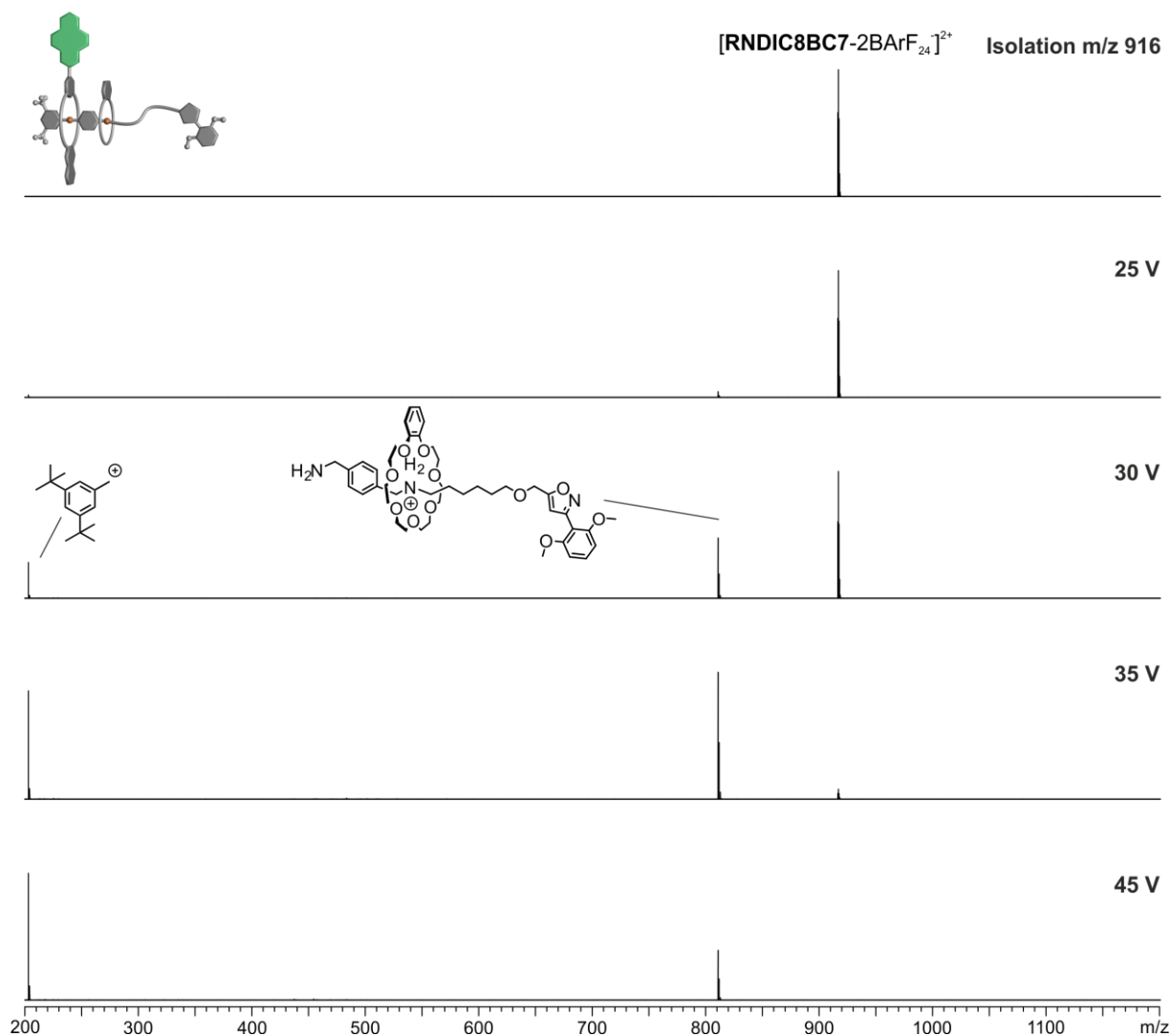


**Figure S51** CID experiment with mass-selected ions at  $m/z$  916 obtained from solution of **RNDIC8BC7** (1  $\mu$ M in acetonitrile). Higher voltages are necessary to induce fragmentation of **RNDIC8BC7** and only axle fragments are observed. This is diagnostic for a mechanically interlocked structure.<sup>3</sup> The loss of **NDIC8** upon cleavage of the axle at the western ammonium station proves the desired sequence in the **RNDIC8BC7** [3]rotaxane.

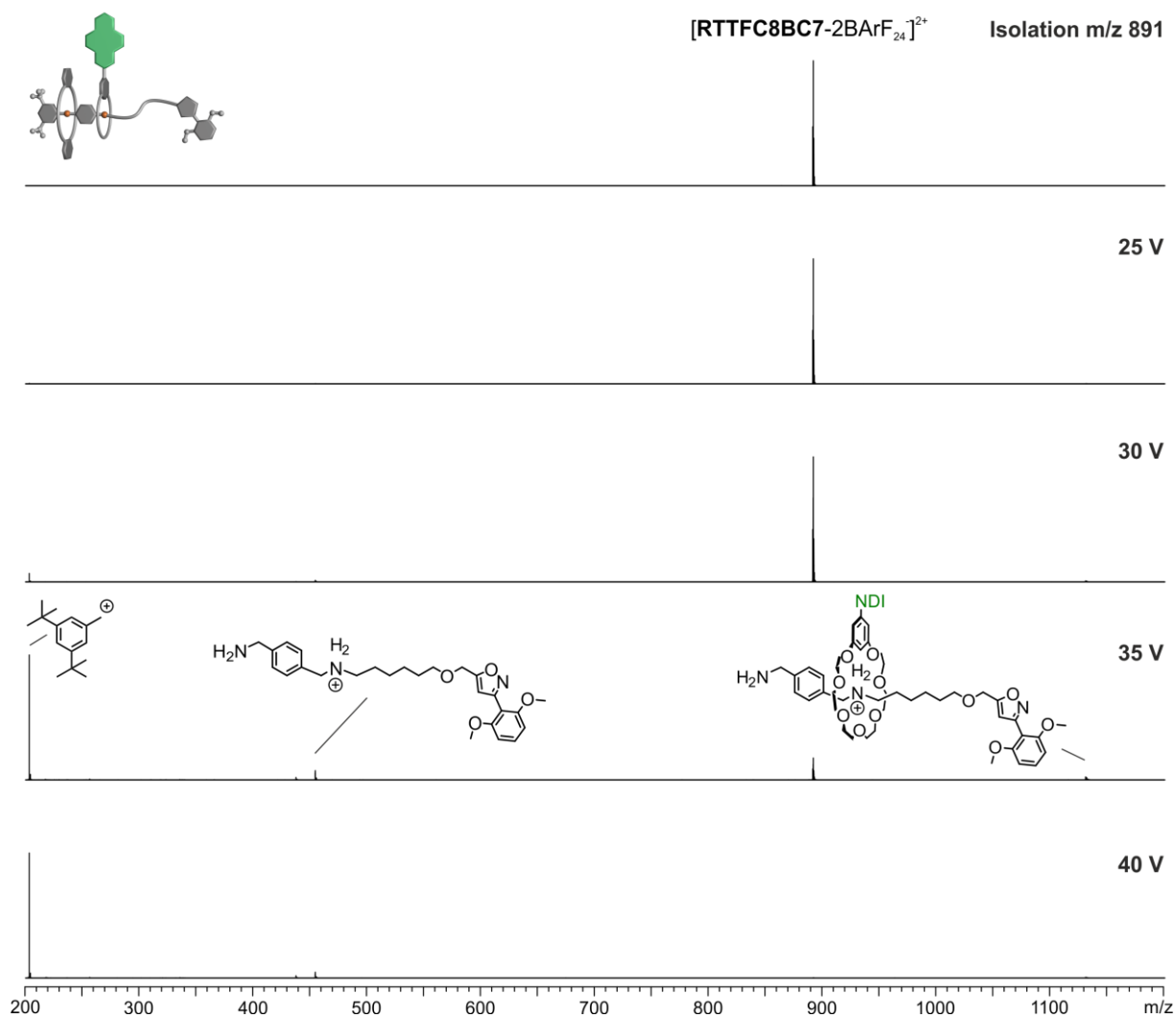


**Figure S52** CID experiment with mass-selected ions at  $m/z$  891 obtained from solution of **RDBC8NDIC7** (1  $\mu\text{M}$  in acetonitrile). Higher voltages are necessary to induce fragmentation of **RDBC8NDIC7** and only axle fragments are observed. This is diagnostic for a mechanically interlocked structure.<sup>3</sup> The loss of **DBC8** upon cleavage of the axle at the western ammonium station proves the desired sequence in the **RDBC8NDIC7** [3]rotaxane.

## 5. Electrochemical measurements

Redox-potentials reported in this study were obtained by DPV. All measurements were at least conducted twice. Measurements were conducted in 1,2-dichloroethane (DCE) with 0.1 M electrolyte and 1.5 mM analyte concentration.

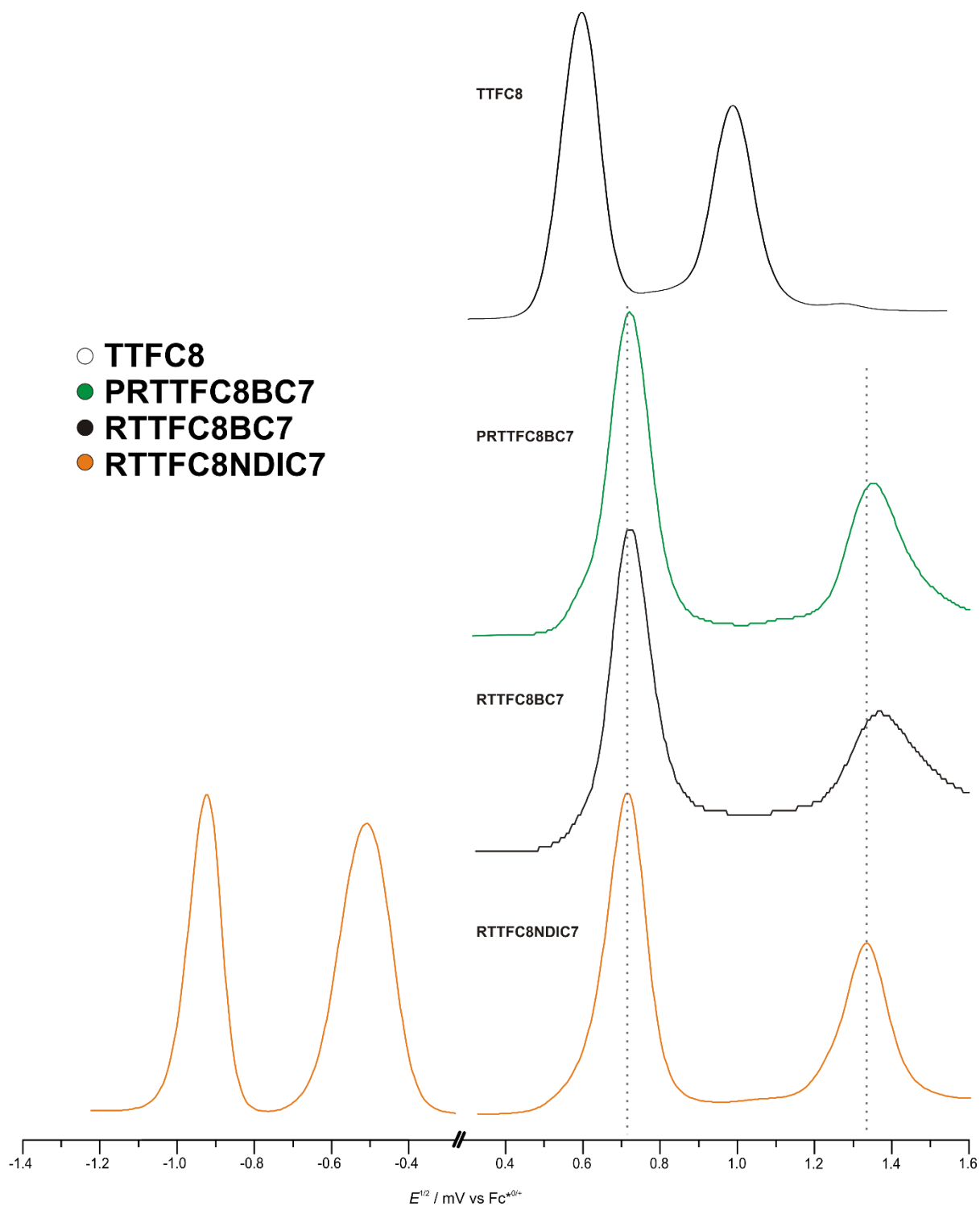


**Fig. S53** Stacked differential pulse voltammograms (DPV, 10 mV/s scan rate, 25 mV modulation amplitude, 50 ms modulation time, 5 mV step potential, 0.5 s interval time) (DCE,  $n\text{-Bu}_4\text{NBArF}_{24}$ , 298 K) of **TTFC8**, **PRTTFC8BC7**, **RTTFC8BC7**, **RTTFC8NDIC7**.

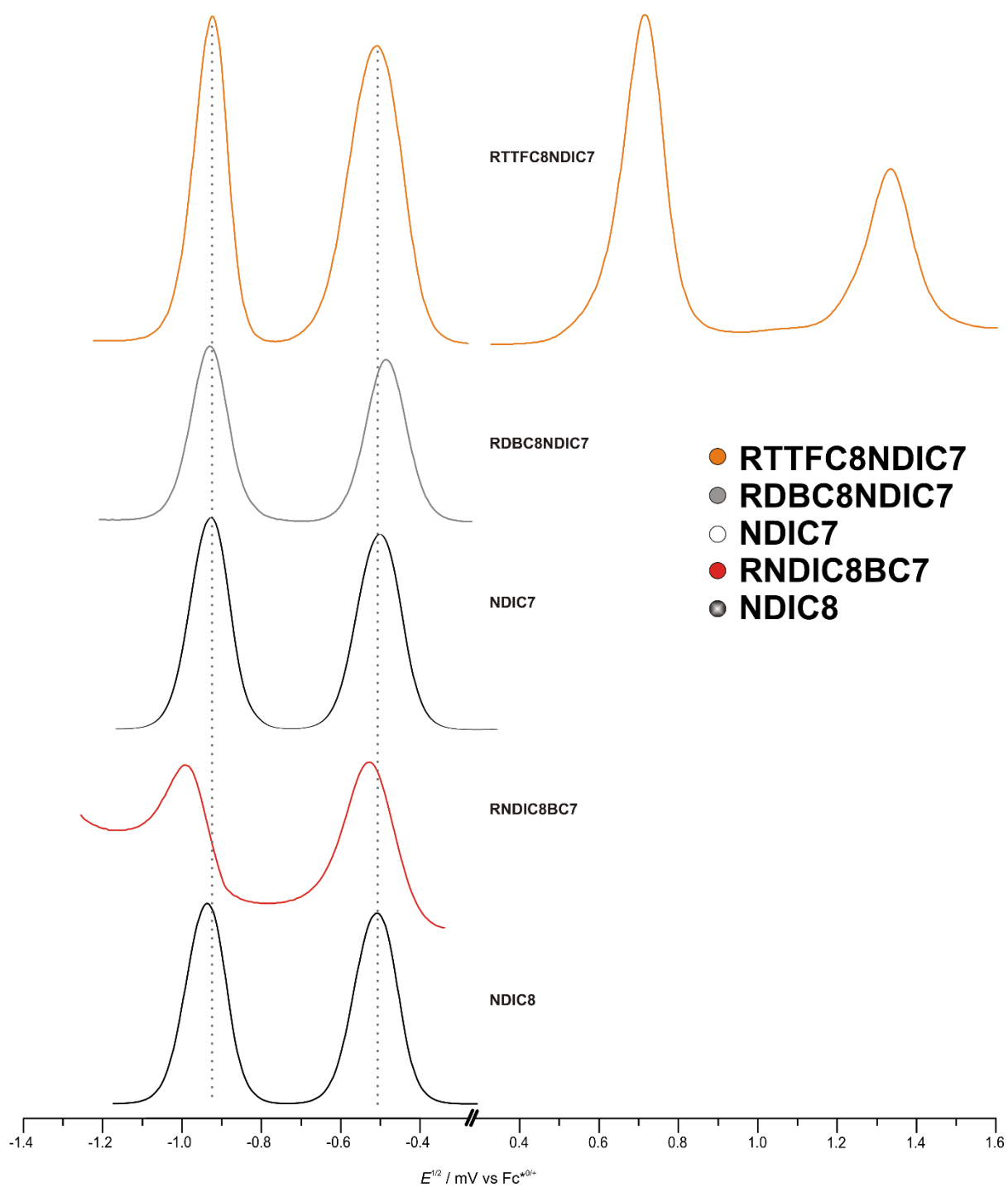


**Fig. S54** Stacked differential pulse voltammograms (DPV, 10 mV/s scan rate, 25 mV modulation amplitude, 50 ms modulation time, 5 mV step potential, 0.5 s interval time) (DCE, n-Bu<sub>4</sub>NBArF<sub>24</sub>, 298 K) of **RTTFC8NDIC7**, **RDBC8NDIC7**, **NDIC7**, **RNDIC8BC7**, **NDIC8**.

**Tab. S2** Electrochemical data obtained from DPV measurements (DCE, with n-Bu<sub>4</sub>NBArF<sub>24</sub> as the electrolyte, 298 K).

<b>-II / mV</b>	<b>-I / mV</b>	<b>species</b>	<b>+I / mV</b>	<b>+II / mV</b>
		<b>TTFC8</b>	594	987
		<b>RTTFC8<sup>8</sup></b>	694	1349
		<b>PRTTFC8BC7</b>	720	1349
		<b>RTTFC8BC7</b>	725	1369
-921	-508	<b>RTTFC8NDIC7</b>	720	1329
-932	-489	<b>RDBC8NDIC7</b>		
-921	-498	<b>NDIC7</b>		
-992	-529	<b>RNDIC8BC7</b>		
-937	-509	<b>NDIC8</b>		

## 6. UV/Vis experiments

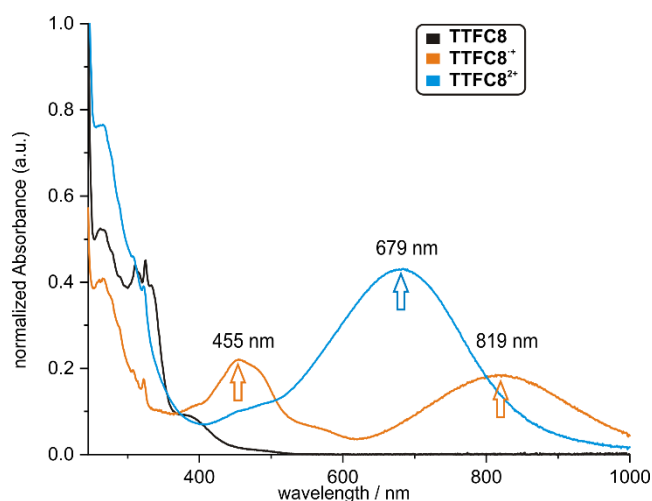


**Fig. S55** UV/Vis spectra of **TTFC8** (15 μM in CH<sub>2</sub>Cl<sub>2</sub>, 298 K, excess bulk Fe(ClO<sub>4</sub>)<sub>3</sub> as the oxidant) in the TTF<sup>0</sup>, TTF<sup>+</sup> and TTF<sup>2+</sup> state.

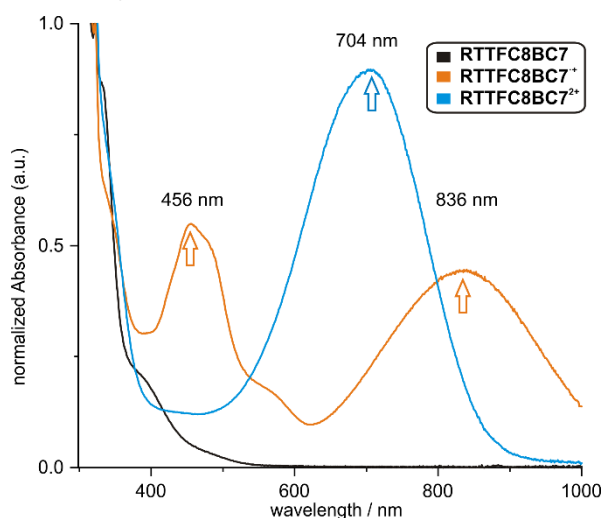


**Fig. S56** UV/Vis spectra of **RTTFC8BC7** (15 μM in CH<sub>2</sub>Cl<sub>2</sub>, 298 K, excess bulk Fe(ClO<sub>4</sub>)<sub>3</sub> as the oxidant) in the TTF<sup>0</sup>, TTF<sup>+</sup> and TTF<sup>2+</sup> state.

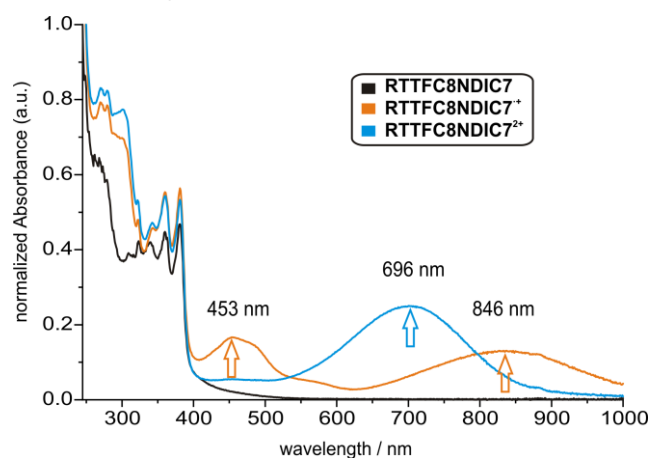


**Fig. S57** UV/Vis spectra of **RTTFC8NDIC7** (15 μM in CH<sub>2</sub>Cl<sub>2</sub>, 298 K, excess bulk Fe(ClO<sub>4</sub>)<sub>3</sub> as the oxidant) in the TTF<sup>0</sup>, TTF<sup>+</sup> and TTF<sup>2+</sup> state.

**Tab. S3** Absorption maxima of TTF<sup>•+</sup> and TTF<sup>2+</sup> in different species (15 μM in CH<sub>2</sub>Cl<sub>2</sub>, 298 K, bulk Fe(ClO<sub>4</sub>)<sub>3</sub> as the oxidant).

species	+I / nm	+II / nm
<b>TTFC8</b>	455, 819	679
<b>RTTFC8BC7</b>	456, 836	704
<b>RTTFC8NDIC7</b>	453, 846	696

The photometric titrations of hetero[3]rotaxanes **RTTFC8BC7** and **RTTFC8NDIC7** with Fe(ClO<sub>4</sub>)<sub>3</sub> show bands similar to those of free wheel **TTFC8** for the three redox states (TTF, TTF<sup>•+</sup> and TTF<sup>2+</sup>).<sup>10</sup> In contrast to a fixed conformation divalent donor-acceptor rotaxane<sup>11</sup> with TTF and NDI, no intramolecular charge transfer band is observable.

## 7. Computational details

A conformational scan of the potential energy surface using Grimme's GFN2-xTB code<sup>12</sup> was conducted for compound **RTTFC8NDIC7** and **RNDIC8BC7** to obtain the most stable structures. Compound **RTTFC8NDIC7** was optimised in charge states 1+, 2+, and 3+, respectively, at the PBEh-3c<sup>13</sup> level of DFT in combination with the COSMO<sup>14</sup> solvation model ( $\epsilon = 8.9$  for  $\text{CH}_2\text{Cl}_2$ )<sup>15</sup> employing the Turbomole program package (Version 7.4).<sup>16</sup> Subsequent single point calculations for an accurate description of the electronic structure were performed at the  $\omega\text{B97X-D3/def2-TZVP}$ <sup>17</sup> level using the CPCM<sup>18</sup> solvent model and the ORCA program package.<sup>19</sup> Spin densities were generated with ORBKIT.<sup>20</sup>

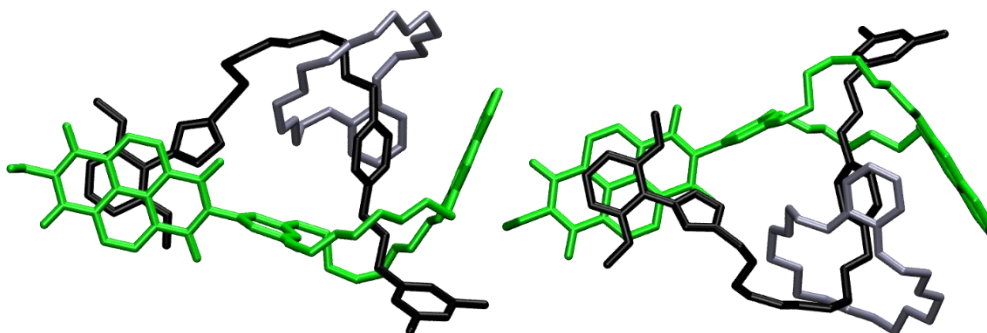


**Fig. S58** Optimised structure of compound **RNDIC8BC7** illustrating the efficient stacking between the NDI and stopper moiety.

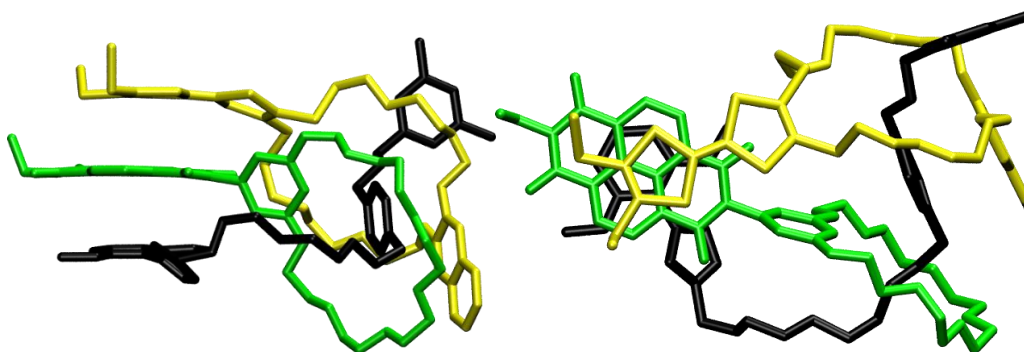


**Fig. S59** Optimised structure of compound **RTTFC8NDIC7** illustrating the efficient stacking between the TTF, NDI and stopper moieties.

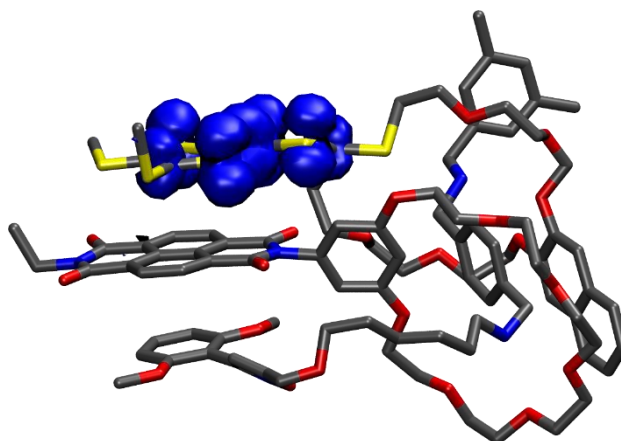


**Fig. S60** Spin density of **RTTFC8NDIC7<sup>+</sup>** localised on the TTF moiety, isovalue =  $0.001 a_0^{-3}$ .

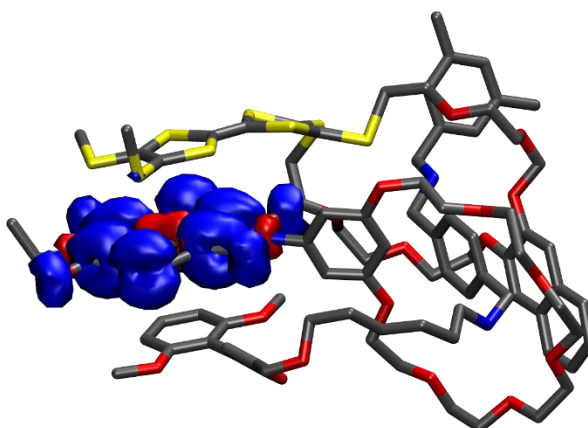


**Fig. S61** Spin density of **RTTFC8NDIC7<sup>-</sup>** localised on the NDI moiety, isovalue =  $0.001 a_0^{-3}$ .

The spin density plots confirm the retained redox-behaviour of the macrocycles within the rotaxane.

## 8. Crystallographic data

The crystals were grown by diffusing pentane into a sat. acetonitrile solution of **NDIC7**. X-ray data were collected on a BRUKER D8 Venture system. Data were collected at 100(2) K using graphite-monochromated Mo K $\alpha$  radiation ( $\lambda_{\alpha} = 0.71073 \text{ \AA}$ ). The strategy for data collection was evaluated by using the Smart software. The data were collected by the standard “ $\psi$ - $\omega$  scan techniques” and were scaled and reduced using Saint+software. The structures were solved by using Olex2,<sup>21</sup> the structure was solved with the XT<sup>22</sup> structure solution program using Intrinsic Phasing and refined with the XL refinement package<sup>23</sup> using Least Squares minimization. Bond length and angles were measured with Diamond Crystal and Molecular Structure Visualization Version 4.6.2.<sup>24</sup> Drawings were generated with POV-Ray.<sup>25</sup> Deposition number CCDC 2047286 contains the supplementary crystallographic data for this paper. These data are provided free of charge by the joint Cambridge Crystallographic Data Centre and Fachinformationszentrum Karlsruhe Access Structures service [www.ccdc.cam.ac.uk/structures](http://www.ccdc.cam.ac.uk/structures).

**Tab. S4** Crystal data of **NDIC7**.

<b>Compound</b>	<b>NDI-MC • ACN</b>
<b>Empirical formula</b>	C <sub>38</sub> H <sub>43</sub> O <sub>11</sub> N <sub>3</sub>
<b>Formula weight</b>	717.75
<b>Temperature/K</b>	100
<b>Crystal system</b>	triclinic
<b>Space group</b>	P $\bar{1}$
<b>a/Å</b>	8.908(11)
<b>b/Å</b>	8.969(9)
<b>c/Å</b>	26.350(3)
<b><math>\alpha</math>/°</b>	84.32(7)
<b><math>\beta</math>/°</b>	85.34(6)
<b><math>\gamma</math>/°</b>	64.95(7)
<b>Volume/Å<sup>3</sup></b>	1896(4)
<b>Z</b>	2
<b><math>\rho_{\text{calc}}/\text{g} \cdot \text{cm}^3</math></b>	1.257
<b><math>\mu/\text{mm}^{-1}</math></b>	0.093
<b>F(000)</b>	760.0
<b>Crystal size/mm<sup>3</sup></b>	0.871 x 0.531 x 0.381
<b>Crystal shape</b>	plate
<b>Radiation</b>	MoK $\alpha$ ( $\lambda$ = 0.71073)
<b>2<math>\theta</math> range for data collection/°</b>	4.664 to 50.996
<b>Index ranges</b>	-10 $\leq$ h $\leq$ 10, -10 $\leq$ k $\leq$ 10, -31 $\leq$ l $\leq$ 31
<b>Reflections collected</b>	42858
<b>Independent reflections</b>	6884 [ $R_{\text{int}}$ = 0.0560, $R_{\text{sigma}}$ = 0.0363]
<b>Data/restraints/parameters</b>	6884/0/625
<b>Goodness-of-fit on F<sup>2</sup></b>	1.057
<b>Final R indexes [<math>I \geq 2\sigma(I)</math>]</b>	$R_1$ = 0.0553, $wR_2$ = 0.1315
<b>Final R indexes [all data]</b>	$R_1$ = 0.0673, $wR_2$ = 0.1385
<b>Largest diff. peak/hole / e<math>\cdot</math>Å<sup>3</sup></b>	0.26/-0.35

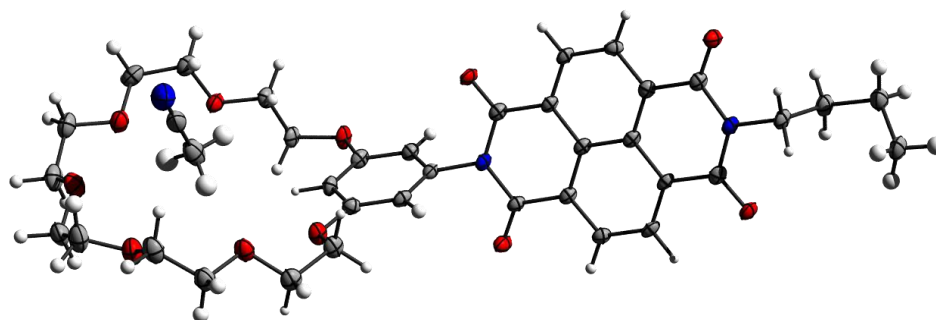


**Fig. S62** Asymmetric unit cell of **NDIC7**.

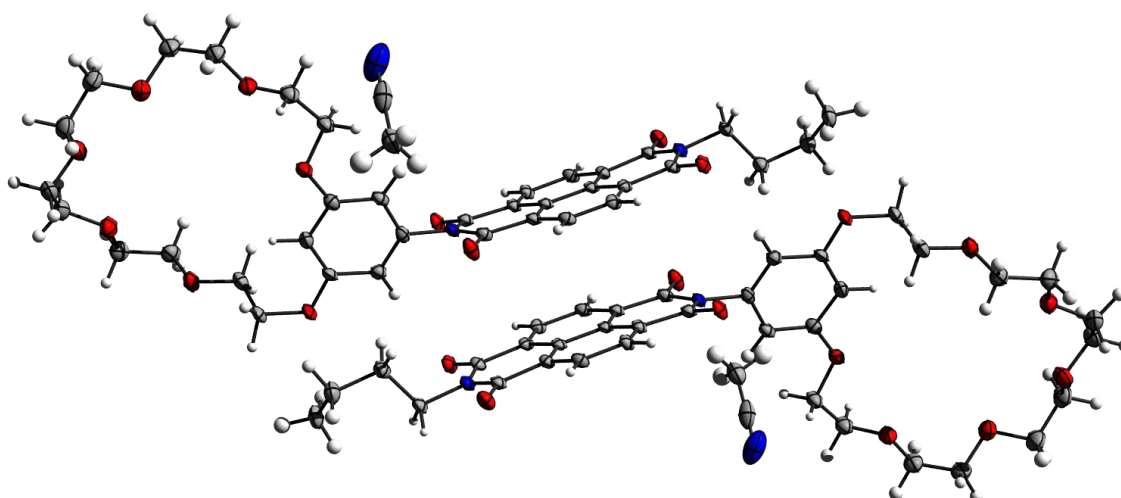


**Fig. S63** Crystal packing of two **NDIC7**, with NDI-NDI plane distance of 3.27 Å.

## 9. References

1. H. V. Schröder, S. Sobottka, M. Nößler, H. Hupatz, M. Gaedke, B. Sarkar and C. A. Schalley, *Chem. Sci.*, 2017, **8**, 6300-6306.
2. T. Matsumura, F. Ishiwari, Y. Koyama and T. Takata, *Org. Lett.*, 2010, **12**, 3828-3831.
3. H. Hupatz, M. Gaedke, H. V. Schröder, J. Beerhues, A. Valkonen, F. Klautzsch, S. Müller, F. Witte, K. Rissanen, B. Sarkar and C. A. Schalley, *Beilstein J. Org. Chem.*, 2020, **16**, 2576-2588.
4. L. Zou and M. J. Webber, *Chem. Commun.*, 2019, **55**, 9931-9934.
5. H. Shao, T. Nguyen, N. C. Romano, D. A. Modarelli and J. R. Parquette, *J. Am. Chem. Soc.*, 2009, **131**, 16374-16376.
6. W. Jiang and C. A. Schalley, *Beilstein J. Org. Chem.*, 2010, **6**, 14.
7. J. R. Aranzaes, M.-C. Daniel and D. Astruc, *Can. J. Chem.*, 2006, **84**, 288-299.
8. M. Gaedke, H. Hupatz, H. V. Schröder, S. Suhr, K. F. Hoffmann, A. Valkonen, B. Sarkar, S. Riedel, K. Rissanen and C. A. Schalley, *Org. Chem. Front.*, 2021, **8**, 3659-3667.
9. M. Gaedke, F. Witte, J. Anhäuser, H. Hupatz, H. V. Schröder, A. Valkonen, K. Rissanen, A. Lützen, B. Paulus and C. A. Schalley, *Chem. Sci.*, 2019, **10**, 10003-10009.
10. S. V. Rosokha and J. K. Kochi, *J. Am. Chem. Soc.*, 2007, **129**, 828-838; M. B. Kirketerp, L. A. Leal, D. Varsano, A. Rubio, T. J. Jørgensen, K. Kilsa, M. B. Nielsen and S. B. Nielsen, *Chem. Commun.*, 2011, **47**, 6900-6902.
11. H. V. Schröder, H. Hupatz, A. J. Achazi, S. Sobottka, B. Sarkar, B. Paulus and C. A. Schalley, *Chem. Eur. J.*, 2017, **23**, 2960-2967.
12. C. Bannwarth, S. Ehlert and S. Grimme, *J. Chem. Theory Comput.*, 2019, **15**, 1652-1671.
13. S. Grimme, J. G. Brandenburg, C. Bannwarth and A. Hansen, *J. Chem. Phys.*, 2015, **143**, 054107.
14. A. Klamt and G. Schüürmann, *J. Chem. Soc., Perkin Trans. 2*, 1993, **5**, 799-805.
15. I. M. Smallwood, *Handbook of Organic Solvent Properties*, Butterworth-Heinemann, Oxford, 1996.
16. R. Ahlrichs, M. Bär, M. Häser, H. Horn and C. Kölmel, *Chem. Phys. Lett.*, 1989, **162**, 165-169.
17. J. D. Chai and M. Head-Gordon, *J. Chem. Phys.*, 2008, **128**, 084106; F. Weigend and R. Ahlrichs, *Phys. Chem. Chem. Phys.*, 2005, **7**, 3297-3305.
18. V. Barone and M. Cossi, *J. Phys. Chem. A*, 1998, **102**, 1995-2001.
19. F. Neese, *WIREs Comput. Mol. Sci.*, 2017, **8**:e1327.
20. G. Hermann, V. Pohl, J. C. Tremblay, B. Paulus, H. C. Hege and A. Schild, *J. Comput. Chem.*, 2016, **37**, 1511-1520.
21. O. V. Dolomanov, L. J. Bourhis, R. J. Gildea, J. A. K. Howard and H. Puschmann, *J. Appl. Crystallogr.*, 2009, **42**, 339-341.
22. G. M. Sheldrick, *Acta Cryst.*, 2015, **A71**, 3-8.
23. G. M. Sheldrick, *SHELXL Version 2014/7, Programm for Crystal Structure Solution and Refinement*, University of Göttingen, 2014; G. M. Sheldrick, *Acta Cryst.*, 2008, **A64**, 112-122.
24. K. Brandenburg, "Diamond: Crystal and Molecular Structure Visualization" can be found under <http://www.crystalimpact.com/diamond>, 2017.
25. Persistence of Vision. Ltd., retrieved from <http://www.povray.org/download/>, 2004.